Spinning Reserve Estimation in Microgrids

Wang Ming Qiang

School of Electrical and Electronic Engineering

A thesis submitted to the
Nanyang Technological University
in fulfillment of the requirement for the degree of
Doctor of Philosophy

2012

Acknowledgements

I would like to express my sincere thanks to my supervisor, Associate Professor Gooi Hoay Beng. Without his ideas, guidance and dedication, my research plan would not have accomplished much. During this 4-year intensive study, I learned from him not only the ways to do research but also the attitude towards life.

I would like to thank the technicians in Laboratory for Clean Energy Research, Mr. Thomas Foo, Mrs. Grace Ong and Mrs. Chia-Nge Tak Heng, for their technical support in the usage of computers, software, and other laboratory equipments. I also like to thank Mr. Chen Shuaixun, and Mr. Gao Zhiyong for their time in engaging constant research discussions with me. Besides, I am thankful to all my classmates and friends in the Laboratory for Clean Energy Research. They have made the laboratory such a wonderful, friendly and intellectually stimulating place.

I am grateful to my parents, sisters, and girlfriend (now my wife) for their encouragements and unconditional support to my study. Their unwavering love is always my source of strength.

Finally, financial support provided by Nanyang Technological University in the form of scholarship throughout my study is deeply appreciated.

Table of Contents

Summary

Spinning reserve (SR) can be defined as the unused capacity which can be activated on decision of the system operator. It is an important resource which can safeguard a power system against loss of load after a sudden outage of generating units, or transmission/distribution network facilities and/or a sudden increase of loads.

Scheduling sufficient SR can reduce the probability and severity of loss of load. Thus it can mitigate considerable social and economical costs of occasional supply interruption caused by outages of power system components. However providing SR has a substantial cost because additional units may need to be committed and some other units may operate less than their optimal output. So the SR requirement needs to be assigned appropriately.

SR can be determined by deterministic techniques or by probabilistic techniques. Among these techniques, the cost/benefit analysis optimizes SR by a tradeoff between security and economics. The major drawback of the cost/benefit analysis is that the calculation of the reliability indices such as the expected energy not supplied (EENS) is computation intensive due to its highly nonlinear and combinatorial characteristics.

EENS can be formulated as a piecewise linear function of system spinning reserve (SSR) because EENS curves under different feasible unit schedules have a cluster property. The parameters of the piecewise function of EENS are determined using capacity outage probability table (COPT) based on a given unit schedule. The nonlinear and combinatorial EENS model is replaced by a piecewise linear one. The computation burden can be greatly reduced.

A multi-step method is proposed to estimate SR in a large traditional power system. In step one, a base UC module is implemented to produce the initial unit schedule. Then

COPT is established. In step two, parameters of the EENS are determined through COPT. Then the optimal SR can be determined by optimizing the schedule cost and the expected interruption cost which is equal to EENS multiplied by the value of lost load. After optimization a convergence criterion is validated. If the convergence criterion is satisfied, the optimization will stop. Otherwise the EENS formuation will be updated based on the newly found unit schedule and the optimizaiton process runs again.

A modified multi-step method is proposed to estimate SR in microgrids. EENS will be classified by outage orders. A first order outage corresponds to a single unit outage while a second order outage corresponds to simultaneous outage of two units. EENS in the modified multi-step method is divided into two parts and calculated using different ways. EENS caused by uncertainties only, and uncertainties and first order of outage events consumes a relatively short time. This part of EENS is calculated directly using UC variables. EENS caused by uncertainties, and second and higher orders of outage events consumes most of the run time. This part of EENS is modeled by a piecewise linear function of SSR and captured step by step. A series of sensitivity analyses are implemented to demonstrate the efficiency and robustness of the proposed method.

List of Figures

List of Tables

List of Variables, Parameters and Abbreviations

◆ List of variables

$b_{s,t}$: a binary variable to represent whether loss of load occurs due to event s during period t;

$b^1_{i,t}$: a binary variable to represent whether loss of load occurs when an outage of unit i occurs during period t;

$b^2_{i,j,t}$: a binary variable to represent whether loss of load occurs when a simultaneous outage of units i and j occurs during period t;

$b^3_{i,j,k,t}$: a binary variable to represent whether loss of load occurs when a simultaneous outage of units i, j and k occurs during period t;

$b_{i,t}$: a binary variable to represent whether loss of load occurs due to the ith outage capacity in COPT during period t;

$b^0_{k,l,m,t}$: 1 if WTG, PV and load uncertainties during period t cause loss of load and 0 otherwise;

$b^1_{i,k,l,m,t}$: 1 if WTG, PV and load uncertainties and the outage of unit i during period t cause loss of load and 0 otherwise;

$b^2_{i,j,k,l,m,t}$: 1 if WTG, PV and load uncertainties and the simultaneous outage of unit i and j during period t cause loss of load and 0 otherwise;

$b^0_{n,t}$: 1 if the aggregated uncertainty during period t causes loss of load and 0 otherwise;

$b^1_{i,n,t}$: 1 if the aggregated uncertainty and the outage of unit i during period t cause loss of load and 0 otherwise;

$b^2_{i,j,n,t}$: 1 if the aggregated uncertainty and the simultaneous outage of unit i and j during period t cause loss of load and 0 otherwise;

$b_{n,t}^{>1}$: 1 if the final combined distribution during period *t* causes loss of load and 0 otherwise;

$C(t)$: energy stored in ESS till period *t*;

$C_{i,t}(\ )$: production cost of unit *i* during period *t*;

$EENS^0$: EENS caused by WTG, PV and load uncertainties with zero order of outage events;

$EENS^1$: EENS caused by WTG, PV and load uncertainties with first order of outage events;

$EENS^2$: EENS caused by WTG, PV and load uncertainties with second order of outage events;

$EENS^{01}$: sum of $EENS^0$ and $EENS^1$;

$EENS^{>1}$: EENS caused by second and higher orders of outage events;

$EENS_{in}^0$: $EENS^0$ calculated during optimization;

$EENS_{after}^0$: $EENS^0$ calculated after optimization via COPT;

$EENS_{in}^1$: $EENS^1$ calculated during optimization;

$EENS_{after}^1$: $EENS^1$ calculated after optimization via COPT;

$EENS_{in}^{>1}$: $EENS^{>1}$ calculated during optimization;

$EENS_{after}^{>1}$: $EENS^{>1}$ calculated after optimization via COPT;

$EENS_t^{during}$: *EENS* of period *t* calculated during optimization;

$EENS_t^{after}$: *EENS* of period *t* calculated after optimization via COPT;

f^{WT}: speed-to-power conversion function;

f_i^{WT}: speed-to-power conversion function of the *i*th WTG;

f^{PV}: irradiance-to-power conversion function;

f_i^{PV}: irradiance-to-power conversion function of the *i*th PV unit;

g : irradiance on the PV panel plane (kW/m^2);

$K_{i,t}$: a binary variable to represent whether unit *i* starts up during period *t*;

$LOLP_t$: LOLP value during period *t*;

p: PV output power (kW);

$p_{s,t}$: probability when event *s* occurs during period *t*;

p_t^0: probability when all online units are available;

$p_{i,t}^1$: probability when an outage of unit *i* occurs during period *t*;

$p_{i,j,t}^2$: probability when a simultaneous outage of units *i* and *j* occurs during period *t*;

$p_{i,j,k,t}^3$: probability when a simultaneous outage of units *i*, *j* and *k* occurs during period *t*;

$P_{i,t}$: output power of unit *i* during period *t*;

P_t^E: output power of ESS during period *t*;

$R_{i,t}$: reserve bid amount of unit *i* during period *t*;

SSR_t: system spinning reserve during period *t*;

$U_{i,t}$: status (0/1) of unit *i* during period *t*;

v: wind speed (m/s or miles/hour);

w: WTG output power (kW or MW);

$\Delta EENS$: normalized relative EENS error;

$\Delta EENS^{01}$: normalized relative $EENS^{01}$ error;

$\Delta EENS^{>1}$: normalized relative $EENS^{>1}$ error;

$\Delta P_{s,t}$: outage power of event *s* during period *t*; and

$\Delta R_{s,t}$: outage reserve of event *s* during period *t*.

◆ **List of parameters**

c: scale factor of speed distribution function;

c_1, c_2 : scale factors of irradiance distribution function;

C_S : starting energy stored in ESS;

C_E : ending energy stored in ESS;

C_{min} : minimum allowable energy stored in ESS;

C_{max} : maximum allowable energy stored in ESS;

d_T : duration time of each interval;

$g_{i,t}^{fcst}$: forecast irradiance of the *i*th PV unit during period *t*;

$g_{i,t}^{trun}$: irradiance value at the truncated point of the *i*th PV unit during period *t*;

k : shape factor (dimensionless) of speed distribution function;

k_1, k_2 : shape factors of irradiance distribution function;

K_c : a certain irradiance point (kW/m^2) on irradiance-to-power curve;

$LOLP_t^{\max}$: maximum allowable LOLP limit;

$MP(t)$: open market active power price;

nWT : number of WTG units;

nPV : number of PV units;

N_{WT} : number of intervals of wind speed distribution;

N_{PV} : number of intervals of irradiance distribution;

N_L : number of intervals of load distribution;

N : number of intervals of the approximated uncertainty distribution;

nI : set of non-dispatchable units;

N_T : number of periods in the optimization horizon;

N_G : number of available generating units;

$N(t)$: number of outage capacity levels during period *t*;

$p_{i,t}$: probability of the *i*th outage capacity level during period *t*;

$p_{k,t}^{WT}$: probability of wind speed falls in the *k*th interval of wind speed distribution function during period *t*;

$p_{m,t}^{PV}$: probability of irradiance falls in the *m*th interval of irradiance distribution function during period *t*;

p_l^L : probability of load falls in the *l*th interval of load forecast distribution function;

$p_{n,t}$: probability when the *n*th interval of the aggregated uncertainty distribution is selected during period *t*;

$p_{n,t}^{>1}$: probability when the *n*th interval of the final combined distribution is selected during period *t*;

$p_E^{\max}$: maximum allowable charge/discharge limit;

$P_i^{\max}$: maximum output power of unit *i*;

$P_i^{\min}$: minimum output power of unit *i*;

P_t^L : system forecast load during period *t*;

$q_{i,t}$: reserve bid price of unit *i* during period *t*;

R_i^{up} : ramp up rate of unit *i*;

R_t^{RCUC} : predefined SR requirement during period *t* in the RCUC problem;

S : the total area of the PV panel (m^2);

S_t : set of all possible events during period *t*;

SUC_i : startup cost of unit *i*;

T : entire period of observation;

u_i : outage replacement rate;

$U_{i,t}^{'}$: exogenous status of a dispatchable unit which is calculated in step one;

v_{mean} : mean of the speed probability distribution;

v_i : cut-in wind speed (m/s or miles/h);

v_r : rated wind speed (m/s or miles/h);

v_o : cut-out wind speed (m/s or miles/h);

$v_{i,t}^{fcst}$: forecast wind speed of the *i*th WTG unit during period *t*;

$v_{i,t}^{trun}$: wind speed value at the truncated point of the *i*th WTG unit during period *t*;

w_r : WTG rated power (kW or MW);

γ_i : failure rate of unit *i*;

$\Delta C_{i,t}$: amount of the *i*th outage capacity during period *t*;

$\Delta P_{l,t}^{L}$: load forecast error when load falls in interval *l* during period *t*;

$\Delta P_{k,t}^{WT}$: WTG power forecast error when wind speed falls in interval *k* during period *t*;

$\Delta P_{m,t}^{PV}$: PV power forecast error when irradiance falls in interval *m* during period *t*;

$\Delta P_{n,t}$: power deviation when the *n*th interval of the aggregated uncertainty distribution is selected during period *t*;

$\Delta P_{n,t}^{>1}$: power deviation when the *n*th interval of the final combined distribution is selected during period *t*;

ε : convergence tolerance of the convergence criterion;

η^{PV} : efficiency of the PV panel (%);

η^{E} : discharge efficiency of ESS;

σ : load standard deviation;

τ : amount of time available for the generators to ramp up their output for delivery of reserve capacity; and

ω: weighted parameter, $0<\omega<1$.

◆ List of abbreviations

CDF	cumulative distribution function
COPT	capacity outage probability table
DG	distributed generation
ESS	energy storage system
EENS	expected energy not supplied
EIC	expected interruption cost
FC	fuel cell
FOR	forced outage rate
Gamma( )	gamma function

LOLP	loss of load probability
MILP	mixed integer linear programming
MT	microturbine
ORR	outage replacement rate
PDF	probability density function
PV	photovoltaic
RCUC	reserve constrained unit commitment
SC	scheduling cost
SR	spinning reserve
SSR	system spinning reserve
UC	unit commitment
VOLL	value of lost load
WT	wind turbine
WTG	wind turbine generator

Chapter 1
Introduction

1.1 Spinning Reserve (SR)

With the restructuring of electricity supply industry and the increasing penetration of various renewable energy sources, modern utilities are under pressure to operate systems with tighter security margin, less scheduling cost as well as conservative reliability. This has heightened concerns over ancillary services which include frequency control, automatic generation control, reactive power control, operating reserve, and black-start capability [1-4]. Keeping a reasonable amount of reserve, especially spinning reserve (SR), is considered as one of the most important ancillary services to maintain the security and reliability of power systems.

SR [5-7] can be defined as the unused capacity which can be activated on decision of the system operator. It is provided by energy generating resources that are synchronized to the network and able to inject the active power into the system. Alternatively, it can be provided by interruptible loads which release their rights to consume electricity. SR is an important resource which can protect a power system against loss of load after a sudden outage of some generating units, or transmission/distribution network facilities and/or a sudden increase of load.

Scheduling sufficient SR can reduce the probability and severity of loss of load. Thus it can mitigate considerable social and economical costs of occasional supply interruption caused by outage of power system components. However providing SR has a substantial cost because additional units may need to be committed and some other units may operate less than their optimal output. When the SR requirement increases, the total operation or

scheduling cost of power systems increases while the social and economical cost caused by unexpected loss of load decreases. Conversely, when the SR requirement decreases, the total operation or scheduling cost of power systems decreases while the social and economical cost increases. So the SR requirement needs to be assigned appropriately.

SR needs some time to be fully deployed in case of contingencies. The reserve deployment time is different in each power system such that each power system has its own definition of deployment time depending on parameters such as the size of synchronized network or the market structure [5-8]. Similar to the SR used in [7], the SR used throughout the thesis refers to that which can be deployed within the tertiary regulation interval [5, 6, 9]. The tertiary regulation interval varies from system to system and it usually ranges from several minutes to more than one hour.

In this thesis, the SR estimation is restricted to a short term system operation problem or a day-ahead power market clearing problem. The SR estimation technique with reasonable accuracy should be implemented within a short interval and this short interval should be no longer than the tertiary regulation interval mentioned above. The determination of SR for long term planning problems [10, 11] is beyond the scope of this thesis and is not taken into account.

1.2 SR Estimation in Large Power Systems

Many approaches are available in regards to how the SR requirement in large power systems is determined. They can be classified as two major categories: deterministic and probabilistic techniques.

1.2.1 Deterministic Technique

Traditionally, the SR requirement is determined based on security consideration rather than on economic rules. The SR requirement is calculated by a deterministic technique where the amount of SR is usually set as a fraction of the total load or the capacity of the largest online unit or their combination [12]. Although this approach is straightforward and easy to implement, it considers neither the stochastic nature of system behavior and component failures nor the economics. The SR requirement is developed specifically for each power system and it varies from system to system. Table 1.1 lists the SR requirement in several different power systems [5, 6, 7] throughout the world.

Table 1.1 SR requirements in different power systems

Power systems	SR requirement
Australia and New Zealand	$\max(U_{i,t}P_{i,t})$
British Columbia (BC) Hydro	$\max(U_{i,t}P_i^{\max})$
Spain	Between $3(P_i^D)^{\frac{1}{2}}$ and $6(P_i^D)^{\frac{1}{2}}$
California	$50\%\times\max(5\%\times P_{hydro}+7\%\times P_{other\ generation}, P_{largest\ contingency})+P_{non\text{-}firm\ import}$
Pennsylvania/new Jersey/Maryland (PJM) (Southern)	$\max(U_{i,t}P_i^{\max})$
PJM (Western)	$1.5\%\times P_t^D$
PJM (other)	$1.1\%\times P_t^D$ + probabilistic calculation on typical days and hours
The Union for the Coordination of Transmission of Electricity (UCTE)	No specific recommendation. The recommended maximum is $\sqrt{10P_t^{zone}+150^2}-150$
The Netherlands	UCTE rules. Currently at least 300 MW
Belgium	UCTE rules. Currently at least 460 MW
France	UCTE rules. Currently at least 500 MW

where

$U_{i,t}$	unit status (0/1) of unit *i* during period *t*;
$P_{i,t}$	power output of unit *i* during period *t*;
$P_i^{\max}$	maximum power output of unit *i*;
P_t^L	load during period *t*;
P_{hydro}	power output from hydroelectric resources;
$P_{other\ generation}$	power output from resources other than hydroelectric;
$P_{largest\ contingency}$	power deviation due to the most severe contingency;
$P_{non\text{-}firm\ import}$	total of all the interruptible power imported from other grid connected systems;
P_t^{zone}	load of the UCTE control area during period *t*;
P_t^D	system load during period *t*; and
UCTE	the union for the coordination of transmission of electricity.

1.2.2 Probabilistic Technique

The nature of the electric power system failure is uncertain. Facility failures which occurred randomly in the past will also occur randomly in the future and therefore the electric power system behaves probabilistically. Thus, it is logical that probabilistic techniques should be considered for the assessment of such behaviors. Various probabilistic techniques have been developed. They can take into account the likelihood of the contingencies and their extent. The value that the customers attach to the continuity of supply is also considered. The probabilistic techniques can be classified as follows:

- **Optimizing SR by successive iteration of Unit Commitment (UC)**

In [8, 13, 14], SR is optimized within the UC problem. This approach postprocesses the UC schedule to compute the system reliability level in each optimization period. If the

reliability level is greater than the specified target, SR is adjusted and the UC optimization process runs again. The flowchart of this approach is shown in Fig. 1.1.

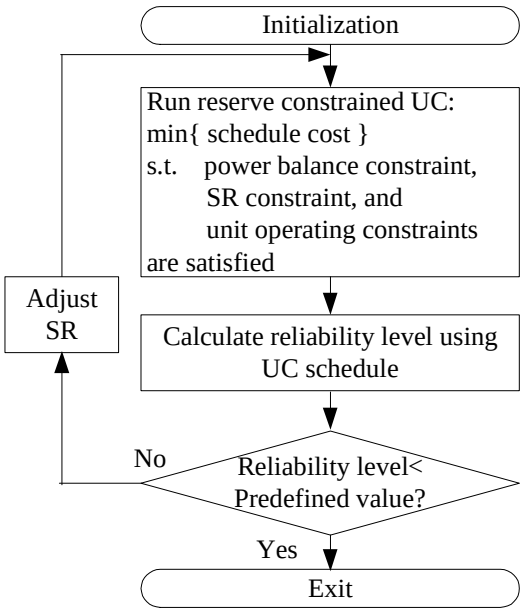

Fig. 1.1 Flowchart of optimizing SR by successive iteration of UC

The advantage of this approach is that it keeps the reserve constrained UC problem intact. The mathematical formulation is straightforward and this approach is easy to solve because the reliability indices are computed after the UC optimization rather than during the UC optimization.

The drawback of this approach is that in practice an acceptable risk level may be difficult to define. Although [13] proposes that the optimal risk can be obtained by an external cost/benefit analysis in each hourly optimization period, the inter-temporal constraints of UC are not fully considered. This approach is computation intensive since several UC computations have to be performed before the specified risk target is realized.

◆ **Optimizing SR by reliability constrained UC**

References [15-19] optimize the SR requirement by solving a reliability constrained UC problem. The reliability metrics, such as loss of load probability (LOLP) and/or expected energy not supplied (EENS), must fall below a predefined threshold are incorporated into the UC model. The mathematical model of reliability constrained UC is shown below.

min { schedule cost }
s.t.
{ power balance constraint,
SR constraint,
unit operating constraints, and
reliability constraints (e.g. $EENS < EENS^{\max}$ or $LOLP < LOLP^{\max}$)
are satisfied
where
$EENS^{\max}$: predefined $EENS$ threshold
$LOLP^{\max}$: predefined $LOLP$ threshold

The advantage of this approach is that the reliability indices are explicitly involved in the optimization. Postprocessing of the UC schedule and successive iteration of UC are avoided. Compared with the conventional UC problem, only a set of reliability constraints is added into the model.

The drawback of this approach is that it is difficult to design a reliability metric ceiling for different power systems. The desired reliability level in one system could represent a completely different level of reliability in other systems because it depends on the number of generating units, generating capacity, loading and reliability of the units as well as the value that the consumers attach to an uninterruptible supply. This approach does not optimize the SR level itself but simply increases the committed capacity until the reliability target is realized. It is also noteworthy that this approach may become infeasible if there are insufficient reserve resources to realize the predefined reliability

threshold. In this approach, the SR requirement is determined more on reliability viewpoint than on cost-effective viewpoint. Therefore the results obtained by an arbitrary selection of reliability ceiling are not economically optimal. Furthermore, using a uniform reliability level during all optimization periods is suboptimal since some expensive reserve may be dispatched in some periods and the benefit that it provides might not justify the cost that it introduces. Finally, when the reliability indices such as EENS and LOLP are explicitly formulated as the functions of UC variables, the formulations of EENS and LOLP are highly nonlinear and their combinatorial characteristic exists. The calculation of EENS and LOLP is computation intensive.

Reference [20] combines successive iteration of UC and reliability constrained UC together in pursuit of better results. This method optimizes SR by successive iteration of reliability constrained UC. Instead of SR, reliability indices are updated within the iteration process. Obviously, this method is computation intensive due to the successive iteration of reliability constrained UC and the complexity of the formulation of reliability indices.

◆ **Optimizing SR by cost/benefit analysis**

In [21-27], the SR requirement is determined by the cost/benefit analysis. The objective is minimizing the scheduling cost (SC) and the expected interruption cost (EIC). The benefit is represented by the reduction of EIC. Compared with the conventional UC problem, an additional term (EIC) is added in the objective function. When SR increases, the SC increases while the EIC decreases. When SR decreases, the SC decreases while the EIC increases. This approach can automatically determine the optimal SR by a tradeoff between reliability and economics. The relationship between SC, EIC, and total cost is illustrated in Fig. 1.2. The mathematical model of this approach is shown in Fig. 1.2.

min { $SC + EIC$ }

s.t.

$$\begin{cases} \text{power balance constraint, and} \\ \text{unit operating constraints} \end{cases}$$

are satisfied

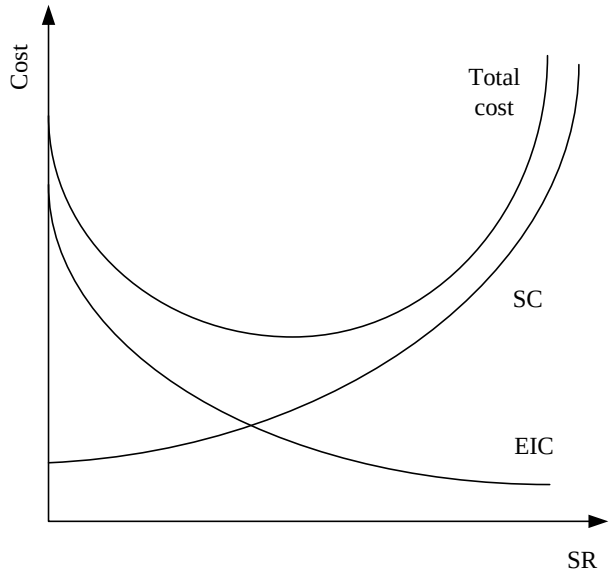

Fig. 1.2 Cost and benefit analysis

This approach has many advantages. It avoids the successive iteration of the UC problem. This approach does not require a predefined system risk or LOLP or EENS target because the SR is automatically determined based on the cost/benefit analysis. Both reliability and economics are considered in the optimization and the final results are economically optimal.

The main drawback of this approach is that the introduction of LOLP and EENS indices is generally cursed by computational intractability due to their nonlinear and combinatorial nature. This makes the main impediment to the wide implementation and adoption of this approach. The computation complexity is explicitly discussed in chapter two.

The characteristics of the three probabilistic approaches are concluded in Table 1.2.

Table 1.2 Characteristics of three probabilistic approaches

	Advantage	Drawback
Successive iteration of UC	Keep the reserve constrained UC intact.	Successive iteration of UC. Difficult to determine a sophisticated reliability threshold.
Reliability constrained UC	Avoid the successive iteration of UC.	Difficult to determine a sophisticated reliability threshold. Complex EENS and LOLP calculation.
Cost/benefit analysis	Avoid the iteration of UC and the selection of reliability threshold.	Complex EENS and LOLP calculation.

Besides the analytical techniques mentioned above, there is another kind of technique called stochastic programming [28-34]. The Monte Carlo simulation is used to create the scenarios and to simulate possible contingencies. Random load variations, outage events of units and transmission lines as well as uncertainties of wind turbine generator (WTG) output are explicitly modeled as scenarios in the Monte Carlo simulation. Similar to the classification of the analytical SR optimization methods, the stochastic SR optimization methods include successive iteration of stochastic UC [28], reliability constrained stochastic UC [29], and stochastic programming based on the cost/benefit analysis [11, 30-34].

When the reliability indices which are caused by possible component outage events with low probability are evaluated using the Monte Carlo simulation, the number of simulation used is two or three orders of magnitude larger than the number of scenarios considered in the decision process. This leads to a model that is so large that a solution cannot be computed within a reasonable amount of time. Stochastic programming does not satisfy the requirement of computation speed for short term SR estimation problems. The computation can be sped up by employing scenario reduction techniques or considering

only a few representative scenarios. However the results will not be representative of the actual system operation when scenarios of smaller subsets are considered.

In stochastic programming the reserve requirement is implicitly involved in the model and the SR requirement is not needed. References [35, 36] try to get a better accuracy by combining stochastic UC with the SR requirement. A scenario reduction technique is used and the SR requirement constraints are added in the model to capture the missing scenarios. But the computation efficiency is still not desirable. In this thesis stochastic programming is not considered and an analytical method is used.

The uncertainties caused by load and intermittent sources such as WTGs should be considered in the SR estimation. In stochastic programming, the load and WTG uncertainties can be explicitly modeled by scenarios through the Monte Carlo simulation. In analytical methods, the SR caused by load uncertainties can be modeled by a fraction of load or combining the load uncertainty into the calculation of reliability. The SR caused by WTGs can be modeled as a ratio of the WTG output power [31, 37, 38], or combining the load uncertainty and WTG uncertainty together and see their combination as the net load [39-43]. The uncertainty of the net load is equal to the total uncertainty of the load and WTGs. The WTG uncertainty can be modeled by a distribution function [39-43] or by a non-parametric probabilistic forecast represented by quantiles or intervals [44-45].

1.2.3 Calculation Complexity of EENS and LOLP

From the above discussion it can be found that optimizing SR using the cost/benefit analysis is the best choice among the existing methods. However, the technique has an obvious drawback that the calculation of EENS and LOLP is computation intensive due to their highly nonlinear formulations and the combinatorial nature caused by unit outage events. This drawback is the major impediment to the widespread use of the cost/benefit

analysis technique. In an attempt to overcome this deficiency, some methods have been developed and they are explicitly shown below.

Reference [15] approximately formulates LOLP as an analytical function of SR only. The constraint that the LOLP must be smaller than a predefined LOLP value can be replaced by a linear function of SR. Its advantage is that the complexity of calculating LOLP is avoided and the computation efficiency can be improved. Its drawback is that some system dependent parameters have to be determined in advance and an approximate LOLP threshold is needed. Besides, LOLP is not very suited for the computation of economics because it only measures the probability of loss of load. The quantity of the loss of load cannot be determined.

Reference [42] approximately formulates EENS and LOLP as an analytical function of SR only based on a Q-function. The calculation complexity of EENS and LOLP can be greatly reduced. However EENS and LOLP considered are only caused by the load and WTG uncertainties. The effect of unit outage events is not considered. Besides, EENS and LOLP calculated using the Q-function lead to upper bounds of the real EENS and LOLP values. The accuracy of the results cannot be guaranteed.

Reference [21] calculates EENS based on exogenous energy scheduling, which means that the reserve schedule is independent of the energy schedule. Ignoring the coupling that exists between the energy and the reserve scheduling can lead to sub-optimal or infeasible solutions [26]. Reference [46] mitigates the computational burden by considering only a few significant events. Reducing the number of contingency events considered cannot guarantee that the whole spectrum of unreliability is captured. The optimization may lose considerable computation accuracy and the results are sub-optimal. In [16, 18], when calculating unit outage probabilities the higher order terms are omitted and only an upper bound is used. The calculation complexity is reduced but the optimality cannot be guaranteed.

In [25, 26, 27], EENS of every optimization period is analytically estimated as a three-segment piecewise linear function of the system committed capacity using a preprocessing auxiliary procedure. The calculation of EENS is greatly reduced. However the proposed EENS approximation is only an upper bound of the real EENS. Using only three segments to represent the EENS curve is not accurate enough. The parameters of the three-segment piecewise linear function are system dependent and they need to be determined by an auxiliary procedure in advance. During preprocessing optimization, the inter-temporal coupling is not considered [27]. This could lead to sub-optimal solutions.

1.3 Microgrids

In the last decade, the interest on distributed generation (DG) has been increasing, essentially due to technical developments of generation systems that address environmental and energy policy concerns. With the penetration of DG, microgrids are becoming more and more attractive in modern distribution networks. Microgrids can be defined as low voltage networks, which include loads, energy storage systems (ESSs), and several small modular generation systems providing both heat and power [47-51]. A simple architecture of a microgrid is shown in Fig. 1.3 [52].

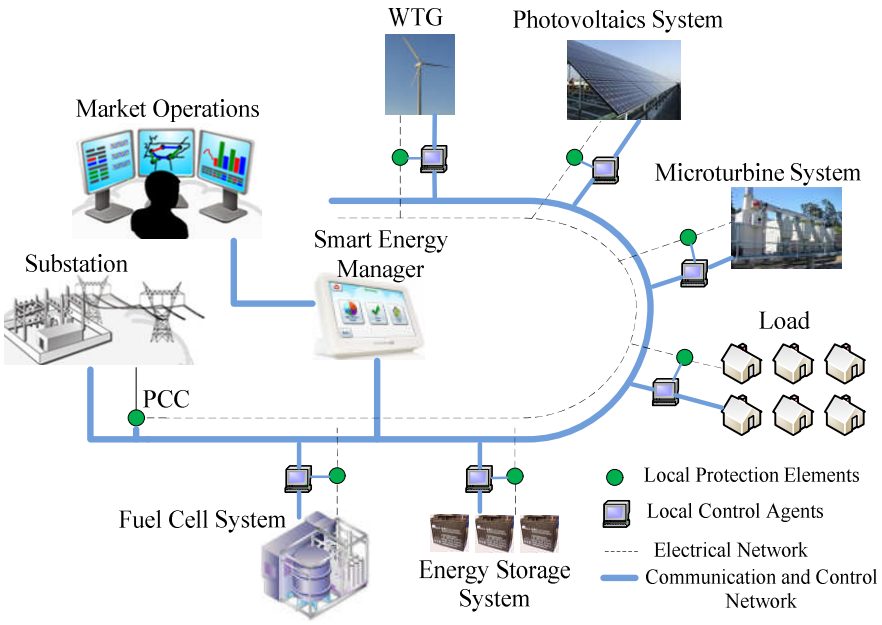

Fig. 1.3 A simple architecture of a microgrid

The key differences between a microsource in microgrids and a generator in conventional power plants are as follows [53]:

1) Microsources are of much smaller capacity with respect to the large generators in conventional power plants.

2) Power generated at distribution voltage levels can be directly fed to the utility distribution network.

3) Microsources are normally installed close to the customer's premises so that the electrical/heat loads can be efficiently supplied with satisfactory voltage and frequency profiles and negligible line losses due to a shorter distance travelled.

Microgrids can operate in two different modes: grid connected or standalone/isolated. In grid connected mode, microgrids are connected to the upstream grid of the distribution network, importing or exporting electricity and/or ancillary services. In isolated mode,

microgrids are disconnected from the upstream grid of the distribution network and can operate as independent entities. They use local resources to cover the power balance. If necessary, they shed load. A typical example of an isolated microgrid is an electricity supply system in a remote village.

Microgrids can coordinate distributed energy resources in a consistently more decentralized way, thereby reducing the control burden on the grid and permitting them to provide its full benefits. From the grid's point of view, a microgrid can be regarded as a controlled entity within the power system that can be operated as a single aggregated load. Given attractive remuneration they can serve as small sources of power or provide ancillary services supporting the network. From the consumer's point of view, microgrids provide their thermal and electricity needs. The supply process is similar to that of the traditional low voltage distribution networks. In addition, they enhance local reliability, reduce emissions, potentially lower costs of energy supply, and improve power quality by providing voltage support.

However, to achieve a stable and secure operation, a number of technical, regulatory and economic issues have to be resolved before microgrids can be widely adopted. Sound operation of microgrids requires well thought energy management strategies. The energy management strategies should accommodate both transient power balancing and short-term energy management requirements. Maintaining an appropriate level of SR is one of the most important aspects of short-term energy management [54].

1.4 SR Estimation in Microgrids

Determining an appropriate SR amount is more difficult in microgrids than in large power systems. Compared with large traditional power systems, microgrids have their own characteristics. The flexibility and usability of microgrids to provide reserves depend on their composition, i.e., the mix of the different sources. The composition of microgrids

varies significantly from one to another. Microgrids usually comprise a lot of intermittent sources, such as WTG, photovoltaic (PV), etc. The wind speed and solar irradiance are different in different microgrids. The load variation in a microgrid is more difficult to predict due to load volatility and the decreased smoothing effect of load forecasting. A sophisticated reliability ceiling is really hard to define. Hence a cost/benefit analysis is the best choice. As mentioned above, when the cost/benefit analysis is used, the calculation of EENS and LOLP is very complex and this problem needs to be analyzed carefully. It is not straightforward to estimate the amount of SR in microgrids.

In the literature very few papers discuss the SR assignment in microgrids. Reference [55] gives an empirical method to determine the SR amount. For PVs, they assume that the SR amount which is used to compensate the uncertainty of PV output is set at 50% of the PV output. For WTGs, they assume that the minimum percentage of reserve is 20% of the nominal capacity. The percentage increases linearly to 100% as the wind power production is reduced as depicted in Fig. 1.4.

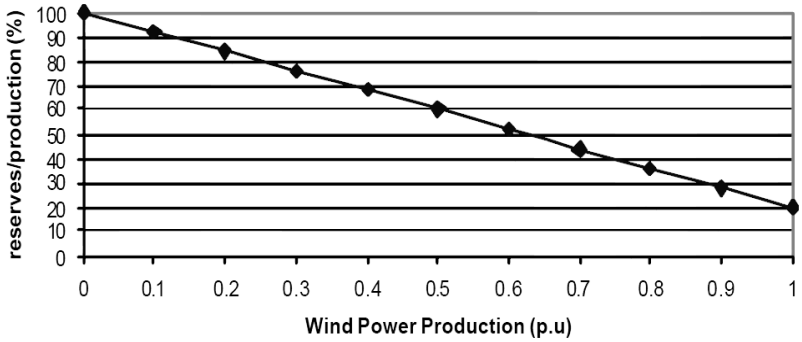

Fig. 1.4 Wind power reserve changes with wind power production

Thus the reserve to compensate for WTG power production uncertainty is:

$$WTG\_reserve = (1 - \frac{0.8}{Ins\_WTG} \times WTG\_production) \times WTG\_production \qquad (1.1)$$

where *Ins_WTG* is the installed capacity of WTG; and *WTG_production* is the power production of WTG.

And for load, they assume that the SR amount which is used to compensate the load uncertainty is set at 6% of the total load. The total reserve amount is equal to the summation of SR which is used to compensate the WTG, PV, and load uncertainties.

Although this method is easy to implement, it is not reasonable when the meteorology conditions change. The microgrid configuration may vary from one form to another and the implementation of the above SR determination criterion may not be applied readily. This empirical method cannot be used for other microgrids. The unreliability of units is also not taken into account. It is a complex problem to decide the SR amount in microgrids and this problem has not been explicitly investigated.

1.5 Major Contribution of This Thesis

In order to reduce the computation complexity caused by the highly nonlinear and combinatorial nature of EENS, an approximated EENS formulation is proposed in this thesis. The procedure of how the approximated EENS is proposed and analyzed forms a part of the main contributions. EENS is formulated as a piecewise linear function of system spinning reserve (SSR) only based on a given unit schedule. The method which is used to calculate the parameters of the EENS model is proposed. The reason why the piecewise linear model can be used is explicitly analyzed.

A SR estimation method which can be used in a large traditional power system is proposed. The SR is determined by a multi-step method in which an approximated EENS formulation discussed in chapter two is used. In step one, a base UC module without the SR constraint is implemented. Based on the exogenous UC results, the capacity outage probability table (COPT) can be established for each optimization period. In step two, an approximated EENS is formulated based on the obtained COPT for each optimization period. This EENS formulation is used in the computation and the SR can be determined by optimizing SC and EIC. A convergence criterion is introduced after step two

completes. If the criterion is satisfied, the total optimization will stop. Otherwise, the EENS is updated based on the newly found unit schedule and a new step is needed.

The proposed multi-step above is extended to microgrids. Due to the poor convergence speed, the multi-step method cannot be directly used and it is modified to suit microgrid applications. The total EENS is divided into two parts and calculated using two different methods. EENS caused by uncertainties only, and a combination of uncertainties and single unit outage events is directly calculated using UC variables. EENS caused by uncertainties and multiple unit outage events, which consume most of the computation resource, is modeled as a piecewise linear function of SSR only. The latter EENS is captured step by step. During optimization EENS caused by simultaneous unit outages are all considered. The optimal SR can be obtained within a desirable time interval with a guaranteed accuracy. The modified multi-step method is used in microgrids.

1.6 Organization of This Thesis

This thesis consists of six chapters. Chapter one is the introduction of the thesis. The motivation of the research is discussed. The definition of SR is introduced. Various SR estimation techniques are presented. The advantages and drawbacks of each technique are elaborately explained. The microgrid is also defined. The difficulty in performing SR estimation in microgrids is explained.

Chapter two studies how to model EENS as a piecewise linear function of SSR. We demonstrate that SSR is the most appropriate variable of the analytical EENS formulation. The characteristic of EENS curve suggests that a piecewise function must be employed. The parameters of the piecewise linear EENS model are by-products of COPT which is established based on the exogenous unit schedule. It is reasonable to model EENS as a piecewise linear function of SSR since EENS curves possess a cluster property. EENS

does not change too much for a fixed SSR when the unit schedule varies in the feasible region.

Chapter three proposes a multi-step method which can be used to estimate the SR in large traditional power systems. The piecewise linear EENS formulation proposed in chapter two is used in the model. In step one, an initial unit schedule is produced. In step two, the SR is determined by optimizing SC and EIC in which EENS is modeled by a piecewise linear function of SSR. The optimization continues till the convergence criterion is satisfied.

Chapter four proposes a modified multi-step method to optimize the SR in microgrids. A microgrid model is introduced. It comprises a WTG, a PV, a fuel cell (FC), a microturbine (MT) and an ESS. The uncertainty distributions of load, WTG and PV are combined and aggregated together. Due to the convergence problem, the multi-step method proposed in chapter three cannot be directly used in microgrids. A modified multi-step method is proposed in which EENS is divided into two parts and calculated using two different methods. The optimal SR can be determined within a desirable time interval.

Chapter five presents the study cases and their simulation results. A series of sensitivity analyses are implemented. The effect of aggregated uncertainty distribution, rounding increment of the final combined distribution, outage probability approximation, and the modified multi-step method are explicitly discussed.

Chapter six concludes the research studies and gives recommendations for future works.

Chapter 2
Analytical Formulation of EENS

2.1 Mathematical Model of SR Estimation Method

In this thesis, the SR requirement is determined by a cost/benefit analysis. The cost includes the unit production cost, startup cost and SR cost. The sum of the unit production cost, startup cost and SR cost is called the schedule cost (SC). The benefit is represented by the reduction of the EIC. So the objective function is to simultaneously optimizing the SC and the EIC [25, 26]. The objective function is

$$\min \{\sum_{t=1}^{N_T}\sum_{i=1}^{N_G}[C_{i,t}(P_{i,t},U_{i,t})+SUC_i\cdot K_{i,t}]+\sum_{t=1}^{N_T}\sum_{i=1}^{N_G}q_{i,t}R_{i,t}+EENS\cdot VOLL\} \tag{2.1}$$

where

N_T: number of periods in the optimization horizon;

N_G: number of available generating units;

$U_{i,t}$: status (0/1) of unit *i* during period *t*;

$P_{i,t}$: output power of unit *i* during period *t*;

$C_{i,t}(\ )$: production cost of unit *i* during period *t* which can be represented by a three-segment piecewise linear function;

SUC_i: startup cost of unit *i*;

$K_{i,t}$: a binary variable to represent whether unit *i* starts up during period *t*. It satisfies

$$\begin{cases} K_{i,t}\geq 0 \\ K_{i,t}\geq U_{i,t}-U_{i,t-1} \qquad \forall i;\forall t\geq 1; \end{cases} \tag{2.2}$$

$R_{i,t}$: reserve bid amount of unit *i* during period *t*; and

$q_{i,t}$: reserve bid price of unit *i* during period *t*.

The first term in the objective function is the operating cost, which includes the production cost and the startup cost. The second term is the SR cost. The final term is the EIC which is equal to EENS multiplied by VOLL. VOLL is defined as the average cost that customers attach to the loss of one kW for one hour [56]. The SC and EIC are conflicting objectives. When SR increases, SC increases while EIC decreases. When SR decreases, SC decreases while EIC increases. The SR requirement can be automatically determined by a tradeoff between reliability and economics.

The formulation of EENS is shown in subsection 2.2.

The objective function must be minimized subject to a number of constraints [57] which are shown below.

Power balance constraint:

$$\sum_{i=1}^{N_G} P_{i,t} = P_t^L \tag{2.3}$$

where P_t^L is system forecast load during period *t*.

SR constraints:

$$\begin{cases} R_{i,t} \le P_i^{\max} U_{i,t} - P_{i,t} \\ R_{i,t} \le U_{i,t}(\tau R_i^{up}) \end{cases} \tag{2.4}$$

where

$P_i^{\max}$: maximum output power of unit *i*;

R_i^{up}: ramp up rate of unit *i*; and

τ: amount of time available for generators to ramp up their output for delivery of reserve capacity [57]. In this thesis, τ is assumed to be 0.5 hour.

Unit operating constraints:

$$(U_{i,t}, P_{i,t}) \in \Psi, \quad \forall i, \forall t. \tag{2.5}$$

The block of constraints (2.5) generally includes upper and lower generation limits, minimum up and down time constraints, initial conditions, ramp up and ramp down rate constraints. They are all considered in this thesis. Their mathematical formulations are explicitly shown in appendix A.3.

2.2 Formulation of EENS

If the unit schedule which includes $U_{i,t}$, $P_{i,t}$, and $R_{i,t}$ are known, EENS can be easily calculated based on COPT [12]. The concepts of EENS and COPT were originally formulated for long-term planning studies. Later these concepts were introduced in short-term operation studies. COPT can be used in short-term operation studies when the unit schedule is known. COPT used in short-term operation studies is different from that used in long-term planning studies. These differences are as follows:

a) In short-term operation studies, only the committed units, i.e. units with on status, are selected to establish COPT. In long-term studies, all units are used to establish COPT.
b) In short-term operation studies, outage replacement rate is used to calculate the unit unreliability. In long-term planning studies, force outage rate is used.
c) In short-term operation studies, ramp rate constraints are considered so the committed capacity which must be larger or equal to output power plus reserve is used to establish COPT. In long-term planning studies, the unit nominal capacity is used.

For each optimization period, a COPT can be established. A COPT gives the probability that the total outage capacity will be greater than or equal to a certain value. EENS is equal to the summation of the products of the probabilities and the associated energy

curtailed when the outage capacity exceeds the SR requirement. EENS will be zero when the loss of capacity is less than the SR requirement.

If $U_{i,t}$, $P_{i,t}$, and $R_{i,t}$ cannot be determined apriori, COPT cannot be formed. EENS can be explicitly formulated by UC variables based on every possible outage event [16]:

$$EENS_t = \sum_{s \in S_t} p_{s,t} b_{s,t} (\Delta P_{s,t} + \Delta R_{s,t} - SSR_t) \cdot d_T \tag{2.6}$$

where

S_t : set of all possible events during period *t*;

$p_{s,t}$: probability when event *s* occurs during period *t*;

$b_{s,t}$: a binary variable to represent whether loss of load occurs due to event *s* during period *t*;

$\Delta P_{s,t}$: outage power of event *s* during period *t*;

$\Delta R_{s,t}$: outage reserve of event *s* during period *t*; and

SSR_t : SSR during period *t*, i.e.

$$SSR_t = \sum_{i=1}^{N_G} R_{i,t} \tag{2.7}$$

d_T : time duration of each period where $d_T = T/N_T$ where T is the entire period of observation, and N_T is the number of optimization periods.

The binary variable $b_{s,t}$ satisfies

$$b_{s,t} = \begin{cases} 1 & if\ \ \Delta P_{s,t} + \Delta R_{s,t} - SSR_t > 0 \\ 0 & otherwise. \end{cases} \tag{2.8}$$

In this thesis, d_T is assumed to be 1 hour. Only random outages of unit are considered. Load forecast errors and the effect of transmission and distribution networks are not taken into account. The outage events can be classified by outage orders. First order outage means outage of a single unit; second order means simultaneous outage of two units; and etc. EENS can be explicitly formulated as below where superscripts ‘1’, ‘2’, and ‘3’

represent first, second and third orders of outage events respectively. For formulation simplicity, EENS caused by fourth and higher orders of outage events are not shown here.

$$\begin{aligned} EENS \approx & \sum_{t=1}^{N_T}\sum_{i=1}^{N_G} p_{i,t}^{1} b_{i,t}^{1} (P_{i,t} + R_{i,t} - SSR_t) \\ & + \sum_{t=1}^{N_T}\sum_{i=1}^{N_G}\sum_{j>i}^{N_G} p_{i,j,t}^{2} b_{i,j,t}^{2} (P_{i,t} + R_{i,t} + P_{j,t} + R_{j,t} - SSR_t) \\ & + \sum_{t=1}^{N_T}\sum_{i=1}^{N_G}\sum_{j>i}^{N_G}\sum_{k>j}^{N_G} p_{i,j,k,t}^{3} b_{i,j,k,t}^{3} (P_{i,t} + R_{i,t} + P_{j,t} + R_{j,t} + P_{k,t} + R_{k,t} - SSR_t) \end{aligned} \tag{2.9}$$

where

$p_{i,t}^{1}$: probability when an outage of unit *i* occurs during period *t*;

$p_{i,j,t}^{2}$: probability when a simultaneous outage of units *i* and *j* occurs during period *t*;

$p_{i,j,k,t}^{3}$: probability when a simultaneous outage of units *i*, *j* and *k* occurs during period *t*.

$b_{i,t}^{1}$: a binary variable to represent whether loss of load occurs when an outage of unit *i* occurs during period *t*;

$b_{i,j,t}^{2}$: a binary variable to represent whether loss of load occurs when a simultaneous outage of units *i* and *j* occurs during period *t*; and

$b_{i,j,k,t}^{3}$: a binary variable to represent whether loss of load occurs when a simultaneous outage of units *i*, *j* and *k* occurs during period *t*.

The binary variables $b_{i,t}^{1}$, $b_{i,j,t}^{2}$, and $b_{i,j,k,t}^{3}$ satisfy

$$b_{i,t}^{1} = \begin{cases} 1 & if\ P_{i,t} + R_{i,t} - SSR_t > 0 \\ 0 & otherwise. \end{cases} \tag{2.10}$$

$$b_{i,j,t}^{2} = \begin{cases} 1 & if\ P_{i,t} + R_{i,t} + P_{j,t} + R_{j,t} - SSR_t > 0 \\ 0 & otherwise. \end{cases} \tag{2.11}$$

$$b_{i,j,k,t}^{3} = \begin{cases} 1 & if\ P_{i,t} + R_{i,t} + P_{j,t} + R_{j,t} + P_{k,t} + R_{k,t} - SSR_t > 0 \\ 0 & otherwise. \end{cases} \tag{2.12}$$

When a two-state model is used to represent the unit reliability, the outage probabilities $p_{i,t}^1$, $p_{i,j,t}^2$ and $p_{i,j,k,t}^3$ can be formulated as [16]:

$$p_{i,t}^1 = u_i U_{i,t} \prod_{j=1,\, j\neq i}^{N_G} (1 - u_j U_{j,t}) \tag{2.13}$$

$$p_{i,j,t}^2 = u_i u_j U_{i,t} U_{j,t} \prod_{k=1,k\neq i,j}^{N_G} (1 - u_k U_{k,t}) \tag{2.14}$$

$$p_{i,j,k,t}^3 = u_i u_j u_k U_{i,t} U_{j,t} U_{k,t} \prod_{l=1,l\neq i,j,k}^{N_G} (1 - u_l U_{l,t}) \tag{2.15}$$

where u_i is the outage replacement rate (ORR).

For short-term operation problems, ORR is used to compute EENS. ORR represents the probability that a unit fails and is not replaced during the lead time. The ORR parameter is similar to the forced outage rate (FOR) used in planning studies. The only difference is that ORR is not a fixed value but is a time-dependent quantity affected by the value of lead time of the unit being considered [58, 59]. It is assumed that unit failures are exponentially distributed and the time to repair is so long that repairs can be ignored. It is also assumed that if a unit is failed during an optimization period, it will not be available for the subsequent periods. The ORR of unit *i* during lead time d_T is given by [12, 16],

$$u_i = 1 - e^{-\gamma_i d_T} \approx \gamma_i d_T \tag{2.16}$$

where γ_i is the failure rate of unit *i*.

2.3 EENS Approximation

2.3.1 Relationship between EENS and SSR

From (2.13)-(2.15) one sees that the outage probabilities are functions of statuses of all units. They are highly nonlinear. So the formulation of EENS is highly nonlinear. From (2.9) one sees that due to the possible permutation of units, the combinatorial nature

exists. The number of first, second, and third orders of outage events are $N_T \cdot N_G$, $N_T \cdot N_G \cdot (N_G - 1)/2$, and $N_T \cdot N_G \cdot (N_G - 1) \cdot (N_G - 2)/6$ respectively. Combined with the UC problem, the curse of dimensionality occurs and the solution space is tremendously large. The calculation of EENS is a major impediment to the optimization process. New methods need to be developed to compute EENS efficiently.

From (2.6) one sees that $EENS_t$ is a function of $p_{s,t}$, $b_{s,t}$, $\Delta P_{s,t}$, $\Delta R_{s,t}$ and SSR_t. The dependent variables $p_{s,t}$, $b_{s,t}$, $\Delta P_{s,t}$ and $\Delta R_{s,t}$ are functions of independent variables $U_{i,t}$, $P_{i,t}$, and $R_{i,t}$. These functions are directly related to every outage event. If any of the four variables, $p_{s,t}$, $b_{s,t}$, $\Delta P_{s,t}$ and $\Delta R_{s,t}$, are kept in the formulation of $EENS_t$, $EENS_t$ cannot be greatly simplified since it is still directly related to every possible outage event and the combinatorial nature still exists. However, SSR_t has no relationship with outage events. It can be concluded that if $EENS_t$ can be analytically expressed as a function of SSR_t only, the formulation of $EENS_t$ can be greatly simplified.

2.3.2 Piecewise Property of EENS Curve

When $EENS_t$ is formulated as a function of SSR_t, extreme turning points occur on the $EENS_t(SSR_t)$ curve. An extreme turning point occurs at the place where the rate of change in $EENS_t$ has a drastic decrease when SSR_t increases. This phenomenon is illustrated by an example. Consider the IEEE-RTS [60, 61] as an example. If the hydro units are omitted, this system consists of 26 units with a total generation capacity of 3,105 MW. The quadratic approximation of the cost functions and ramp-up limits are taken from [60]. For more details of this test system, refer to appendix A.1. For simplicity only the first hour is considered in this subsection. VOLL is 1,000 $/MWh. The $EENS_t(SSR_t)$ curve of Fig. 2.1 is obtained by a sensitivity analysis. When SSR_t increases from zero to the maximum available value, the corresponding $EENS_t$ can be obtained for each fixed SSR_t by optimizing (2.1) using EENS of (2.9). In Fig. 2.1, two insets show the magnifications

of $EENS_t$ when SSR_t is larger than 400 MW and 800 MW. The variations of $EENS_t$ when SSR_t is around 400 MW and 800 MW in the first hour are shown in Fig. 2.2.

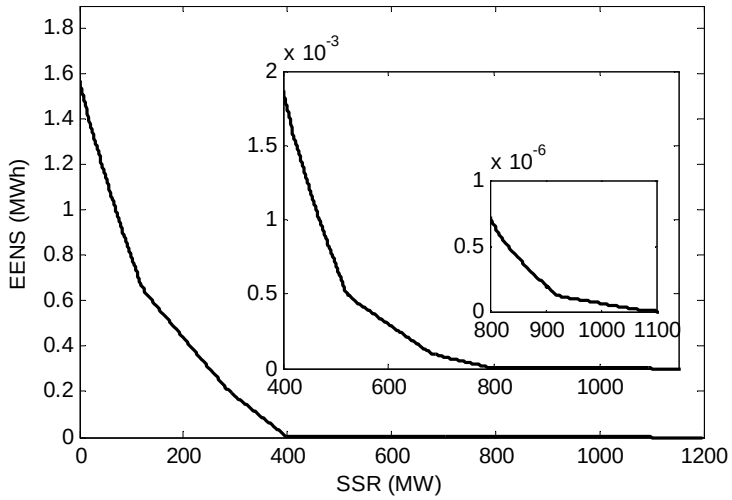

Fig. 2.1 Variation of EENS versus SSR in the first hour

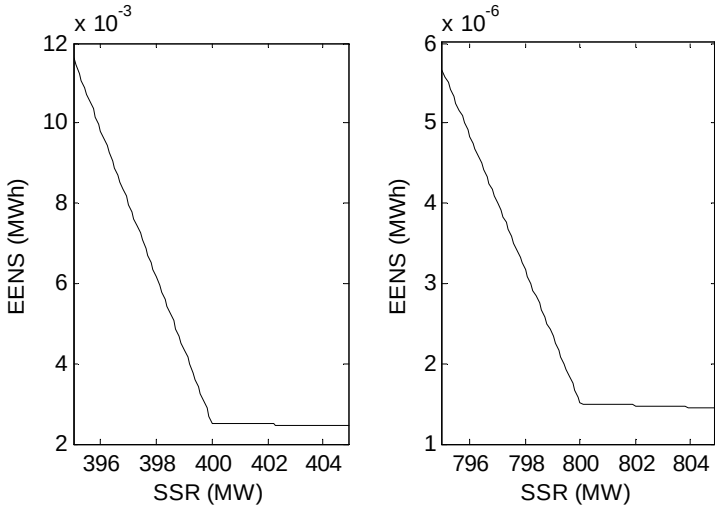

Fig. 2.2 Variations of EENS when SSR is around 400 MW and 800 MW

From Figs. 2.1 and 2.2, it can be concluded that $EENS_t$ decreases drastically when SSR_t increases initially. The rate of decrease in $EENS_t$ decreases as the SSR_t increases. From Fig. 2.2 one sees that the rate of decrease in $EENS_t$ decreases sharply when the SSR_t is

around 400 MW and 800 MW. For example, when the SSR_t increases from less than 400 MW to larger than 400 MW, the rate of decrease in $EENS_t$ changes from 1.821 to 0.0155. When the SSR_t increases from less than 800 MW to larger than 800 MW, the rate changes from 8.332×10^{-4} to 1.143×10^{-5}. Here 400 MW is equal to the largest committed capacity of a single unit. The committed capacity of a unit is equal to the output power plus the committed SR. Likewise, 800 MW is equal to the sum of the committed capacities of two largest units. When the SSR_t is smaller than 400 MW, $EENS_t$ is relatively large because $EENS_t$ is caused by some first order of outage events, and all second and higher orders of outage events. When the SSR_t becomes larger than 400 MW, the system is able to withstand any first order of outage events. The outage probabilities of the second and higher orders of outage events decrease several orders of magnitude compared with those of the first order of outage events. However the outage capacities caused by the second and higher orders of outage events increase linearly compared with those of the first order of outage events. Obviously the effect of decrease of outage probabilities on $EENS_t$ outperforms the effect of the increase of outage capacities. That is why the rate of decrease in $EENS_t$ drops sharply when the SSR_t is around 400 MW. A similar situation occurs when the SSR_t is around 800 MW. The existence of extreme turning points suggests that the relationship between $EENS_t$ and SSR_t should be modeled by a piecewise function.

To facilitate the integration of EENS in the UC problem, a linear model can be used. When the linear model is used, the complexity of the model can be greatly reduced. The approximation error caused by a linear model can be compensated by increasing the number of segments of the piecewise linear model. The EENS curve will be linearized starting from SSR at 0 MW to the leftmost extreme turning point and between any two successive extreme turning points. Then EENS of an optimization period can be modeled by a piecewise linear function of SSR of that period.

2.3.3 Formulating EENS as A Function of SSR

When the unit schedule is determined, calculating $EENS_t$ through state enumeration method by (2.6) or through COPT is essentially the same. But using COPT has some advantages over using enumeration method. For example, the COPT can be truncated when the cumulative probability is smaller than a predefined value; and rounding technique can be used in COPT. These advantages can greatly reduce the computation burden.

An event in (2.6) corresponds to an outage capacity line in COPT. If some outage events have the same outage capacity, their total effect corresponds to one outage capacity line. The sum of outage power and outage reserve, namely $\Delta P_{s,t}+\Delta R_{s,t}$ in (2.6), corresponds to the unit outage capacity in COPT. The variable $p_{s,t}$ in (2.6) corresponds to the outage probability in COPT. By comparing the two techniques, it can be found that the outage capacity, outage probability and number of outage capacity levels in COPT are the parameters of the EENS piecewise linear function which is shown in (2.17).

Based on the given unit schedule, COPT can be established and $EENS_t$ can be formulated from COPT as

$$EENS_t = \sum_{i=1}^{N(t)} \{ p_{i,t} b_{i,t} (\Delta C_{i,t} - SSR_t) \} \tag{2.17}$$

where

$N(t)$: number of unit outage capacity levels during period t;

$\Delta C_{i,t}$: amount of the ith unit outage capacity during period t;

$p_{i,t}$: probability of the ith outage capacity level during period t; and

$b_{i,t}$: a binary variable to represent whether loss of load occurs due to the ith unit outage capacity in COPT during period t. It satisfies

$$b_{i,t} = \begin{cases} 1 & if \ \Delta C_{i,t} - SSR_t > 0 \\ 0 & otherwise. \end{cases} \tag{2.18}$$

The parameters $N(t)$, $\Delta C_{i,t}$ and $p_{i,t}$ are all derived from COPT. The number of segments of the piecewise linear function $N(t)$ is equal to the number of outage capacity levels in COPT. From (2.17) one sees that $EENS_t$ has been formulated as a piecewise linear function of SSR_t only. Compared with (2.6) and (2.9), the formulation of EENS is greatly simplified and the computation efficiency is greatly improved. Equation (2.18) can be linearized [6, 20] to

$$\frac{\Delta C_{i,t} - SSR_t}{\sum_{i=1}^{N_G} P_i^{\max}} \le b_{i,t} \le 1 + \frac{\Delta C_{i,t} - SSR_t}{\sum_{i=1}^{N_G} P_i^{\max}} \tag{2.19}$$

Finally, EENS can be formulated as the summation of the products of some binary variables and a bounded continuous variable, which can be linearized [16, 62]. For more details of the expression of linearization refer to appendices A.4 and A.5. After EENS is linearized, the SR estimation problem becomes a piecewise linear function and a MILP can be used to solve it.

2.3.4 Cluster Property of EENS Curves

From the above subsection, one sees that $EENS_t$ can be formulated as a piecewise linear function of SSR_t based on a given unit schedule. However, the unit schedule $U_{i,t}$, $P_{i,t}$ and $R_{i,t}$ are unknown before optimization. If $U_{i,t}$, $P_{i,t}$ and $R_{i,t}$ take arbitrary values, $EENS_t$ may have a large variation.

As far as the above problem is concerned, the unit schedule parameters $U_{i,t}$, $P_{i,t}$ and $R_{i,t}$ are constrained to a small feasible region because they must satisfy the power balance constraint, SR constraint, and unit operating constraints. Besides, the total cost which is a function of $U_{i,t}$, $P_{i,t}$ and $R_{i,t}$, needs to be minimized. When $U_{i,t}$, $P_{i,t}$ and $R_{i,t}$ vary in this feasible region, it can be found that the $EENS_t(SSR_t)$ curves have a cluster property.

Take the IEEE-RTS system as an example. For simplicity only the first hour is considered. Fig. 2.3 shows the $EENS_t(SSR_t)$ curves under different feasible unit schedules. These unit schedules are obtained based on a family of reserve constrained unit commitment (RCUC) solutions. The RCUC in which SSR must satisfy the SR requirement is only used in this subsection. The purpose of introducing a family of RCUC solutions is to produce a series of representative unit schedules. Then $EENS_t(SSR_t)$ curves can be plotted and analyzed based on these unit schedules. The objective function of RCUC is

$$\min \{\sum_{t=1}^{N_T}\sum_{i=1}^{N_G}[C_{i,t}(P_{i,t},U_{i,t})+K_i\cdot SC_{i,t}]+\sum_{t=1}^{N_T}\sum_{i=1}^{N_G}q_{i,t}R_{i,t}\} \tag{2.20}$$

Equation (2.20) is the same as the first and second terms of (2.1). The objective function must be minimized subject to constraints (2.2)-(2.5). Besides, the following constraint should also be satisfied in the RCUC problem.

$$SSR_t \geq R_t^{RCUC} \tag{2.21}$$

where R_t^{RCUC} is the predefined SR requirement during period *t* in the RCUC problem.

Fig. 2.3 is obtained using the following procedure:

1) Specify the SR requirement R_t^{RCUC} to be enforced. At the beginning, R_t^{RCUC} is zero.
2) Perform RCUC and the unit schedule can be obtained. If RCUC is feasible, go to step 3. Otherwise, R_t^{RCUC} exceeds the maximum reserve supported by the system and the iterative process aborts.
3) Calculate $N(t)$, $\Delta C_{i,t}$ and $p_{i,t}$ using COPT based on the unit schedule obtained in step 2. Plot $EENS_t$ by varying SSR_t via (2.17).
4) Increase R_t^{RCUC} and go to step 2 above.

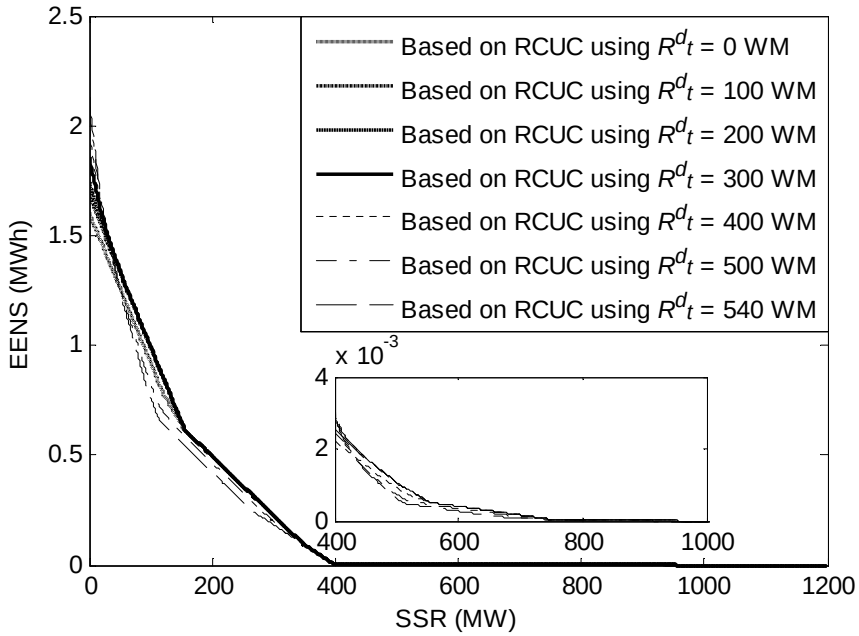

Fig. 2.3 $EENS_t(SSR_t)$ curves under different feasible unit schedules

In Fig. 2.3 the maximum R_t^{RCUC} is 540 MW. When R_t^{RCUC} is larger than 540 MW, the RCUC becomes infeasible. For clarity the inset shows the magnification of $EENS_t$ when the SSR_t increases from 400 MW to 1000 MW. From Fig. 2.3 one sees that $EENS_t$ is sensitive to SSR_t. When SSR_t increases from 0 MW to 1,000 MW, $EENS_t$ decreases several orders of magnitude. However, $EENS_t$ is not so sensitive to the variation of unit schedules. For a fixed SSR_t, $EENS_t$ does not change too much. i.e., $EENS_t$ varies within a narrow band as seen in Fig. 2.3. Thus, the $EENS_t(SSR_t)$ curves under different feasible unit schedules have a cluster property.

It should be noted that when plotting the $EENS_t(SSR_t)$ curves via (2.17) in step three above, SSR_t is seen as the independent variable and all other constraints in the optimization is relaxed during this step. So the $EENS_t(SSR_t)$ curves shown in Fig. 2.3 are relaxed curves. The feasible $EENS_t(SSR_t)$ of the whole optimization model belongs to a subset of the plotted curves of Fig. 2.3. From Fig. 2.3 one sees that even the relaxed

$EENS_t(SSR_t)$ curves satisfy the cluster property. As a subset of the plotted curves, the feasible $EENS_t(SSR_t)$ should also satisfy the cluster property.

The $EENS_t(SSR_t)$ curve which corresponds to the optimal unit schedule also belongs to the cluster curves. Hence it is logical to formulate $EENS_t$ as a function of SSR_t only based on a feasible unit schedule.

2.4 Summary

In this chapter, the mathematical model of SR estimation using the cost/benefit analysis is introduced. EENS is formulated explicitly using UC variables such as unit status and output power. From the formulation of EENS, it can be found that the calculation of EENS is computation intensive since it is highly nonlinear and exhibits combinatorial characteristics.

An approximated EENS function is proposed. In this chapter the following questions are answered. What are the best input variables of the EENS function? What is the best mathematical model of the EENS function? How to determine the parameters of the EENS function? Why the proposed approximated EENS function can be used?

EENS is formulated as a function of SSR only because SSR is not related to any specific contingency events. The piecewise linear model is used since the EENS curve has a strong piecewise property. When the linear model is used, the complexity of the model can be greatly reduced. The approximation error caused by the linear model can be compensated by increasing the number of segments of the piecewise linear model. The parameters of the piecewise linear function are by-products of COPT. Finally it can be found that EENS does not change too much for a fixed SSR when the unit schedule varies in the feasible region. So it can be concluded that it is reasonable to model EENS as a piecewise linear function of SSR only.

Chapter 3
SR Estimation in Large Traditional Power Systems

3.1 Proposed Multi-Step Method

From chapter two, it can be found that EENS for each optimization period can be formulated as a piecewise linear function which is shown in (2.17). However, when this piecewise linear function is used in the model, two problems occur. First, a feasible unit schedule must be known before the optimization can proceed. Second, even though the cluster property exists, EENS calculated using (2.17) may have some approximation errors. Accordingly, a multi-step method is proposed in this chapter. A feasible unit schedule is produced using a base UC module in step one and the approximation error of EENS is gradually eliminated in the following steps.

In the first step, a base UC module without reserve constraint is used to produce a feasible unit schedule. Then for each optimization step, a COPT is established. In the second step, EENS for each optimization period is formulated as a piecewise linear function of SSR only via (2.17). Then (2.1) is optimized and a new unit schedule can be obtained. After optimization a convergence criterion is introduced:

$$\Delta EENS = \max_t \{ \frac{\left| EENS_t^{druing} - EENS_t^{after} \right|}{EENS_t^{after}} \} \le \varepsilon \tag{3.1}$$

where

$\Delta EENS$: normalized relative EENS error;

$EENS_t^{during}$: *EENS* of period *t* calculated during optimization via (2.17);

$EENS_t^{after}$: *EENS* of period *t* calculated after optimization via COPT based on the optimization results; and

ε : convergence tolerance.

The convergence criterion guarantees that the EENS approximation error introduced by the multi-step method is within a certain accuracy. If (3.1) is satisfied, the optimal SR requirement is obtained and the optimization will stop. Otherwise, the EENS formulation is updated based on the COPT formed using the newly found unit schedule. A new step will be implemented till (3.1) is satisfied.

The proposed multi-step method replaces the nonlinear and combinatorial EENS formulation by a piecewise linear function. The accuracy can be guaranteed and the computation efficiency is greatly improved. The flowchart of the proposed multi-step method is shown in Fig. 3.1.

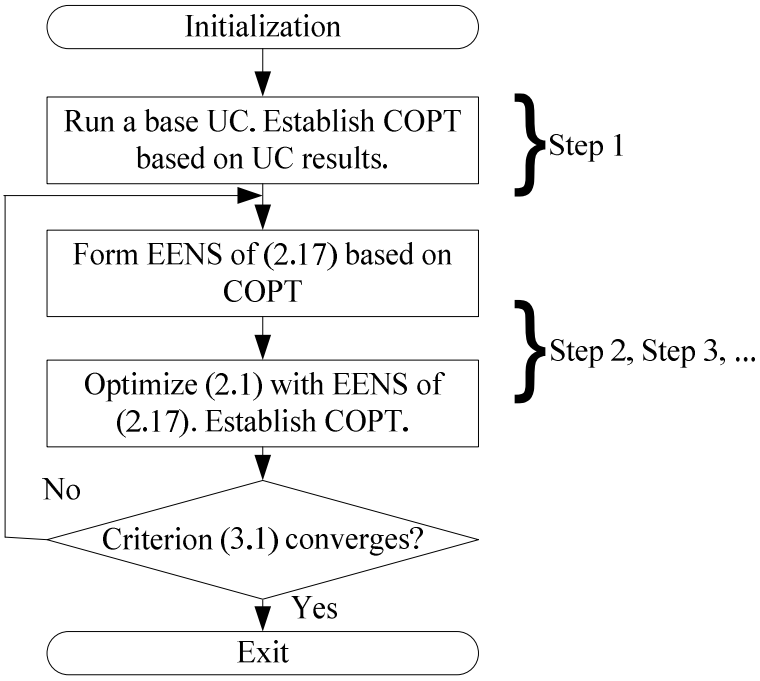

Fig. 3.1 Flowchart of the proposed multi-step method

3.2 Convergence of Multi-Step Method

In the proposed multi-step method, a base UC module without reserve constraint is implemented in step one. In step two, EIC is considered and the system committed capacity increases in the most economical way. The SR requirement is computed and the system operation becomes more reliable. In step three, the EENS curve is updated based on the unit schedule of step two. More units are scheduled and more capacity is committed for the scheduled units. The EENS curve used in step three moves slightly upward compared with that used in step two. A higher SR requirement is scheduled and the system reliability is further improved.

As the iteration continues, the sytem committed capacity gradually increases and the EENS curve moves monotonously and asymptotically close to the final curve due to the cluster property of the EENS curves. The variations of unit status and output power of two successive steps become smaller and smaller. The difference in EENS values of two successive steps becomes negligible. The proposed multi-step method will finally converge when creterion (3.1) is satisfied.

Take the IEEE-RTS system as an example and consider only the first hour. VOLL is 1,000 $/MWh. The convergence tolerance ε is 0.5% and the MILP duality gap is 0.01%. After step two $\Delta EENS$ is 4.07%. After step three $\Delta EENS$ is 0.0024% and the convergence criterion is satisfied. Unit status, output power and reserve in three different steps are shown in Table 3.1. The variations among different steps are shown in bold. The EENS curves formed using the unit schedule of each step are shown in Fig. 3.2.

Table 3.1 Unit status, output power and reserve in three different steps

Index of unit	Step 1			Step 2			Step 3		
	$U_{i,t}$	$P_{i,t}$ (MW)	$R_{i,t}$ (MW)	$U_{i,t}$	$P_{i,t}$ (MW)	$R_{i,t}$ (MW)	$U_{i,t}$	$P_{i,t}$ (MW)	$R_{i,t}$ (MW)
1-9	0	0	0	0	0	0	0	0	0
10	0	0	0	**1**	**53.7**	**19.25**	**1**	**31.3**	**19.25**
11	0	0	0	0	0	0	0	0	0
12	0	0	0	0	0	0	**1**	**15.2**	**19.25**
13	0	0	0	0	0	0	0	0	0
14-16	0	0	0	0	0	0	0	0	0
17	1	**121.42**	**0**	1	**127.5**	**27.5**	1	**127.5**	**27.5**
18	1	**121.42**	**0**	1	**127.5**	**27.5**	1	**127.5**	**27.5**
19	1	**152.16**	**0**	1	**127.5**	**27.5**	1	**127.5**	**27.5**
20	1	**155**	**0**	1	**127.5**	**27.5**	1	**127.5**	**27.5**
21-23	0	0	0	0	0	0	0	0	0
24	1	**350**	**0**	1	**336.3**	**13.7**	1	**343.5**	**6.5**
25	1	400	0	1	400	0	1	400	0
26	1	400	0	1	400	0	1	400	0

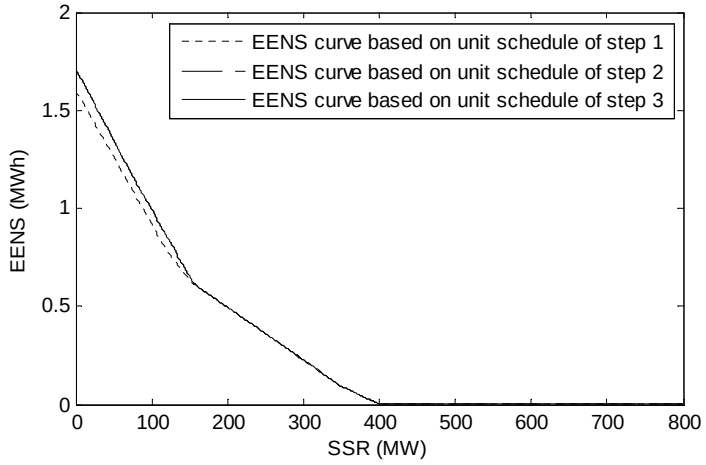

Fig. 3.2 EENS curves formed using unit schedule of each step

In step one, a base UC module without the reserve constriant is implemented. No reserve is scheduled. The unit committed capacity is defined as the output power plus reserve and the sum of output power is always equal to the system load value. So in step one the committed capacity is 1700 + 0, namely 1700 MW. In step two, one more unit, unit 10, is

scheduled. The SSR is 142.95 MW and the committed capacity is 1700 + 142.95, namely 1842.95 MW. In step three, unit 12 is scheduled. The SSR is 155 MW and the committed capacity is 1855 MW. It can be found that the committed capacity gradually increases but the increment decreases.

Based on the unit schedule of step one, an EENS curve is formed and this EENS formulation is used in step two. After step two, the committed capacity increases but it does not increase too much. For a fixed SSR, EENS calculated based on the unit schedule of step two does not increase very much compared with the EENS calculated based on the unit schedule of step one. This corresponds to the EENS curve formed using the unit schedule of step two. The curve moves slightly upwards compared with the EENS curve formed using the unit schedule of step one. Similarly after step three the EENS curve still moves upwards but with a smaller increment. In Fig. 3.2, the EENS curves based on the unit schedules of step two and step three overlap each other. In the following steps, EENS curves will not shift anymore and the following steps will not be implemented as they are not necessary.

3.3 Accuracy of Multi-Step Method

The accuracy of the proposed multi-step method depends on whether the piecewise linear formulation of EENS can model the real EENS curve exactly. When criterion (3.1) is satisfied, the EENS caluclated using (2.17) during optimization is approximately the same as that calculated using COPT after optimization. This means that the accuracy of the approximation is guaranteed.

Take the IEEE-RTS system as an example and only the first hour is considered. VOLL is 1,000 $/MWh. The convergence tolerance ε is 0.5% and the MILP duality gap is 0.01%. The results obtained by the proposed multi-step method and the results obtained by optimizing (2.1) with EENS of (2.9) are shown in Table 3.2. When the multi-step method

is implemented, three steps are needed. The value of $\Delta EENS$ in steps two and three are 4.07% and 0.02% respectively. As the iteration proceeds, more SR is scheduled. Finally the solution converges at step three and the SR meets the optimal SR requirement. The SR requirement and various costs obtained by the multi-step method are approximately the same as those obtained by minimizing (2.1) using EENS of (2.9).

Table 3.2: SR requirement, SC, EIC and TC obtained by multi-step method and by optimizing (2.1) with EENS of (2.9)

	Results of minimizing (2.1) with EENS (2.9)	Results of step 1 in multi-step method	Results of step 2 in multi-step method	Results of step 3 in multi-step method
Optimal SR (MW)	155.00	0.00	142.95	155.00
SC ($)	18,677.05	18,242.93	18,601.05	18,678.48
EIC ($)	618.12	0.00	671.86	618.11
TC ($)	19,295.17	18,242.93	19,272.91	19,296.58

When VOLL is extremely large, say 10,000 $/MWh, the EENS obtained using the multi-step method is somewhat overestimated compared with that obtained by optimizing (2.1) using EENS (2.9). However, the SC obtained by the multi-step method is smaller than that obtained by optimizing (2.1) using EENS of (2.9). The increase of EIC is mainly compensated by the decrease of SC and the total cost computed by the multi-step method is only slightly larger. The small error, about 2.1% in this case, occurs because $EENS_t$ is formulated as a function of SSR_t only. The direct interaction between $EENS_t$ and $U_{i,t}$, $P_{i,t}$ in the EENS formulation is neglected. This error is the price one pays for using an approximated EENS formulation which greatly improves the computation efficiency. In normal system operation, an extremely large VOLL is seldom used though.

3.4 Case Studies and Discussion of Simulation Results

The proposed multi-step method is tested using the IEEE-RTS system without the hydro generation. This system consists of 26 units and 24 hours are considered. The UC data

and ramp rate limits were obtained from [61], and the startup costs and reliability data were obtained from [60]. The power generated by the units committed at $t = 0$ is given by the economic dispatch of the committed units for the first hour at a load level of 1,700 MW. The system lead time is 1 hour. For simplicity, it is assumed that all generating units offer SR at prices equal to 10% of their highest incremental cost of energy production. COPT is truncated by omitting the MW outage levels in which the cumulative probabilities are less than 10^{-10}. The outage capacity levels are rounded to a fixed rounding increment [12] of 1 MW. VOLL is 1,000 $/MWh. The convergence tolerance ε is 0.5% and the MILP duality gap is 0.01%.

3.4.1 Simulation Results

After the third step, the convergence criterion is satisfied and the optimization procedure stops. The value of $\Delta EENS$ in steps two and three are 8.22% and 0.02% respectively. The SR requirement of steps two and three are shown in Fig. 3.3. The itemization of cost and EENS of each step is shown in Table 3.3. The unit output power and reserve are shown in Tables 3.4 and 3.5. It should be noted that units 3-9 and 23 are not dispatched during the entire optimization period. Their output power and reserve are all zero and they are not shown in the two tables. From Fig. 3.3 and Table 3.3 it can be found that in step two, an approximated solution is determined. In step three, the solution is improved and finally the optimal solution is obtained.

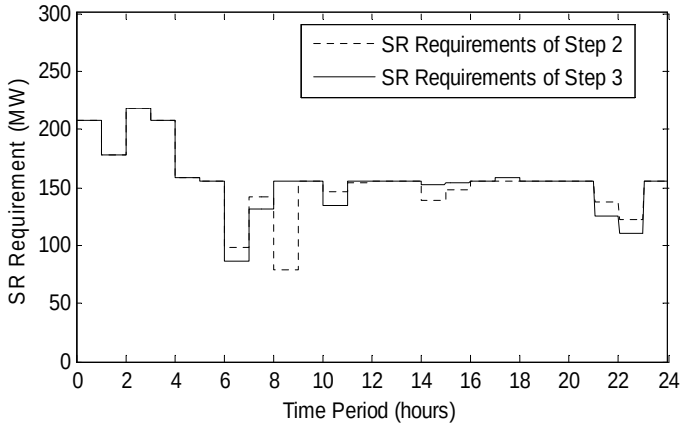

Fig. 3.3 SR requirement of every hour

Table 3.3 Itemization of cost and EENS

	Step 1	Step 2	Step 3
Operating cost ($)	715,799.87	723,838.97	723,856.44
SR cost ($)	0	7,004.53	7,012.51
SC ($)	0	730,843.5	730,868.95
EIC ($)	0	16,064.59	16,201.31
Total Cost ($)	715,799.87	746,908.09	747,070.26
$EENS^1$ (MWh)	0	15.8716	15.8513
$EENS^2$ (MWh)	0	0.3487	0.3485
$EENS^3$ (MWh)	0	0.0000	0.0000

3.4.2 Discussion of Simulation Results

◆ **Effect of ORR**

In order to analyze the effect of unit ORR, several sets of ORR values were created by multiplying the original ORR value by the factors of 0.5, 1 and 2.0. Fig. 3.4 shows how the SR requirement varies under different ORR values. As expected, the SR requirement increases with the ORR of the generating units. This is because with the increase of ORR, the outage probabilities of various outage orders increase, EENS increases and the optimization tends to schedule more SR. Conversely, when the units in the system are more reliable, the SR requirement is lower.

Table 3.4 Unit output power (MW) of every optimization period

t \ *i*	1	2	3	10	11	12	13	14	15	16	17	18	19	20	21	22	24	25	26
1	0	0	0	15.2	15.2	15.2	15.2	0	0	0	127.5	127.5	127.5	127.5	0	0	329.2	400	400
2	0	0	0	15.2	15.2	15.2	15.2	0	0	0	136.7	127.5	127.5	127.5	0	0	350	400	400
3	0	0	0	15.2	15.2	15.2	15.2	0	0	0	127.5	127.5	127.5	127.5	0	0	319.2	400	400
4	0	0	0	15.2	15.2	15.2	15.2	0	0	0	127.5	127.5	127.5	127.5	0	0	329.2	400	400
5	0	0	0	15.2	15.2	15.2	15.2	0	0	0	155	129.2	127.5	127.5	0	0	350	400	400
6	0	0	0	51.6	35.5	35.5	35.5	0	0	0	155	132	127.5	127.5	0	0	350	400	400
7	2.4	0	0	57.4	56.8	56.8	56.8	0	0	0	155	155	155	155	0	0	350	400	400
8	2.4	2.4	2.4	76	76	76	76	75	75	75	155	155	155	155	123.8	0	350	400	400
9	2.4	2.4	2.4	76	76	76	76	75	75	75	155	155	155	155	122.2	111.6	350	400	400
10	2.4	2.4	2.4	76	76	76	76	78.8	75	75	155	155	155	155	154.3	135.7	350	400	400
11	2.4	2.4	2.4	76	76	76	76	99.8	75	75	155	155	155	155	169.5	169.5	350	400	400
12	2.4	2.4	2.4	76	76	76	76	78.8	75	75	155	155	155	155	154.3	125.7	350	400	400
13	2.4	2.4	2.4	76	76	76	76	78.8	75	75	155	155	155	155	154.3	125.7	350	400	400
14	2.4	2.4	2.4	76	76	76	76	78.8	75	75	155	155	155	155	128.4	111.6	350	400	400
15	2.4	2.4	2.4	76	76	76	76	80.2	75	75	155	155	155	155	154.3	154.3	350	400	400
16	2.4	2.4	2.4	76	76	76	76	79.8	75	75	155	155	155	155	169.5	169.5	350	400	400
17	2.4	2.4	2.4	76	76	76	76	78.8	75	75	155	155	155	155	128.4	111.6	350	400	400
18	2.4	2.4	2.4	76	76	76	76	75.5	75	75	155	155	155	155	111.6	111.6	350	400	400
19	2.4	2.4	2.4	76	76	76	76	78.8	75	75	155	155	155	155	111.6	78.4	350	400	400
20	2.4	2.4	2.4	76	76	76	76	78.8	75	75	155	155	155	155	128.4	111.6	350	400	400
21	2.4	2.4	2.4	76	76	76	76	75	75	75	155	155	155	155	154.3	139.5	350	400	400
22	2.4	2.4	2.4	76	76	76	76	80.9	75	75	155	155	155	155	168	0	350	400	400
23	2.4	2.4	2.4	76	76	65.1	56.8	74.5	74.5	0	155	155	155	155	0	0	350	400	400
24	0	0	0	55.8	55.7	55.7	0	0	0	0	140.3	127.5	127.5	127.5	0	0	350	400	400

Table 3.5 Unit reserve (MW) of every optimization period

t \ *i*	1	2	3	10	11	12	13	14	15	16	17	18	19	20	21	22	24	25	26
1	0	0	0	19.3	19.3	19.3	19.3	0	0	0	27.5	27.5	27.5	27.5	0	0	20.8	0	0
2	0	0	0	19.3	19.3	19.3	19.3	0	0	0	18.3	27.5	27.5	27.5	0	0	0	0	0
3	0	0	0	19.3	19.3	19.3	19.3	0	0	0	27.5	27.5	27.5	27.5	0	0	30.8	0	0
4	0	0	0	19.3	19.3	19.3	19.3	0	0	0	27.5	27.5	27.5	27.5	0	0	20.8	0	0
5	0	0	0	19.3	19.3	19.3	19.3	0	0	0	0	25.8	27.5	27.5	0	0	0	0	0
6	0	0	0	19.3	19.3	19.3	19.3	0	0	0	0	23	27.5	27.5	0	0	0	0	0
7	9.6	0	0	18.7	19.3	19.3	19.3	0	0	0	0	0	0	0	0	0	0	0	0
8	9.6	9.6	9.6	0	0	0	0	25	25	25	0	0	0	0	27.5	0	0	0	0
9	9.6	9.6	5.8	0	0	0	0	25	25	25	0	0	0	0	27.5	27.5	0	0	0
10	9.6	9.6	9.6	0	0	0	0	21.2	25	25	0	0	0	0	27.5	27.5	0	0	0
11	9.6	9.6	9.6	0	0	0	0	0.21	25	25	0	0	0	0	27.5	27.5	0	0	0
12	9.6	9.6	9.6	0	0	0	0	21.2	25	25	0	0	0	0	27.5	27.5	0	0	0
13	9.6	9.6	9.6	0	0	0	0	21.2	25	25	0	0	0	0	27.5	27.5	0	0	0
14	9.6	9.6	9.6	0	0	0	0	21.2	25	25	0	0	0	0	27.5	27.5	0	0	0
15	9.6	9.6	8	0	0	0	0	19.9	25	25	0	0	0	0	27.5	27.5	0	0	0
16	9.6	9.6	9.6	0	0	0	0	20.2	25	25	0	0	0	0	27.5	27.5	0	0	0
17	9.6	9.6	9.6	0	0	0	0	21.2	25	25	0	0	0	0	27.5	27.5	0	0	0
18	9.6	9.6	9.6	0	0	0	0	24.5	25	25	0	0	0	0	27.5	27.5	0	0	0
19	9.6	9.6	9.6	0	0	0	0	21.2	25	25	0	0	0	0	27.5	27.5	0	0	0
20	9.6	9.6	9.6	0	0	0	0	21.2	25	25	0	0	0	0	27.5	27.5	0	0	0
21	9.6	9.6	5.8	0	0	0	0	25	25	25	0	0	0	0	27.5	27.5	0	0	0
22	9.6	9.6	9.6	0	0	0	0	19.2	25	25	0	0	0	0	27.5	0	0	0	0
23	9.6	9.6	9.6	0	0	11	19.3	25.5	25.5	0	0	0	0	0	0	0	0	0	0
24	0	0	0	19.3	19.3	19.3	0	0	0	0	14.75	27.5	27.5	27.5	0	0	0	0	0

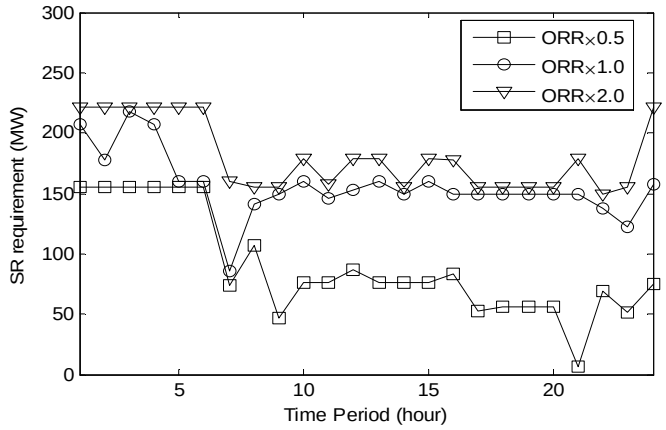

Fig. 3.4 SR requirement under different ORR

◆ **Effect of Ramp rates**

From (2.4) it can be found that the value of ramp rate has an important effect on the SR assignment. In order to illustrate its effect, the value of ramp rate is scaled by the factors of 0.5 and 1.5. Fig. 3.5 shows how the SR requirement varies under different ramp rate values. As ramp rate increases, the system deploys more SR resources that can be scheduled and the optimal SR tends to increase. Similarly, when the ramp rate decreases, the optimal SR tends to decrease.

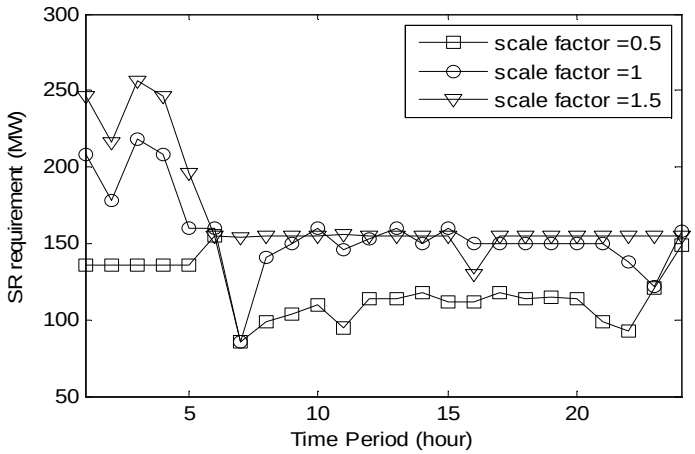

Fig. 3.5 SR requirement under different ramp rates

◆ **Effect of VOLL**

VOLL plays a very important role in the estimation of SR. A time-dependent VOLL could also be used and it can be incorporated easily in the model. Fig. 3.6 shows how the SR requirement varies under different VOLLs. As VOLL increases, the trade-off balance between SC and EIC tends to make the system more reliable and more SR is scheduled. For the 26-unit system, when VOLL increases from 1,000 $/MWh to 10,000 $/MWh, the optimal SR increases to 400 MW. This is equal to the capacity of the largest online unit. It can be concluded that setting the SR amount as the capacity of the largest online unit is relatively conservative for the 26-unit system.

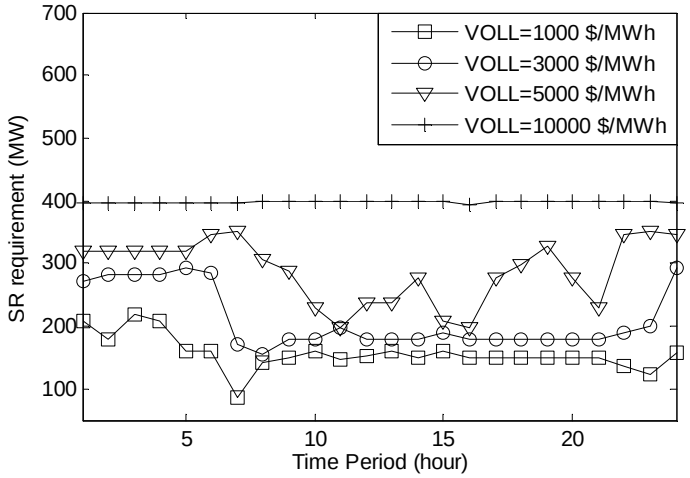

Fig. 3.6 SR requirement under different VOLL

◆ **Effect of system size**

In order to illustrate the effect of system size, systems with similar characteristics but different sizes were created by duplicating the IEEE-RTS and by proportionally scaling the load profile. Three larger systems with 3, 5 and 10 times the number of units in the base system were created. The rounding increment is 10 MW. The convergence tolerance is 0.5% and duality gap is 0.1%. Table 3.6 gives the itemization of cost and EENS for systems with different sizes. Fig. 3.7 shows how the SR requirements vary under different

system sizes when VOLL is 1,000 $/MWh. Fig. 3.8 shows how the SR requirements vary under different system sizes when VOLL is 5,000 $/MWh. As expected, for larger power systems, more SR is needed. When VOLL is 1,000 $/MWh and with the increase of system size, the SR requirement becomes independent of the system size. The optimal SR is around 400 MW, which is equal to the value that is determined by the deterministic approach. When VOLL becomes larger, such as 5,000 $/MWh, and for systems with a small number of units, the SR requirement is around 400 MW, which is equal to the value determined by the deterministic approach. For systems with a larger number of units, the SR requirement increases somewhat as the system size increases.

Table 3.6 Itemization of cost and EENS for systems with different sizes

	26 units	78 units	130 units	260 units
Operating cost ($)	723,856.44	2,160,283.64	3,586,823.09	7,146,910.68
SR cost ($)	7,012.51	16,536.95	19,174.48	20,557.20
SC ($)	730,868.95	2,176,820.59	3,605,997.57	7,167,467.88
EIC ($)	16,201.31	7,221.36	3,035.35	7,325.58
Total Cost ($)	747,070.26	2,184,041.95	3,609,032.92	7,174,793.46
EENS (MWh)	16.2013	6.7182	3.0393	7.3256

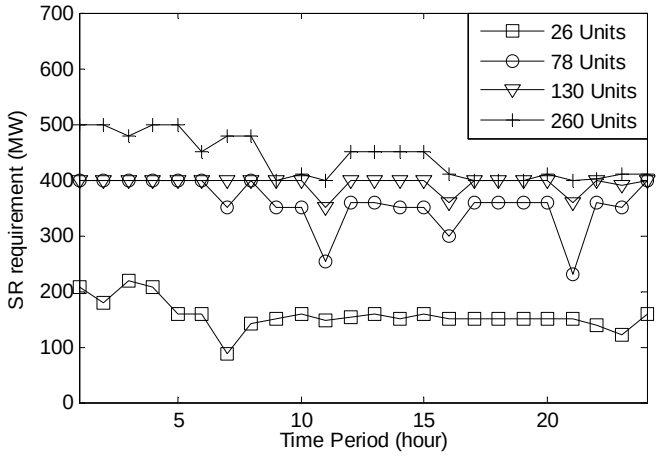

Fig. 3.7 SR requirements under different system sizes when VOLL is 1,000 $/MWh

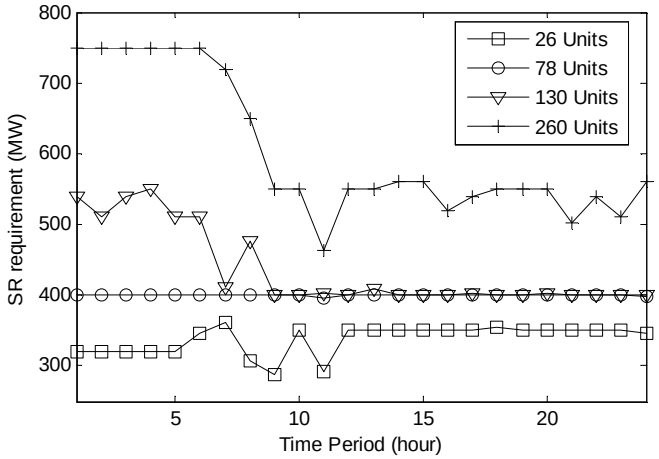

Fig. 3.8 SR requirements under different system sizes when VOLL is 5,000 $/MWh

◆ **Effect of load levels**

In order to demonstrate how the SR varies under different load levels, IEEE-RTS is used as an example and only the first hour is considered. VOLL is 1,000 $/MWh. Figs. 3.9 and 3.10 show how the optimal SR requirements vary under the normalized load levels and system sizes. As expected, when the load level increases, the SR requirement increases. The variations of these two figures are very similar to those in [26].

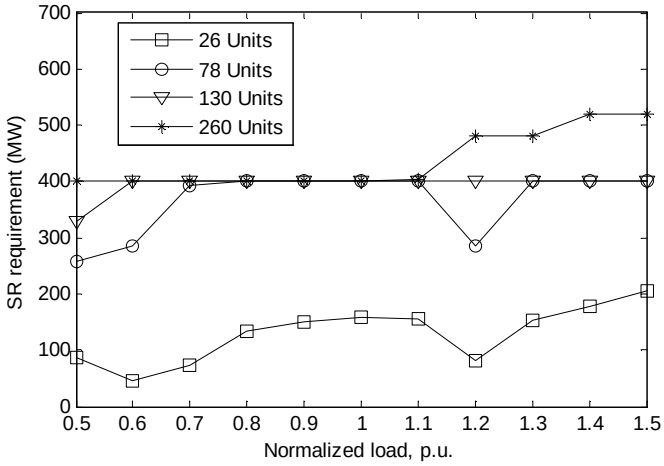

Fig. 3.9 SR requirements under different load levels when VOLL is 1,000 $/MWh

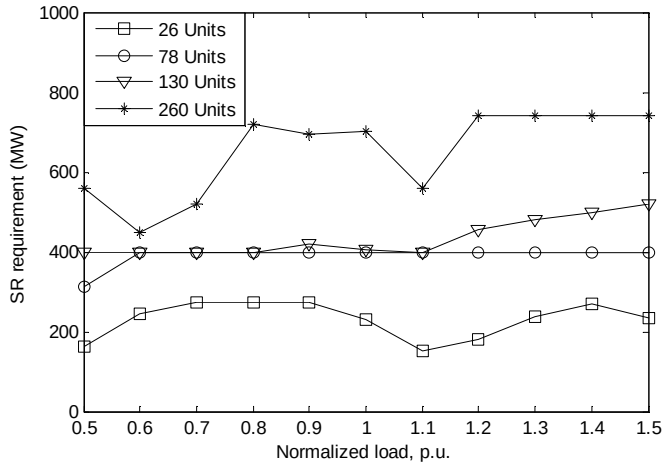

Fig. 3.10 SR requirements under different load levels when VOLL is 5,000 $/MWh

◆ **Computation Time**

From the above case studies it can be found that due to the cluster property of EENS, an approximated EENS can be achieved in the second step. The unit status and output power have been determined roughly. After step two, the status and output power only need a little adjustment to satisfy the accuracy requirement. Usually three or four steps are all it takes for the solution to converge.

Compared with the base UC module, a piecewise linear EENS of (2.17) is added in the objective function in the second and subsequent steps. Only $N(t)$ binary variables are introduced in (2.17) for each optimization period. These binary variables are related to SSR only and it has no relationship with unit commitment variables such as unit status and output power. The computation time does not increase too much compared with that of the base UC module.

The total required computation time of the multi-step method is related to the maximum acceptable MILP duality gap, convergence tolerance, rounding increment of COPT, VOLL, system size, load condition and types of generators. Relaxing the MILP duality gap, convergence tolerance or COPT resolution can reduce the computation time at the

expense of accuracy. In order to illustrate effect of the system size on computation time, systems with similar characteristics but 3, 5 and 10 times the number of units in the base system were used. For all these systems, 24 hours are considered. The rounding increment is 10 MW and VOLL is 1,000 $/MWh. The convergence tolerance is 0.5% and the MILP duality gap is 0.1%. Fig. 3.11 shows how the computation times as a function of the system size.

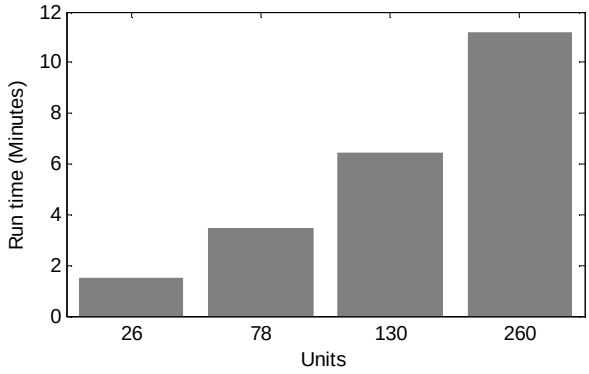

Fig. 3.11 Computation times as a function of system size

Fig. 3.10 shows that with the increase of the system size, the computation time tends to increase. However, as the highly nonlinear and combinatorial characteristics of the problem have been extracted and replaced by a piecewise linear model, the increase of the computation time is nearly linear rather than exponential with the increase of system size. High orders of outage events are all considered in the proposed multi-step method and the proposed method is not time consuming. For the 26-unit IEEE-RTS system, if the SR requirement is determined by minimizing (2.1) using EENS of (2.9) rather than the proposed multi-step method, the system will run out of the memory even only the first hour is considered. This is because too many binary variables are introduced.

The model is coded in GAMS [63] and solved using a large-scale MILP solver CPLEX 11.2 combined with Visual C. The CPU solution time was recorded on a Windows-based server with 2.6-GHz processor and 3.3 G bytes of RAM.

CPLEX is an optimization software package. It can solve integer programming problems, and very large linear programming problems using primal, dual variants of the simplex method or the barrier interior point method, as well as convex quadratic programming problems, and convex quadratically constrained programming problems [64]. Until the release of CPLEX, no mixed-integer programming solver had the power to handle real-world UC problems effectively.

The SR estimation problem is solved by MILP. MILP has many advantages [65-69]. The formulation of MILP is straightforward and it has enhanced modeling capability and adaptability. MILP can make developers focus on problem definition rather than algorithmic development. When the configurations of the model are changed or upgraded, such as new constraints are involved, no significant efforts are needed to change the algorithm. MILP can yield a more accurate measure of optimality. It could guarantee a solution that is globally optimal or one within an acceptable tolerance. The disadvantage of the MILP approach is its computational complexity. However the MILP technique has experienced rapid development in the last decade because of improvements in the linear programming solver and the incorporation of cutting plane techniques in the branch-and-bound algorithm.

3.5 Summary

In this chapter, a multi-step method is proposed to solve the SR estimation problem in large traditional power systems. In the first step, a base UC module without SR constraint is implemented to produce an initial unit schedule. Then COPT is established based on the unit schedule for each optimization period. In step two, a piecewise linear EENS model is formed based on the COPT obtained in step one. The EENS formulation is used in the model for the optimization. If the convergence criterion is satisfied, the optimization will stop. Otherwise the EENS formulation is updated based on the newly found optimization results and a new step is needed.

The convergence and accuracy problems have been discussed. The EENS curve used in the optimization gradually shifts close to the final actual curve. When VOLL varies in the feasible region, the accuracy of the proposed method is desirable. The convergence and accuracy problems are demonstrated using the IEEE-RTS system.

The proposed multi-step method is illustrated using the IEEE-RTS system and several larger systems. The simulation results are presented. A series of sensitivity analyses are implemented. The effects of ORR, VOLL, load level and system size are exhaustively studied. Several aspects which can affect the computation time are also discussed. The proposed multi-step method can obtain accurate results in a desirable time interval.

Chapter 4
SR Estimation in Microgrids

4. 1 Probabilistic Load, WTG and PV Models

Various intermittent energy sources such as WTGs and PVs exist in microgrids. Their outputs are uncertain and usually not controllable. Time varying load in microgrids is usually determined by an approach based on forecasting techniques. The uncertainties introduced by forecasting errors are significant in microgrids compared with those in large traditional power systems. These uncertainties must be considered when optimizing SR in microgrids. The load, WTG, and PV uncertainties are represented by probability distribution models in this thesis. The probabilistic load, WTG, and PV models are introduced below.

4.1.1 Probabilistic Load Model

The load forecasting model in a microgrid can be derived from historical data. Similar to large power systems, a normal distribution is used to represent the load forecast uncertainty. To simplify the calculation, a seven-step distribution model (0, $\pm1\delta$, $\pm2\delta$, $\pm3\delta$) is often used [12], where δ is the standard deviation. Such a model is considered sufficient since it encompasses more than 99% of the load uncertainty distribution. Because the smoothing effect of system load is reduced and the uncertainty is increased due to smaller load in microgrids, a relatively larger standard deviation must be used. The distribution model of load forecast errors is shown in Fig. 4.1.

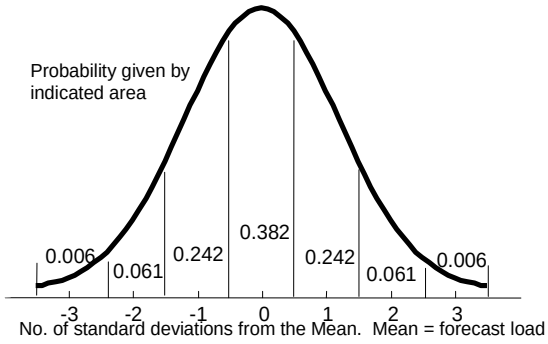

Fig. 4.1 Seven-step approximation of the normal distribution

4.1.2 Probabilistic WTG Model

In microgrids WTG and PV units are normally operated based on the maximum power tracking concept to extract the maximum possible power from these primary energy sources. They are seen as non-dispatchable units. WTG output power varies according to the wind speed conditions. The wind speed variations over the period can be described by a probability distribution function. Prior research [70-74] has shown that the wind speed profile at a given location closely follows a Weibull distribution over time.

The probability density function (PDF) for a Weibull distribution is given by

$$f(v) = \left(\frac{k}{c}\right)\left(\frac{v}{c}\right)^{(k-1)} e^{-\left(\frac{v}{c}\right)^k}, \qquad 0 < v < \infty \tag{4.1}$$

where

v: wind speed (m/s or miles/hour);

k: shape factor (dimensionless); and

c: scale factor (it shares the unit of wind speed).

The Weibull cumulative distribution function (CDF) is

$$F(v) = \int_0^v f(\tau) d\tau = 1 - e^{-\left(\frac{v}{c}\right)^k} \tag{4.2}$$

Most wind sites would have the scale parameter ranging from 10 to 20 miles per hour (mph) and the shape parameter ranging from 1.5 to 2.5 [71]. Some typical Weibull PDFs of wind speed are shown in Fig. 4.2. For greater values of *c*, the curves shift right to the higher wind speeds. As the value of *k* decreases from 2.5 to 1.5, the shapes shift from bell to flatter shapes. Many methods can be used to forecast the wind speed [75, 76] and estimate the Weibull distribution parameters [74]. Because the focus of this thesis is on reserve estimation and not on forecasting, the wind speed profile and the corresponding Weibull distribution parameters are assumed known for each period.

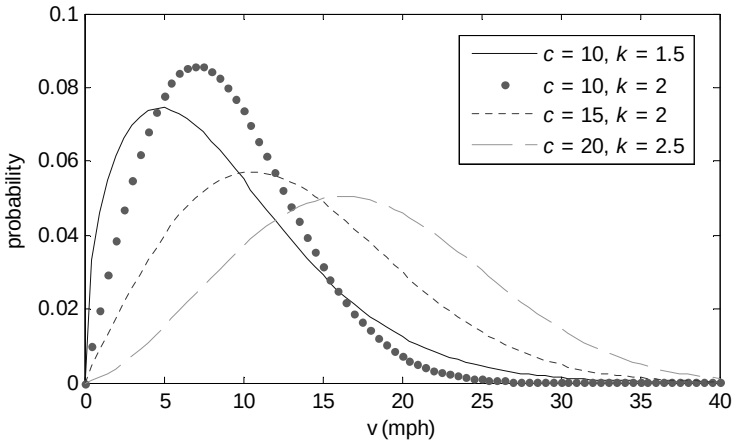

Fig. 4.2 Some Weibull PDFs of wind speed

For computational simplicity, the forecast probability distribution of wind speed will be truncated and discretized. Firstly at each period the random wind speed is normalized by the forecast wind speed which is used as the mean of the probability distribution v_{mean}. For the Weibull distribution function, *c* and *k* are related to v_{mean}. They can be approximated by a Gamma function [71]:

$$v_{mean} = c \cdot Gamma\left(1+\frac{1}{k}\right) \tag{4.3}$$

So when the wind speed is normalized, (4.3) is independent of *c*. An appropriate truncated point can be selected to encompass the overwhelming majority of the

distribution. The truncated point could increase from v_{mean} in a fixed step until the desired precision is received. For the mostly used value $k = 2$, if $0.5 \cdot v_{mean}$ is used as the fixed step, the truncated point and the encompassed probability are shown in Table 4.1. From this table one can find that if the probability distribution is truncated at 2.5 times of v_{mean}, it encompasses more than 99% of the distribution.

Table 4.1 Truncated points and the encompassed probabilities

Truncated point	$1 \cdot v_{mean}$	$1.5 \cdot v_{mean}$	$2 \cdot v_{mean}$	$2.5 \cdot v_{mean}$	$3 \cdot v_{mean}$
Encompassed probability	54.40%	82.92%	95.68%	99.26%	99.91%

Like in the case of load, the truncated distribution can be divided into class intervals. The number of which depends upon the accuracy desired. A larger number of intervals increase the accuracy at the expense of computation burden. The probability of every interval can be easily calculated by integration. An indicative 5-interval wind speed distribution model is shown in Fig. 4.3. The probability of every interval is also given.

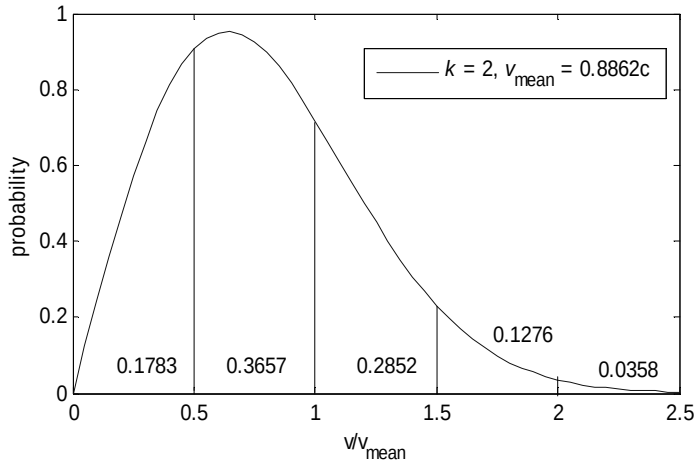

Fig. 4.3 An indicative wind speed distribution model

Given the forecast distribution of wind speed and the speed-to-power conversion function, the wind output power distribution can be obtained. In this thesis, a linear speed-to-power conversion function [72, 74, 77, 78] is used and it is shown in Fig. 4.4.

$$w = f^{WT}(v) = \begin{cases} 0, & for\ v < v_i\ and\ v > v_o \\ w_r \dfrac{(v - v_i)}{(v_r - v_i)}, & for\ v_i \le v \le v_r \\ w = w_r, & for\ v_r \le v \le v_o \end{cases} \tag{4.4}$$

where

f^{WT}: speed-to-power conversion function;

w: WTG output power (kW or MW);

w_r: WTG rated power (kW or MW);

v_i : cut-in wind speed (m/s or miles/h);

v_r: rated wind speed (m/s or miles/h); and

v_o: cut-out wind speed (m/s or miles/h).

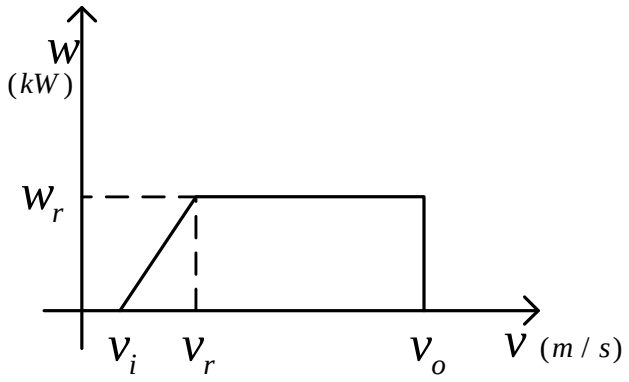

Fig. 4.4 Speed-to-power conversion function

Usually several WTG are present in a microgrid. Different WTG may have different speed-to-power conversion functions. However, due to the geographic proximity, all WTGs could share the same wind speed distribution model. For simplicity, if the random wind speed falls into an interval, we take the mid value of this interval. Then each WTG unit can be treated as a multi-state unit in which the total state number is equal to the number of intervals [79].

4.1.3 Probabilistic PV Model

The output of PV mainly depends on irradiance and ambient temperature. A fairly good approximation of a PV module could neglect the effects of temperature variations by taking only the average cell temperature [74]. Irradiance varies with sites and seasons. The distribution of hourly irradiance at a particular location usually follows a bimodal distribution function [74, 78, 80-82] which can be seen as a linear combination of two unimodal distribution functions [83]. The unimodal distribution functions can be modeled by Beta, Weibull, and Log-normal PDFs [74, 78, 80, 82, 84, 85]. Here the Weibull distribution is employed as:

$$f(g) = \varpi \left(\frac{k_1}{c_1}\right)\left(\frac{g}{c_1}\right)^{k_1-1} e^{-\left(\frac{g}{c_1}\right)^{k_1}} + (1-\varpi)\left(\frac{k_2}{c_2}\right)\left(\frac{g}{c_2}\right)^{k_2-1} e^{-\left(\frac{g}{c_2}\right)^{k_2}}, \quad 0 < g < \infty \qquad (4.5)$$

where

g: irradiance on the PV panel plane (kW/m^2).

ω: weighted parameter, $0<\omega<1$;

k_1, k_2: shape factors; and

c_1, c_2: scale factors.

Irradiance PDFs can be calculated for each hour of a typical day in a month [74]. Historical data collected over long periods of time can be utilized to characterize the probabilistic behavior of irradiance [74, 78, 84]. In case of non-availability of site-specific data, one can use the data taken from the nearest meteorological station, which will reproduce the on-site environmental conditions with unknown degree of similarity [83]. The irradiance prediction and the determination of irradiance PDF are beyond the scope of this thesis and we assume that they are known or given prior to the SR estimation studies.

Similar to the wind speed distribution model, the irradiance distribution function can also be truncated and then divided into class intervals [85]. The probability of every interval

can be calculated by integration. An indicative 5-interval irradiance probability distribution model is shown in Fig. 4.5.

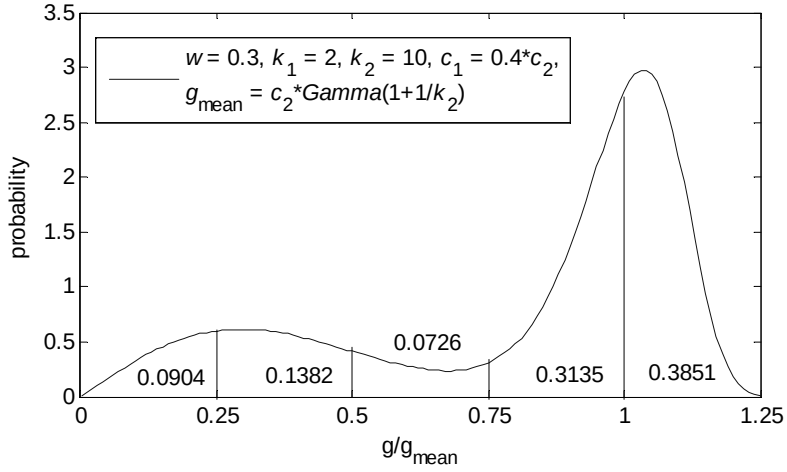

Fig. 4.5 PV irradiance probability function

Given the irradiance probability distribution and the irradiance-to-power conversion function, the PV output power distribution can be obtained. The irradiance-to-power conversion function used in this report is similar to those given in references [86-88]. It is shown in Fig. 4.6.

$$p = f^{PV}(g) = \begin{cases} \dfrac{g^2}{K_c} S\eta^{PV} & 0 < g < K_c \\ gS\eta^{PV} & g > K_c \end{cases} \tag{4.6}$$

where

f^{PV}: irradiance-to-power conversion function;

p: PV output power (kW);

η^{PV}: efficiency of the PV panel (%);

K_c: a certain irradiance point (kW/m^2); and

S: the total area of the PV panel (m^2).

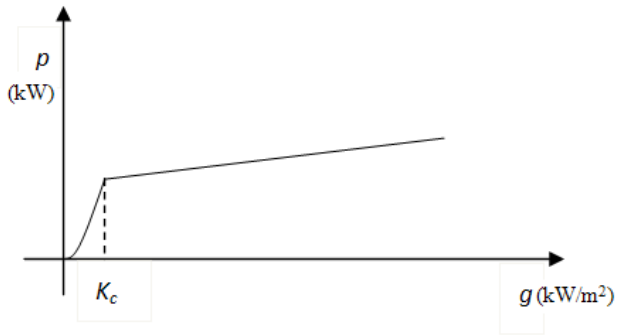

Fig. 4.6 Irradiance-to-power conversion function

The relationship between the PV output power and irradiance is different for each type of PV cells. Obviously, all PV units present in a microgrid face the same meteorology and they share the same irradiance distribution model. For simplicity, if the random irradiance falls into an interval, we take the mid value of this interval. Then each PV unit can also be treated as a multi-state unit in which the total state number is equal to the number of intervals.

4.2 Mathematical Model of SR Estimation in Microgrids

Microgrids can operate in isolated or grid connected mode. When microgrids operate in isolated mode, the aim is to minimize the total cost. When microgrids operate in grid connected mode, the aim is to maximize the profit [89]. These two models are formulated below.

4.2.1 Microgrids in Isolated Mode

When microgrids operate in isolated mode, they try to minimize the total cost which includes the operating cost, reserve cost, and EIC. The objective function is the same as (2.1) and it is reproduced as follows:

$$\min \{\sum_{t=1}^{N_T}\sum_{i=1}^{N_G}[C_{i,t}(P_{i,t},U_{i,t})+SUC_i\cdot K_{i,t}]+\sum_{t=1}^{N_T}\sum_{i=1}^{N_G}q_{i,t}R_{i,t}+EENS\cdot VOLL\} \quad (4.7)$$

The formulation of EENS is different from that used in chapter two since the effect of various uncertainties are involved. The formulation of EENS used in microgrids is shown in section 4.3.

The objective function must be minimized subject to a number of constraints [57]. The power balance constraint and SR constraints are the same as (2.3) and (2.4) respectively in chapter two.

The LOLP constraint is:

$$LOLP_t \le LOLP_t^{max} \quad (4.8)$$

where

$LOLP_t$: LOLP value during period t; and

$LOLP_t^{max}$: maximum allowable LOLP limit during period t.

The LOLP constraint is treated as an additional security constraint and it can be inactivated by setting a large enough LOLP cap. The LOLP constraint can protect microgrids from suffering a high risk at some periods. The formulation of LOLP is shown in section 4.3.

Various DG units exist in microgrids. In this thesis the WTG, PV, MT, FC, and ESS are considered. The output of the WTG and PV depends on wind speed and solar irradiance respectively. They are seen as non-dispatchable units whereas MT [90-93] and FC [94] are seen as dispatchable units.

An ESS such as a battery bank plays an important role in microgrid operation. It can provide a wide array of solutions to the key issues that affect the system. These issues include, but not limited to SR, load leveling, frequency control, voltage regulation, relief of overloaded network components, and capacity release [95-104]. ESS can be used to

store the energy at the time of surplus and re-dispatch it appropriately later. In microgrids ESS is taken as a special dispatchable unit which has the ability to absorb energy. An ESS should satisfy the following constraints [105, 106]:

Output power limits: $| p_t^E | \leq p_E^{\max}$ (4.9)

Charge equation: $C(t+1) = C(t) - d_T \; p_t^E$ (4.10)

Discharge equation: $C(t+1) = C(t) - d_T \; p_t^E / \eta^E$ (4.11)

Starting/Ending limits: $C(0) = C_S, C(N_T) = C_E$ (4.12)

Stored energy limits: $C_{min} \leq C(t) \leq C_{max}$ (4.13)

where

p_t^E: output power of ESS during period t;

$p_E^{\max}$: maximum allowable charge/discharge limit;

$C(t)$: energy stored in ESS till period t;

d_T: duration time of each interval;

η^E: discharge efficiency of ESS;

C_S: starting energy stored in ESS;

C_E: ending energy stored in ESS;

C_{min}: minimum allowable energy stored in ESS; and

C_{max}: maximum allowable energy stored in ESS.

Besides, each generating unit is subject to its own operating constraints which include upper and lower generation constraints, minimum up- and down-time constraints, initial conditions constraints, and ramp-up and ramp-down constraints. They are all considered in this thesis. Their mathematical formulation is shown in appendix A.3.

4.2.2 Microgrids in Grid Connected Mode

When microgrids operate in grid connected mode, it tries to maximize its benefit or profit from power exchange with the upstream grid. The profit is equal to revenue minus total

cost. Customers are assumed to be charged at open market prices. Under this circumstance, the objective function is shown as follows:

$$\max\{\sum_{t=1}^{N_T}\sum_{i=1}^{N_G} MP(t)\cdot P_{i,t} - \sum_{t=1}^{N_T}\sum_{i=1}^{N_G}[C_{i,t}(P_{i,t},U_{i,t}) + SUC_i \cdot K_{i,t}] - \sum_{t=1}^{N_T}\sum_{i=1}^{N_G} q_{i,t}R_{i,t} - EENS\cdot VOLL\} \quad (4.14)$$

where

$MP(t)$: open market active power price.

The revenue is equal to the market price multiplied by unit output power. The total cost is the same as that when the microgrid operates in isolated mode.

In this model, the upstream grid is taken as an equivalent unit. The capacity of this unit is the available capacity of the tie lines. Its bid price is the real price of the market. All constraints are not changed. This model is similar to the model in isolated mode. Only the objective function is changed slightly.

4.3 Formulations of EENS and LOLP

In this chapter, when optimizing SR in microgrids, random outages of units and uncertainties caused by load, WTGs, and PVs are considered. The effect of distribution networks is not taken into account.

The universal formulation of EENS used in microgrids is the same as that used in large traditional power system, namely, equation (2.6). d_T is assumed to be 1 hour. In microgrids, the EENS is caused by not only random outages of units, but also uncertainties introduced by WTGs, PVs and load. The outage events are classified by outage order. For formulation simplicity, EENS caused by third and higher orders of outage events are not shown. The EENS in microgrids can be explicitly formulated as shown below.

$$
\begin{aligned}
&EENS = EENS^0 + EENS^1 + EENS^2 \\
&= \sum_{t=1}^{N_T} \sum_{k=1}^{N_{WT}} \sum_{l=1}^{N_L} \sum_{m=1}^{N_{PV}} p_t^0 \, p_{k,t}^{WT} \, p_{m,t}^{PV} \, p_l^L b_{k,l,m,t}^0 (\Delta P_{k,t}^{WT} + \Delta P_{m,t}^{PV} + \Delta P_{l,t}^L - R_t) \\
&+ \sum_{t=1}^{N_T} \sum_{i=1}^{N_G} \sum_{k=1}^{N_{WT}} \sum_{l=1}^{N_L} \sum_{m=1}^{N_{PV}} p_{i,t}^1 \, p_{k,t}^{WT} \, p_{m,t}^{PV} \, p_l^L b_{i,k,l,m,t}^1 (P_{i,t} + R_{i,t} + \Delta P_{k,t}^{WT} + \Delta P_{m,t}^{PV} + \Delta P_{l,t}^L - R_t) \\
&+ \sum_{t=1}^{N_T} \sum_{i=1}^{N_G} \sum_{j>i}^{N_G} \sum_{k=1}^{N_{WT}} \sum_{l=1}^{N_L} \sum_{m=1}^{N_{PV}} p_{i,j,t}^2 p_{k,t}^{WT} \, p_{m,t}^{PV} \, p_l^L b_{i,j,k,l,m,t}^2 (P_{i,t} + R_{i,t} + P_{j,t} + R_{j,t} + \Delta P_{k,t}^{WT} + \Delta P_{m,t}^{PV} + \Delta P_{l,t}^L - R_t)
\end{aligned}
\tag{4.15}
$$

where

$EENS^0$: EENS caused by WTG, PV and load uncertainties with zero order of outage events;

$EENS^1$: EENS caused by WTG, PV and load uncertainties with first order of outage events;

$EENS^2$: EENS caused by WTG, PV and load uncertainties with second order of outage events;

N_{WT}: number of intervals of wind speed distribution;

N_{PV}: number of intervals of irradiance distribution;

N_L: number of intervals of load distribution;

p_t^0: probability when all online units are available;

$p_{i,t}^1$: probability of unit *i* outage during period *t*;

$p_{i,j,t}^2$: probability of units *i* and *j* simultaneous outage during period *t*;

$p_{k,t}^{WT}$: probability of wind speed falls in the *k*th interval of wind speed distribution function during period *t*;

$p_{m,t}^{PV}$: probability of irradiance falls in the *m*th interval of irradiance distribution function during period *t*;

p_l^L: probability of load falls in the *l*th interval of load forecast distribution function;

$\Delta P_{l,t}^L$: load forecast error when load falls in interval *l* during period *t*;

$\Delta P_{k,t}^{WT}$: WTG power forecast error when wind speed falls in interval *k* during period *t*;

$\Delta P_{m,t}^{PV}$: PV power forecast error when irradiance falls in interval *m* during period *t*;

$b_{k,l,m,t}^{0}$: 1 if WTG, PV and load uncertainties during period *t* cause loss of load and 0 otherwise;

$b_{i,k,l,m,t}^{1}$: 1 if WTG, PV and load uncertainties and the outage of unit *i* during period *t* cause loss of load and 0 otherwise; and

$b_{i,j,k,l,m,t}^{2}$: 1 if WTG, PV and load uncertainties and the simultaneous outage of unit *i* and *j* during period *t* cause loss of load and 0 otherwise.

The outage probabilities $p_{i,t}^{1}$ and $p_{i,j,t}^{2}$ are the same as those introduced in chapter two. The probabilities p_{t}^{0}, $p_{i,t}^{1}$ and $p_{i,j,t}^{2}$ can be formulated as:

$$p_t^0 = \prod_{i=1}^{N_G}(1-u_i U_{i,t}) \tag{4.16}$$

$$p_{i,t}^1 = u_i U_{i,t} \prod_{j=1,\, j\neq i}^{N_G}(1-u_j U_{j,t}) \tag{4.17}$$

$$p_{i,j,t}^2 = u_i u_j U_{i,t} U_{j,t} \prod_{k=1,k\neq i,j}^{N_G}(1-u_k U_{k,t}) \tag{4.18}$$

$$p_{i,j,k,t}^3 = u_i u_j u_k U_{i,t} U_{j,t} U_{k,t} \prod_{l=1,l\neq i,j,k}^{N_G}(1-u_l U_{l,t}) \tag{4.19}$$

In (4.15),

$$\Delta P_{k,t}^{WT} = \sum_{i=1}^{nWT}[\, f_i^{WT}(v_{i,t}^{fcst}) - f_i^{WT}(\frac{v_{i,t}^{trun}}{K}\cdot(k-0.5))] \tag{4.20}$$

$$\Delta P_{m,t}^{PV} = \sum_{i=1}^{nPV}[\, f_i^{PV}(g_{i,t}^{fcst}) - f_i^{PV}(\frac{g_{i,t}^{trun}}{M}\cdot(m-0.5))] \tag{4.21}$$

$$\Delta P_{l,t}^{L} = P_t^L \cdot \sigma \cdot (l-4) \tag{4.22}$$

where

nWT: number of WTG units;

nPV: number of PV units;

f_i^{WT}: speed-to-power conversion function of the *i*th WTG unit;

f_i^{PV}: irradiance-to-power conversion function of the *i*th PV unit;

$v_{i,t}^{fcst}$: forecast wind speed of the *i*th WTG unit during period *t*;

$g_{i,t}^{fcst}$: forecast irradiance of the *i*th PV unit during period *t*;

$v_{i,t}^{trun}$: wind speed value at the truncated point of the *i*th WTG unit during period *t*;

$g_{i,t}^{trun}$: irradiance value at the truncated point of the *i*th PV unit during period *t*; and

σ: load standard deviation.

In equation (4.20) or (4.21), the first term in the square bracket is the forecast value. The second term is the actual value under a possible event. $\Delta P_{k,t}^{WT}$, $\Delta P_{m,t}^{PV}$ and $\Delta P_{l,t}^{L}$ are all forecast errors. It is assumed that the uncertainties of WTG, PV and load are uncorrelated and the forecast errors can be added up directly.

The binary variables $b_{k,l,m,t}^{0}$, $b_{i,k,l,m,t}^{1}$ and $b_{i,j,k,l,m,t}^{2}$ can be formulated as:

$$b_{k,l,m,t}^{0} = \begin{cases} 1 & \text{if } \Delta P_{k,t}^{WT} + \Delta P_{m,t}^{PV} + \Delta P_{l,t}^{L} - R_t > 0 \\ 0 & \text{otherwise.} \end{cases} \tag{4.23}$$

$$b_{i,k,l,m,t}^{1} = \begin{cases} 1 & \text{if } P_{i,t} + R_{i,t} + \Delta P_{k,t}^{WT} + \Delta P_{m,t}^{PV} + \Delta P_{l,t}^{L} - R_t > 0 \\ 0 & \text{otherwise.} \end{cases} \tag{4.24}$$

$$b_{i,j,k,l,m,t}^{2} = \begin{cases} 1 & \text{if } P_{i,t} + R_{i,t} + P_{j,t} + R_{j,t} + \Delta P_{k,t}^{WT} + \Delta P_{m,t}^{PV} + \Delta P_{l,t}^{L} - R_t > 0 \\ 0 & \text{otherwise.} \end{cases} \tag{4.25}$$

$b_{k,l,m,t}^{0}$ can be linearized [62] to

$$\frac{\Delta P_{k,t}^{WT} + \Delta P_{m,t}^{PV} + \Delta P_{l,t}^{L} - R_t}{\sum_{i=1}^{N_G} P_i^{max}} \le b_{k,l,m,t}^{0} \le 1 + \frac{\Delta P_{k,t}^{WT} + \Delta P_{m,t}^{PV} + \Delta P_{l,t}^{L} - R_t}{\sum_{i=1}^{N_G} P_i^{max}} \tag{4.26}$$

$b_{i,k,l,m,t}^{1}$ and $b_{i,j,k,l,m,t}^{2}$ can be linearized in the same way.

$LOLP_t$ can be formulated as:

$$LOLP_t = \sum_{k=1}^{N_{WT}} \sum_{l=1}^{N_L} \sum_{m=1}^{N_{PV}} (p_t^0 p_{k,t}^{WT} p_{m,t}^{PV} p_l^L b_{k,l,m,t}^0) + \sum_{i=1}^{N_G} \sum_{k=1}^{N_{WT}} \sum_{l=1}^{N_L} \sum_{m=1}^{N_{PV}} (p_{i,t}^1 p_{k,t}^{WT} p_{m,t}^{PV} p_l^L b_{i,k,l,m,t}^1) + \sum_{i=1}^{N_G} \sum_{j>i}^{N_G} \sum_{k=1}^{N_{WT}} \sum_{l=1}^{N_L} \sum_{m=1}^{N_{PV}} (p_{i,j,t}^2 p_{k,t}^{WT} p_{m,t}^{PV} p_l^L b_{i,j,k,l,m,t}^2) \quad (4.27)$$

4.4 Aggregation of Uncertainties

One can find that with the introduction of uncertainties, the dimension of contingency events in (4-15) increases $N_{\mathrm{WT}} \cdot N_{\mathrm{PV}} \cdot N_{\mathrm{L}}$ times. The introduction of uncertainties heavily increases the computational burden. In order to reduce the computational burden, the combination of various uncertainties can be aggregated together and rounded to an approximated distribution model before optimization. The uncertainties can be rounded by a fixed number of intervals or by a fixed kW rounding increment. The two methods are the same in essence because if the number of intervals is fixed, only one rounding increment will be mapped. Rounding uncertainties by a fixed number of intervals is directly correlated to computation complexity and it is used in this paper. The procedure of rounding is described as follows:

1) The number of intervals of the rounded uncertainty distribution N is defined by the user.

2) For each set of (k, l, m), a combined power deviation value $\Delta P_{k,t}^{WT} + \Delta P_{m,t}^{PV} + \Delta P_{l,t}^{L}$ and a combined probability $p_{k,t}^{WT} \cdot p_{m,t}^{PV} \cdot p_l^L$ are mapped. The uncertainties combination which has the largest absolute power deviation value is selected and the largest power deviation is denoted as $max_{(k,m,l)}(\Delta P_{k,t}^{WT} + \Delta P_{m,t}^{PV} + \Delta P_{l,t}^{L})$. The aggregated uncertainty distribution is centered at zero. Then the length of every interval is $max_{(k,m,l)}(\Delta P_{k,t}^{WT} + \Delta P_{m,t}^{PV} + \Delta P_{l,t}^{L}) / (N/2)$.

3) For each set of (*k*, *l*, *m*), if $\Delta P_{k,t}^{WT}+\Delta P_{m,t}^{PV}+\Delta P_{l,t}^{L}$ falls in an interval of the aggregated uncertainty distribution, $p_{k,t}^{WT}\cdot p_{m,t}^{PV}\cdot p_{l}^{L}$ will be added in the same interval too. The first term of (4.15) is changed to (4.28):

$$\begin{aligned}&\sum_{t=1}^{N_T}\sum_{k=1}^{N_{WT}}\sum_{l=1}^{N_L}\sum_{m=1}^{N_{PV}} p_{k,t}^{WT}\, p_{m,t}^{PV}\, p_{l}^{L} b_{k,l,m,t}^{0}(\Delta P_{k,t}^{WT}+\Delta P_{m,t}^{PV}+\Delta P_{l,t}^{L}-R_t)\\ &\approx \sum_{t=1}^{N_T}\sum_{n=1}^{N} p_{n,t} b_{n,t}^{0}(\Delta P_{n,t}-R_t)\end{aligned} \tag{4-28}$$

Then the formulation of the total EENS is changed from (4.15) to (4.29):

$$\begin{aligned}EENS \approx &\sum_{t=1}^{N_T}\sum_{n=1}^{N} p_t^0\, p_{n,t} b_{n,t}^{0}(\Delta P_{n,t}-R_t)+\sum_{t=1}^{N_T}\sum_{i=1}^{N_G}\sum_{n=1}^{N} p_{i,t}^{1}\, p_{n,t} b_{i,n,t}^{1}(P_{i,t}+R_{i,t}+\Delta P_{n,t}-R_t)\\ &+\sum_{t=1}^{N_T}\sum_{i=1}^{N_G}\sum_{j>i}^{N_G}\sum_{n=1}^{N} p_{i,j,t}^{2}\, p_{n,t} b_{i,j,n,t}^{2}(P_{i,t}+R_{i,t}+P_{j,t}+R_{j,t}+\Delta P_{n,t}-R_t)\end{aligned} \tag{4.29}$$

where

N: number of intervals of the approximated uncertainty distribution;

$p_{n,t}$: probability when the *n*th interval of the aggregated uncertainty distribution is selected during period *t*;

$\Delta P_{n,t}$: power deviation when the *n*th interval of the aggregated uncertainty distribution is selected during period *t*;

$b_{n,t}^{0}$: 1 if the aggregated uncertainty during period *t* causes loss of load and 0 otherwise;

$b_{i,n,t}^{1}$: 1 if the aggregated uncertainty and the outage of unit *i* during period *t* cause loss of load and 0 otherwise; and

$b_{i,j,n,t}^{2}$: 1 if the aggregated uncertainty and the simultaneous outage of unit *i* and *j* during period *t* cause loss of load and 0 otherwise.

The binary variables $b_{n,t}^{0}$, $b_{i,n,t}^{1}$ and $b_{i,j,n,t}^{2}$ can be formulated as:

$$b_{n,t}^{0}=\begin{cases}1 & if\ \Delta P_{n,t}-R_t>0\\ 0 & otherwise.\end{cases} \tag{4.30}$$

$$b_{n,t}^{1}=\begin{cases}1 & if\ P_{i,t}+R_{i,t}+\Delta P_{n,t}-R_t>0\\ 0 & otherwise.\end{cases} \tag{4.31}$$

$$b_{n,t}^{2}=\begin{cases}1 & if\ P_{i,t}+R_{i,t}+P_{j,t}+R_{j,t}+\Delta P_{n,t}-R_t>0\\ 0 & otherwise.\end{cases} \tag{4.32}$$

For binary variable $b_{n,t}^{0}$, it satisfies

$$\frac{\Delta P_{n,t}-R_t}{\sum_{i=1}^{N_G}P_i^{max}}\le b_{n,t}^{0}\le 1+\frac{\Delta P_{n,t}-R_t}{\sum_{i=1}^{N_G}P_i^{max}} \tag{4.33}$$

$b_{i,n,t}^{1}$, $b_{i,j,n,t}^{2}$ can be presented in the same way.

Similarly, the formulation of LOLP is changed from (4.27) to (4.34):

$$LOLP_t\approx\sum_{n=1}^{N}p_t^0p_{n,t}b_{n,t}^{0}+\sum_{i=1}^{N_G}\sum_{n=1}^{N}p_{i,t}^{1}p_{n,t}b_{i,n,t}^{1}+\sum_{i=1}^{N_G}\sum_{j>i}^{N_G}\sum_{n=1}^{N}p_{i,j,t}^{2}p_{n,t}b_{i,j,n,t}^{2} \tag{4.34}$$

By comparison it can be found that the combined power deviation value $\Delta P_{k,t}^{WT}+\Delta P_{m,t}^{PV}+\Delta P_{l,t}^{L}$ is replaced by $\Delta P_{n,t}$. The combined probability $p_{k,t}^{WT}\cdot p_{m,t}^{PV}\cdot p_l^{L}$ is replaced by $p_{n,t}$; and $b_{k,l,m,t}^{0}$, $b_{i,k,l,m,t}^{1}$ and $b_{i,j,k,l,m,t}^{2}$ are changed to $b_{n,t}^{0}$, $b_{i,n,t}^{1}$ and $b_{i,j,n,t}^{2}$ respectively. After aggregation of uncertainties, the calculation dimension of EENS and LOLP decreases $N_{\mathrm{WT}}\cdot N_{\mathrm{PV}}\cdot N_{\mathrm{L}}/N$ times. The computation efficiency is greatly improved.

4.5 Modified Multi-Step Method in Microgrids

In chapter three, the SR estimation problem in large power systems is solved using the multi-step method. EENS is approximated as a piecewise linear function of SSR. The proposed multi-step method solves the large traditional power system well. However, when the multi-step method is applied in microgrids, it usually needs many iterations to

converge and sometimes it even diverges. The reason is that the configuration of microgrids is very different from that of large traditional power systems. Due to the introduction of various intermittent DG units and the increased load forecasting error in microgrids, the degree of uncertainties in microgrids is high compared with that of the large traditional power systems. The proposed multi-step method cannot be directly used in microgrids. When optimizing SR in microgrids, EENS must be computed elaborately.

In this chapter, a modified multi-step method is proposed to solve the SR estimation problem in microgrids. The mathematical formulations of the multi-step method and the modified method are the same, except for the formulations of EENS and LOLP. In the modified multi-step method, EENS is divided into two parts. The first part is the sum of EENS caused by uncertainties only and EENS caused by first order of outage events and uncertainties. The second part is EENS caused by second and higher orders of outage events and uncertainties. Compared with the first order of outage events, the second and higher orders of outage events consume most of the computation resources, but they usually contribute a small proportion in the total cost. So these two parts are captured using different methods. The first part of EENS is calculated using unit commitment variables. The second part of EENS is modeled approximately as a piecewise linear function of SSR and its calculation is performed step by step. The procedure of the proposed modified multi-step method is shown below:

In the first step, the SR is determined by optimizing SC and EIC. The EENS formulation used in this step is

$$EENS \approx EENS^0 + EENS^1 = \sum_{i=1}^{N_T}\sum_{n=1}^{N} p_t^0 p_{n,t} b_{n,t}^0 (\Delta P_{n,t} - R_t) + \sum_{i=1}^{N_T}\sum_{i=1}^{N_G}\sum_{n=1}^{N} p_{i,t}^1 p_{n,t} b_{i,n,t}^1 (P_{i,t} + R_{i,t} + \Delta P_{n,t} - R_t) \quad (4.35)$$

It can be found that (4.35) is just the first two terms of (4.29). After optimization an approximate unit schedule can be obtained. Based on the obtained unit schedule, a COPT for each period is established in which only the second and higher orders of outage events

are considered. The COPT is combined with the aggregated uncertainty distribution and a final combined distribution can be achieved. Similar to COPT, The final combined distributions are used to calculate the parameters of EENS and LOLP caused by the second and higher orders of outage events and uncertainties in step two. For computation simplicity, the final combined distributions will be rounded by a rounding increment.

In the second step, when calculating EENS, all orders of outage events are considered. The calculation of EENS which is caused by uncertainties only, first order of outage events and uncertainties is the same as that of (4.35). EENS caused by the second and higher orders of outage events and uncertainties is calculated based on the final combined distributions. EENS used in step two is

$$\begin{aligned} EENS &= EENS^{0} + EENS^{1} + EENS^{>1} \\ &= \sum_{t=1}^{N_T}\sum_{n=1}^{N} p_t^0\, p_{n,t}\, b_{n,t}^0 (\Delta P_{n,t} - R_t) + \sum_{t=1}^{N_T}\sum_{i=1}^{N_G}\sum_{n=1}^{N} p_{i,t}^1\, p_{n,t}\, b_{i,n,t}^1 (P_{i,t} + R_{i,t} + \Delta P_{n,t} - R_t) \\ &+ \sum_{t=1}^{N_T}\sum_{n=1}^{N(t)} p_{n,t}^{>1} b_{n,t}^{>1} (\Delta P_{n,t}^{>1} - R_t) \end{aligned} \tag{4.36}$$

where

$EENS^{>1}$: EENS caused by second and higher orders of outage events;

$p_{n,t}^{>1}$: probability when the *n*th interval of the final combined distribution is selected during period *t*;

$\Delta P_{n,t}^{>1}$: power deviation when the *n*th interval of the final combined distribution is selected during period *t*; and

$b_{n,t}^{>1}$: 1 if the final combined distribution during period *t* causes loss of load and 0 otherwise.

For $b_{n,t}^{>1}$, it satisfies

$$b_{n,t}^{>1} = \begin{cases} 1 & if\ \ \Delta P_{n,t}^{>1} - R_t > 0 \\ 0 & otherwise. \end{cases} \tag{4.37}$$

It can be linearized as

$$\frac{\Delta P_{n,t}^{>1}-R_t}{\sum_{i=1}^{N_G}P_i^{\max}} \le b_{n,t}^{>1} \le 1+\frac{\Delta P_{n,t}^{>1}-R_t}{\sum_{i=1}^{N_G}P_i^{\max}} \tag{4.38}$$

Similarly LOLP can be formulated as

$$LOLP=\sum_{t=1}^{N_T}\sum_{n=1}^{N} p_t^0 p_{n,t} b_{n,t}^0 + \sum_{t=1}^{N_T}\sum_{i=1}^{N_G}\sum_{n=1}^{N} p_t^1 p_{n,t} b_{i,n,t}^1 + \sum_{t=1}^{N_T}\sum_{n=1}^{N(t)} p_{n,t}^{>1} b_{n,t}^{>1} \tag{4.39}$$

After step two, a convergence criterion (4.40) is introduced. In (4.40), $EENS_{during}$ is the EENS value computed during optimization. It is calculated by (4.36). $EENS_{after}$ is the EENS value computed after optimization. It is calculated using the optimization results based on the final combined distribution. $\Delta EENS$ is the normalized relative EENS error. It quantifies the accuracy of the EENS approximation. Parameter ε is the convergence tolerance. Equation (4.40) is similar to (3.1). If (4.40) is satisfied, the optimization procedure will stop. Otherwise, as in step two, new final combined distribution is formed based on the results of the last step. EENS and LOLP are then updated. A new step is implemented till (4.40) is satisfied.

$$\Delta EENS = \frac{\left|EENS_{during}-EENS_{after}\right|}{EENS_{after}} \le \varepsilon \tag{4.40}$$

The outage probabilities p_t^0 and $p_{i,t}^1$ which are used in (4.35), (4.36) and (4.39) are shown in (4.41) and (4.42). It can be found that the outage probabilities are functions of unit statuses. The statuses of non-dispatchable units are known and only the statuses of dispatchable units are unknown variables. So the probabilities p_t^0 and $p_{i,t}^1$ are the functions of statuses of dispatchable units only. Similar to reference [16], these probabilities can be simplified.

In the first step, for p_t^0, only the constant terms are kept. For $p_{i,t}^1$, only terms with the first order of unknown variables are considered. The formulations of p_t^0 and $p_{i,t}^1$ are changed from (4.16) and (4.17) to:

$$p_t^0 = \prod_{i=1}^{N_G}(1-u_iU_{i,t}) = \prod_{i\in nI}(1-u_iU_{i,t})\prod_{i\notin nI}(1-u_iU_{i,t}) \approx \prod_{i\in nI}(1-u_iU_{i,t}) \tag{4.41}$$

$$\begin{aligned} p_{i,t}^1 &= u_iU_{i,t}\prod_{j\in nI,\, j\neq i}(1-u_jU_{j,t})\prod_{j\notin nI,\, j\neq i}(1-u_jU_{j,t}) \\ &\approx u_iU_{i,t}\prod_{j\in nI,\, j\neq i}(1-u_jU_{j,t}) \approx u_iU_{i,t}\prod_{j\in nI}(1-u_jU_{j,t}) \end{aligned} \tag{4.42}$$

where

nI : set of non-dispatchable units.

Because the statuses of non-dispatchable units are known, $\prod_{i\in nI}(1-u_iU_i)$ is just a constant in (4.42) and (4.41). Then p_t^0 becomes a constant value and $p_{i,t}^1$ becomes the product of a binary variable and a constant value. The formulation of EENS in (4.35) and (4.36) can be presented as the summation of the products of some binary variables and a bounded continuous variable, which can be linearized [16, 62]. LOLP in (4.39) can be presented as the summation of the products of some binary variables and it can also be linearized. After linearization of LOLP and EENS, the first step of the modified step method can be solved by MILP.

In the second step and beyond, the formulations of p_t^0 and $p_{i,t}^1$ are shown below:

$$p_t^0 = \prod_{i=1}^{N_G}(1-u_iU_{i,t}) \approx \prod_{i\in nI}(1-u_iU_{i,t})\prod_{i\notin nI}(1-u_iU_{i,t}^{'}) \tag{4.43}$$

$$\begin{aligned} p_{i,t}^1 &= u_iU_{i,t}\prod_{j=1,\, j\neq i}^{N_G}(1-u_jU_{j,t}) = u_iU_{i,t}\prod_{j\in nI,\, j\neq i}(1-u_jU_{j,t})\prod_{j\notin nI,\, j\neq i}(1-u_jU_{j,t}) \\ &\approx u_iU_{i,t}\prod_{j\in nI,\, j\neq i}(1-u_jU_{j,t})\prod_{j\notin nI,\, j\neq i}(1-u_jU_{j,t}^{'}) \approx u_iU_{i,t}\prod_{j\in nI}(1-u_jU_{j,t})\prod_{j\notin nI}(1-u_jU_{j,t}^{'}) \end{aligned} \tag{4.44}$$

where

$U_{i,t}^{'}$: exogenous status of a dispatchable unit which is calculated in step one.

Equations (4.43) and (4.44) are calculated based on (4.41) and (4.42). When calculating the products of series of probabilities in (4.41) and (4.42), the exogenous unit status $U_{i,t}^{'}$ which is computed from step one is used. $\prod_{i \in nI}(1-u_i U_i)$ and $\prod_{i \in nI}(1-u_i U_i^{'})$ are all constants. Then p_t^0 becomes a constant and $p_{i,t}^1$ becomes the product of a binary variable and a constant. The formulation of EENS and LOLP can be linearized [16, 62]. Refer to appendices A.4 and A.5 for the details. So the entire modified multi-step method can be solved by MILP.

A flow chart of the proposed method is shown in Fig. 4.7. The proposed modified multi-step method which is used estimate the SR requirement in microgrids is concluded below. Before optimization, load, WTG and PV uncertainties are aggregated together and rounded to an approximated distribution model. In step one, optimize the objective function (4.7) or (4.14) subject to the constraints with EENS as described in (4.35). Using optimization results of step one, the unit schedule is obtained. A COPT is established based on the known unit schedule for each optimization interval. In step two the aggregated uncertainty and the COPT obtained in step one are combined together to produce the new EENS formulation (4.36). Then optimize the objective function (4.7) or (4.14) with the newly formed EENS (4.36). A convergence criterion is introduced and validated. If the convergence criterion is satisfied, the total optimization will stop. Otherwise, the EENS is updated based on the newly found unit schedule and a new step is needed.

The proposed method replaces the combinatorial characteristic of outage events by their equivalent piecewise linear functions. All higher orders of outage events and various uncertainties are taken into account. The proposed method can yield accurate results within desirable execution time.

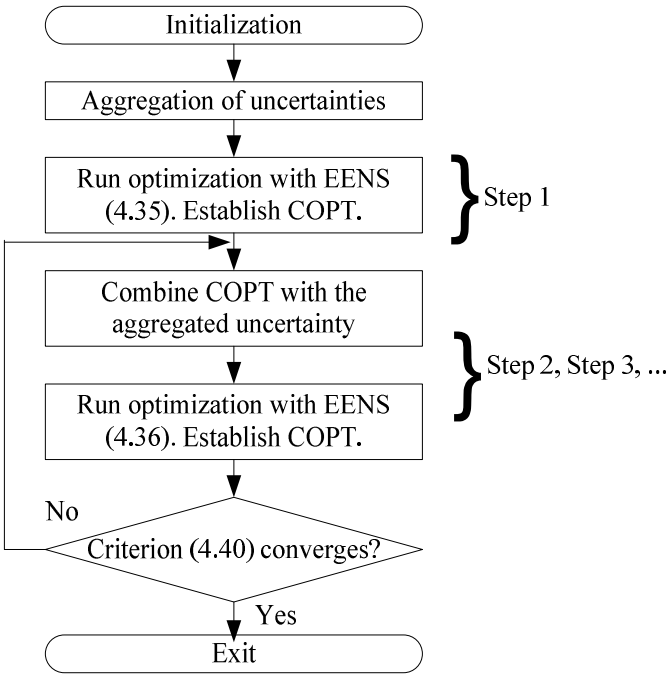

Fig. 4.7 Flowchart of the modified multi-step method

4.6 Summary

In this chapter, a modified multi-step is proposed to estimate the SR requirement in microgrids. First the uncertainty models of load, WTG, and PV are introduced. Load is modeled by a seven-step normal distribution. Wind speed is modeled by a Weibull distribution and irradiance is modeled by a bimodal distribution function. The wind speed and irradiance distributions are truncated and divided into class intervals. Given the speed-to-power and irradiance-to-power conversion functions, the WTG and PV output uncertainties distribution can be obtained.

Second, the mathematical model of SR estimation in microgrids is introduced. When microgrids operate in grid connected mode, the objective function is to maximize the profit while in isolated mode the objective function is to minimize the total cost. The corresponding constraints such as LOLP constraint and ESS constraints are all discussed.

Third, the formulations of EENS and LOLP are presented. With the in introduction of uncertainties, the calculation dimension expands and this further increases the computation burden.

Fourth the procedure of aggregation of total uncertainties is given. Load, WTG and PV uncertainties are aggregated together and rounded by a fixed kW rounding increment. The computation complexity caused by uncertainty can be controlled by the value of rounding increment.

Finally the modified multi-step method is presented. The difference between multi-step and modified multi-step exists in how to calculate the EENS value. In the modified multi-step method, EENS is divided into two parts and calculated using different methods. EENS caused by uncertainties only and a combination of first order outage events and uncertainties is represented using unit commitment variables and computed by optimization. EENS caused by the combination of second and higher order outage events and uncertainties is modeled by a piecewise linear function of SSR and its calculation is performed step by step. The case studies and result discussions on SR estimation in microgrids are explicitly discussed in the next chapter.

Chapter 5
Case Studies and Result Discussions on SR Estimation in Microgrids

5.1 Case Studies

To set up a study case, a hypothetical microgrid model is used in this thesis. The load profile and energy price are derived from [89]. They are shown in Figs. 5.1 and 5.2.

Four DG units are installed in this microgrid: a WTG, a PV, a FC and a MT. When a microgrid which includes an ESS is connected to the upstream grid, it can be seen as a 6-unit system. Table 5.1 summarizes their parameters. Here a linear bidding production cost function is used. The offer coefficients of DG units are derived from [89]. For the ESS, P_{max}^{E} is 20 kW; η^{E} is 0.9; and C_S, C_E, C_{min}, C_{max} are 180, 180, 100, 260 kWh respectively. The standard deviation σ of the load is 0.08; *VOLL* is 10 \$/kWh and $LOLP_t^{max}$ is 0.005. $q_{i,t}$ is 0.4 cent/kW; τ is 10 minutes and ε is 0.005. The predefined duality gap of MILP algorithm is 0.001.

The average hourly wind speed and irradiance profiles of the WTG and PV are taken from [107]. They are shown in Figs. 5.3 and 5.4. For the WTG, v_i, v_r and v_o are 5, 15 and 45 miles/hour respectively. Assume that J = 10, k = 2 and $c = v_{mean}/0.9$ miles/hour for all hours. For the PV, η^{PV} = 12%, and S^{PV} = 270 m^2 while K = 10, ω = 0.3, k_1 = 2, k_2 = 10, $c_2 = g_{mean}/0.95$ and $c_1 = 0.4c_2$ for all hours. For the aggregated uncertainty distribution, M = 7 is used. For the final combined distribution, the fixed rounding increment is 5 kW. An indicative combinatorial distribution of WTG, PV and load uncertainties at hour 12 is

shown in Fig. 5.5. The corresponding aggregated uncertainty distribution is shown in Fig. 5.6. The data of the microgrid is also explicitly shown in appendix A.2.

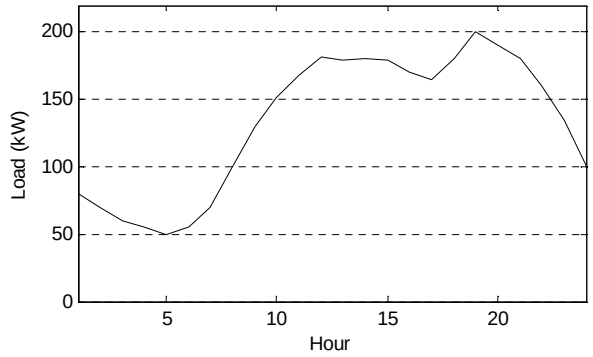

Fig. 5.1 Load profile of the study case

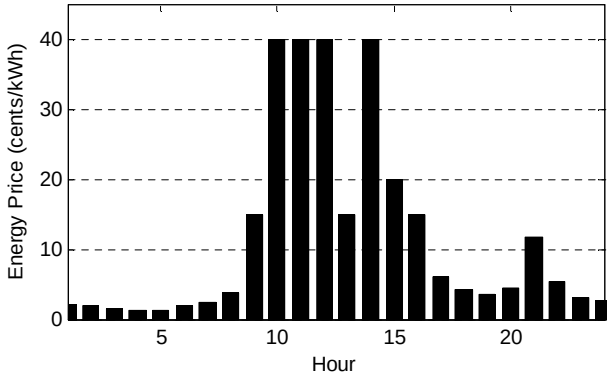

Fig. 5.2 Energy price of every hour

Table 5.1 Some parameters of DG units, ESS and upstream grid

Unit type	MT	FC	WTG	PV	ESS	Upstream grid
Min power (kW)	30	10	0	0	−	-100
P_i^{max} (kW)	150	100	40	30	−	100
Min up/down time (h)	1	1	1	1	1	0
Ramp up/down rate (kW/h)	900	900	600	600	600	600
Failure rate γ_i	0.006	0.006	0.006	0.006	0.006	0.006
$b_{i,t}$ (cents/kWh)	4.37	2.84	10.63	54.84	0	$MP(t)$
$c_{i,t}$ (cents/h)	425	850	0	0	10	0
SC_i (cents)	45	53	0	0	0	0

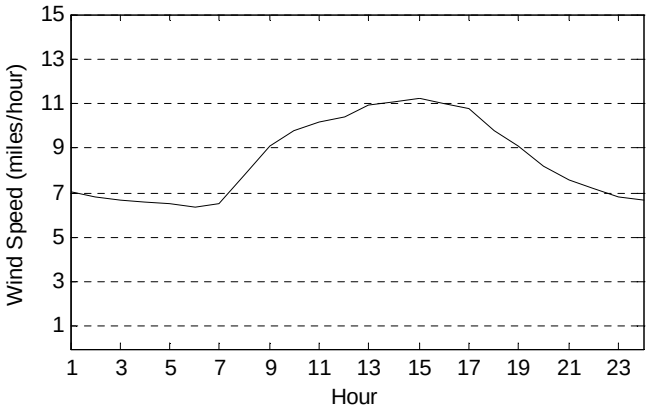

Fig. 5.3 Hourly wind speed of WTG

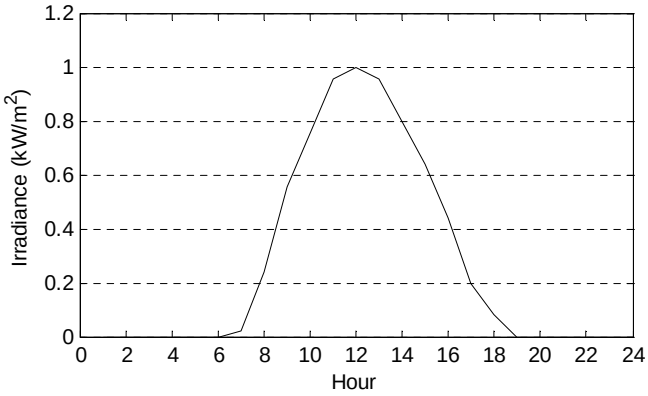

Fig. 5.4 Hourly irradiance of PV

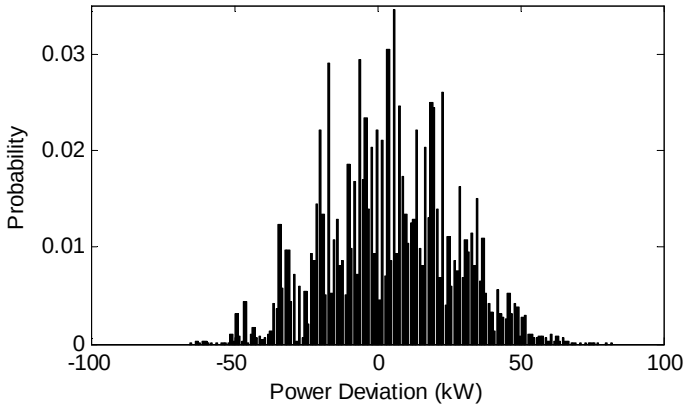

Fig. 5.5 Combined uncertainty distribution

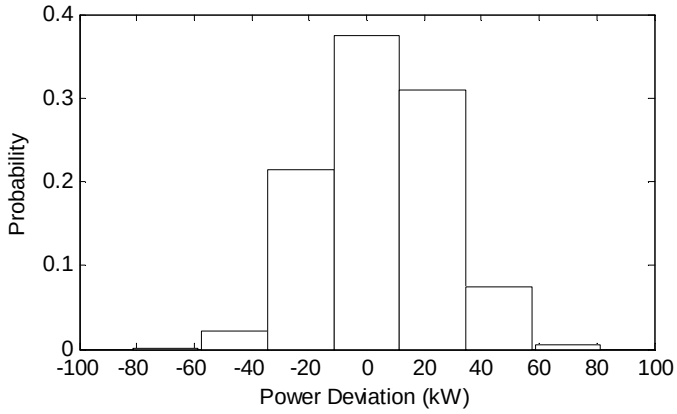

Fig. 5.6 Aggregated uncertainty distribution

5.2 Simulation Results

5.2.1 Simulation Results of 6-unit Microgrid System

◆ **Microgrid in grid connected mode**

A base UC module without the reserve constraint is implemented. After step one, a COPT in which only the second and higher orders of outage events are considered is established for each optimization period. An indicative COPT (at hour 12) is shown in Fig. 5.7. Combined with the uncertainty distribution described in Fig. 5.5, the final combined distribution at this hour is shown in Fig. 5.8.

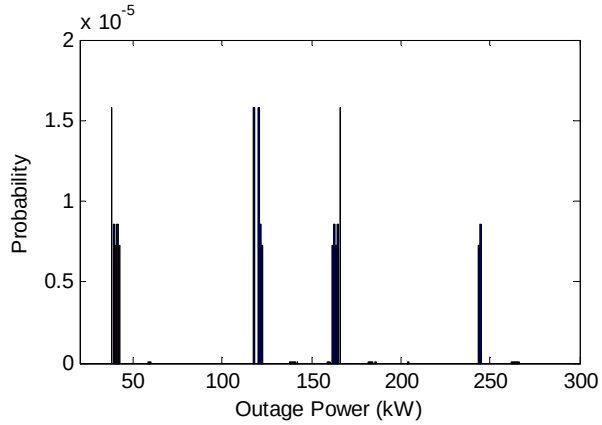

Fig. 5.7 An indicative distribution of unreliability of units at hour 12

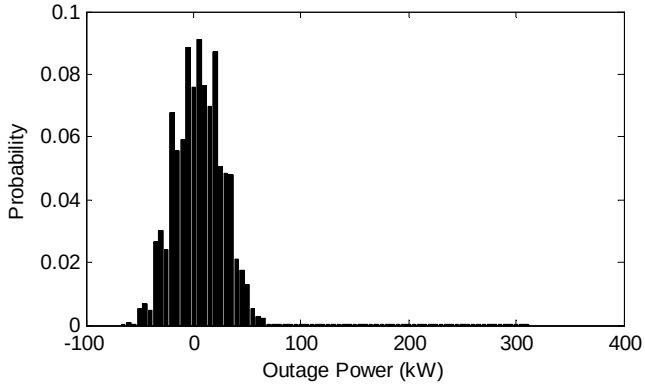

Fig. 5.8 Final combined distribution at hour 12

Next step two is run. After step two, Δ*EENS* is 0.070%. The convergence criterion is satisfied and the optimization stops. The itemization of cost and EENS is shown in Table 5.2. In Table 5.2 the optimal results in the fourth column are calculated by simultaneously optimizing SC and caused by uncertainties, the first and the second outage events. The results in the fourth column are assumed to be the perfect results. This assumption is reasonable since the EENS caused by third and higher orders of outage events are negligible in this example. The output power and the optimal SR of the multi-step method are shown in Figs. 5.9 and 5.10. The maximum available SR, namely $\min\{P_i^{\max}U_{i,t} - P_{i,t}, U_{i,t}(\tau R_i^{up})\}$ where R_i^{up} is the ramp up rate, and τ = 10 minutes is also

given. The corresponding LOLP and energy stored in ESS are shown in Figs. 5.11 and 5.12.

Table 5.2 Itemization of cost, EENS and run time

	Results of step 1	Results of step 2	Optimal results
$EENS^0$ (kW)	0.000	0.000	0.000
$EENS^1$ (kW)	0.817	0.815	0.817
$EENS^{>1}$(kW)	N/A	0.124	0.125
Operating cost ($)	437.857	437.857	437.857
Reserve cost ($)	11.131	11.171	11.131
EIC ($)	8.170	9.391	9.423
Total cost ($)	457.158	458.419	458.411
Revenue ($)	205.791	204.531	204.539
Run Time (s)	10	33	505

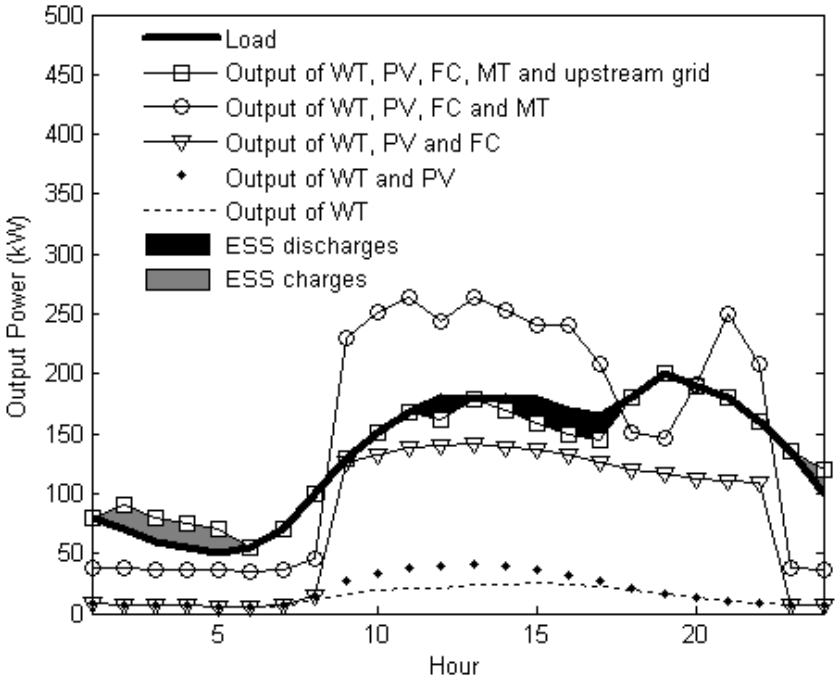

Fig. 5.9 Production of units

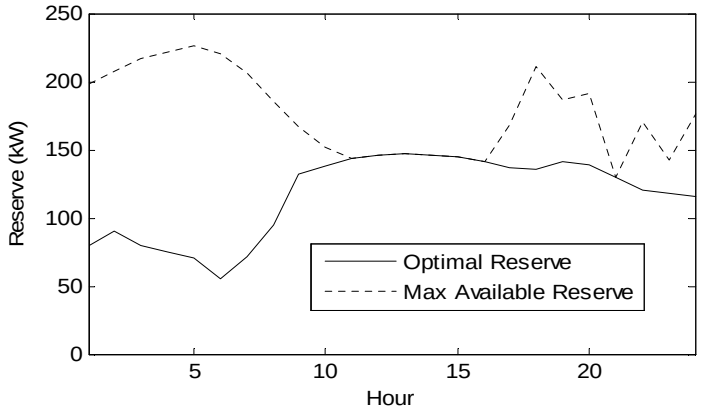

Fig. 5.10 Optimal SR of every hour

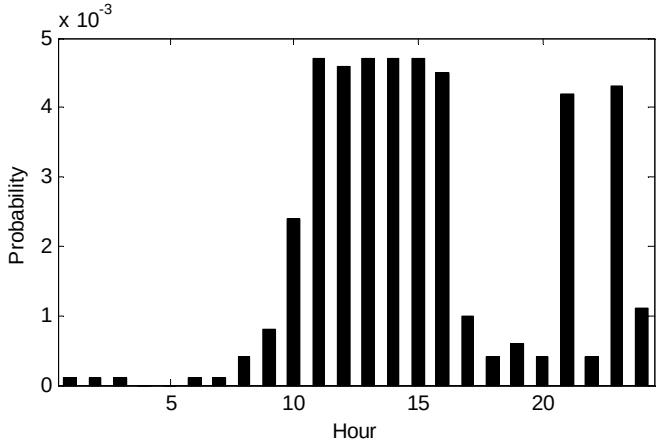

Fig. 5.11 LOLP of every hour

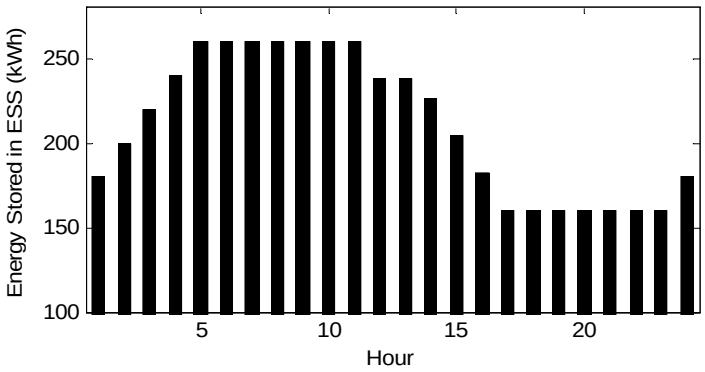

Fig. 5.12 Energy stored in ESS

From Table 5.2 one sees that an approximated solution is obtained in step one. This is because in step one only the first order of outage events and uncertainties are considered. The EENS caused by second and higher orders of outage events which are not considered in step one only accounts for a small proportion in total EENS. In step two all higher orders of outage events are considered and a more accurate solution is obtained. Step two improves the results of step one. The results of step two are nearly the same as the optimal results but it consumes much less time. The proposed multi-step method captures the total unreliability very efficiently.

For MT, the operating cost is $4.37P + 425$. For FC, the operating cost is $2.84P + 850$ where P is the output power. Comparing the cost functions of MT and FC, when $4.37P + 425 = 2.84P + 850$, $P = 278$ kW, which is larger than the capacity of MT (150 kW) and FC (100 kW). When MT and FC have the same output power, the operating cost of MT is smaller than that of FC. It is more economical to dispatch MT than to dispatch FC. Hence MT has a higher priority to be dispatched. From Fig. 5.9 it can be found that MT is always dispatched during the entire optimization period. But FC has a relatively small incremental cost (2.84 cents/kWh < 4.37 cents/kWh). Hence when FC is dispatched, it usually operates very close to the maximum output power. Due to the characteristic that ESS cannot produce cheap energy by itself, ESS mainly works as a source of SR most of the time. When the market price is volatile, ESS can make profits by buying cheap storing energy and selling dear later.

From the legend of Fig. 5.9 it can be found that the difference between the circle line and square line is the output of the upstream grid. In Fig. 5.9, when the circle line is higher than the square line, the microgrid sells energy to the upstream gird. Likewise when the circle line is lower than the square line, the microgrid buys energy from the upstream gird. From Fig. 5.9 one sees that when the market price is low (t = hour 1-8, 18-20, 23-24 in Fig. 5.2), the microgrid generates some energy and purchases the remaining energy from the upstream grid to lower its cost. When the market price is relatively high (t = hour 9-17, 21-22), the microgrid generates energy and sells the surplus energy to the upstream grid

for profit. The grey area means ESS charges up and the black area means ESS discharges its energy. Combined with Fig. 5.12 one sees that ESS charges up when the market price is low and discharges its energy when market price is relatively high.

In Fig. 5.10, during hours 1-8, the optimal reserve is relatively small compared with those in other hours. This is mainly because the load level is small. During hours 11-16, 21, and 23, the optimal reserve reaches or nearly reaches the maximum available reserve. At these hours the SR resource is relatively tense. From Fig. 5.11 one can find that at these hours the LOLP level is relatively high.

◆ **Microgrid in isolated mode**

When the microgrid operates in isolated mode, the total capacity of the dispatchable units, namely microturbine and fuel cell, is 150kW+100kW=250kW, which is obviously larger than the maximum load 200kW. The 6-unit microgrid has the ability to operate in isolated mode.

When the microgrid operates in isolated mode, the unit which represents the upstream grid is not allowed to be scheduled during the entire optimization period. In isolated mode, the generating power sources become tighter compared with those in grid connected mode. If $LOLP_t^{\max}$ takes 0.005 the operation of the microgrid will become infeasible. So $LOLP_t^{\max}$ is assumed to be 0.015 in isolated mode.

After step two, $\Delta EENS$ is 0.02%. The convergence criterion is satisfied and the optimization stops. The itemization of cost and EENS values and run time are shown in Table 5.3. The outputs of the DG units are shown in Fig. 5.13. The optimal reserve and the maximum available reserve are shown in Fig. 5.14. The corresponding LOLP is given in Fig. 5.15.

Table 5.3 Itemization of cost, EENS and run time

	Results of step 1	Results of step 2	Optimal results
$EENS^0$ (kW)	0.036	0.036	0.0355
$EENS^1$ (kW)	6.168	6.158	6.156
$EENS^{>1}$(kW)	N/A	0.193	0.193
Operating cost ($)	416.433	416.433	416.433
Reserve cost ($)	7.885	7.999	8.041
EIC ($)	62.594	63.856	64.408
Total cost ($)	486.912	488.287	488.882
Run Time (s)	2.3	4	18

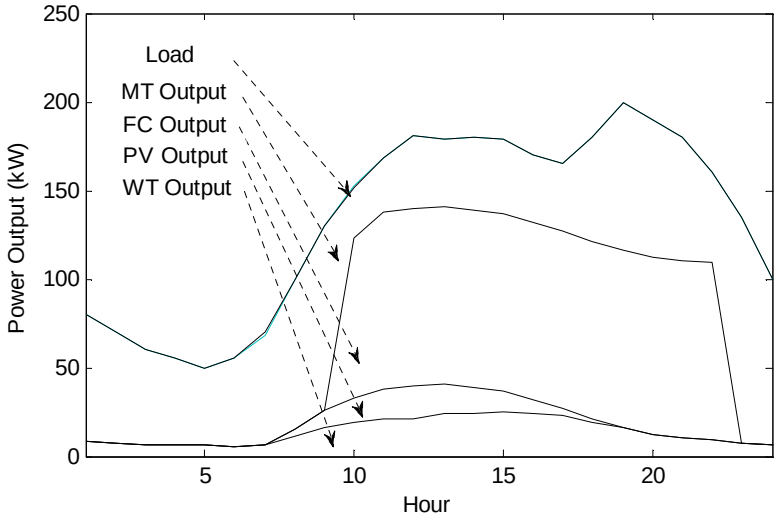

Fig. 5.13 Production of DG units

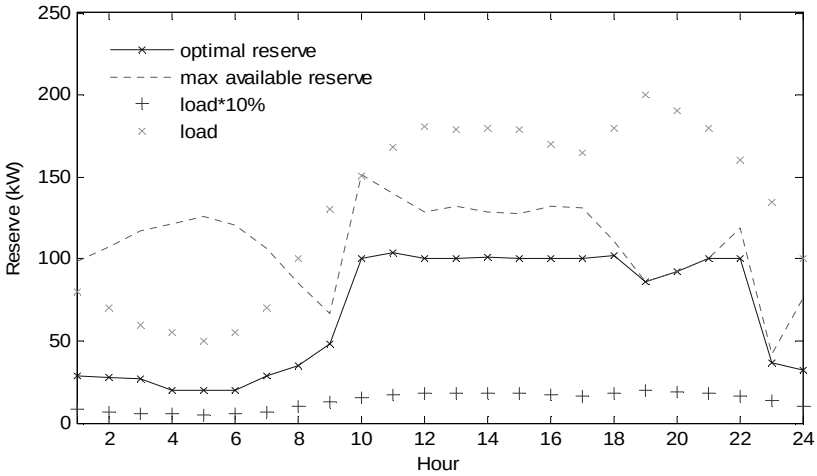

Fig. 5.14 Reserve of every hour

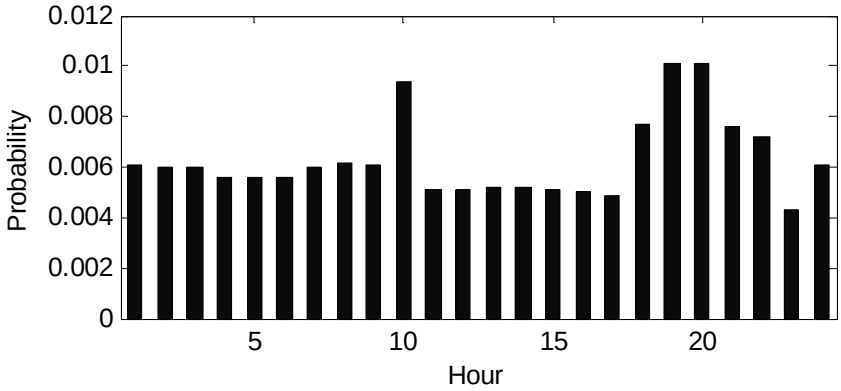

Fig. 5.15 LOLP of every hour

From Table 5.3 one sees that a rough solution is obtained in step one. In step two all higher orders of outage events are considered and a more accurate solution is obtained. Step two improves the results of step one. The results of step two are nearly the same as the optimal results but it consumes much less time. The proposed modified multi-step method captures the total hourly system unreliability index very efficiently.

When the microgrid operates in isolated mode, the run time is smaller than that of grid connected mode. The reason is that the upstream grid is not scheduled in the entire optimization period. When the microgrid operates in isolated mode, the market price is

not considered. Under this condition, ESS is mainly used as a source of SR and it is seldom scheduled during optimization.

As discussed above, MT has a higher priority to be dispatched since it has a relatively lower operation cost. FC has a relatively small incremental cost so when FC is dispatched it usually reaches the maximum output power. It can be found that in Fig. 5.13, MT is always scheduled. When FC is scheduled, it reaches its maximum output power. ESS does not charge up or discharge its energy during the entire optimization period.

In Fig. 5.14, during hours 1-9 and 23-24, the reserve is small because load level is small. During hours 10-18, likewise, the reserve is large because the load level is high. The reserve during hours 19-20 decreases compared with that during hours 10-18. At these hours the SR reaches the maximum available reserve.

According to Fig. 5.15, one can find that the LOLP value is much higher than the value obtained in grid connected mode. Since the reserve is mainly supplied by MT, this reserve cannot compensate the outage events caused by MT itself. The LOLP value is relatively high, especially, when the SR amount reaches the maximum available reserve (t = hour 9, and hours 19-21).

5.2.2 Simulation Results of 42-unit Microgrid System

A more complex 42-unit microgrid is used in this subsection. It includes 10 WTGs, 10 PV units, 10 FC units, 10 MT units, and an ESS. Compared with the data of the 6-unit system, the parameters of the ESS, upstream grid and load are not changed. The capacity of each WTG, PV, FC, and MT is set to 0.1 of the original value. The corresponding ramp rate limits are also changed accordingly. Only grid connected operation mode is considered.

The modified multi-step method is implemented. Based on the results of step one, a COPT for each period is established by considering unreliabilities caused by the second and higher orders of outage events. An indicative COPT (at hour 12) is shown in Fig. 5.16. Combined with the uncertainties, the final combined distribution which is shown in Fig. 5.17 can be obtained. The final combined distribution is rounded at 5 kW.

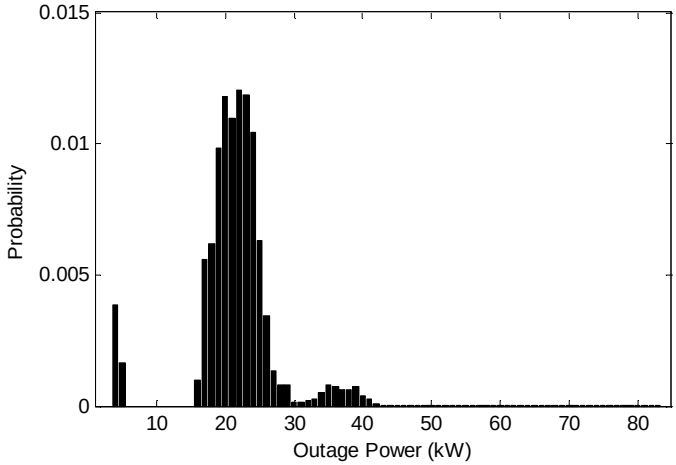

Fig. 5.16 An indicative distribution of unreliabilities of units at hour 12

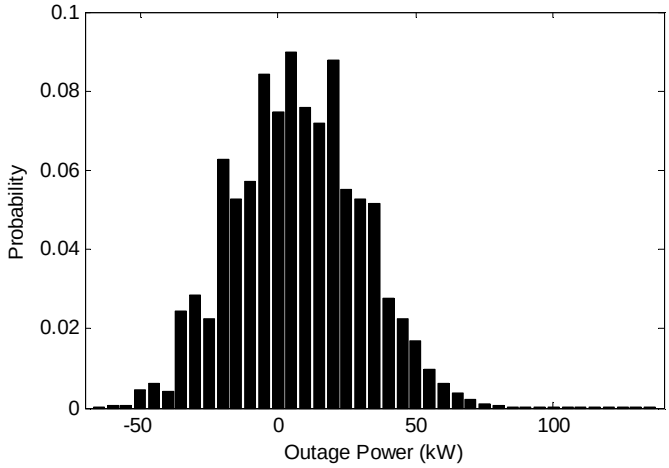

Fig. 5.17 Final combined distribution at hour 12

During the optimization, the variations of Δ*EENS* and revenue versus each solution step are shown in Fig. 5.18. Δ*EENS* and the revenue decrease step by step. The optimization is terminated after step four and Δ*EENS* is 0.022% when the convergence criterion is satisfied. The total run time is about 8 minutes with a pre-specified duality gap of 0.1%.

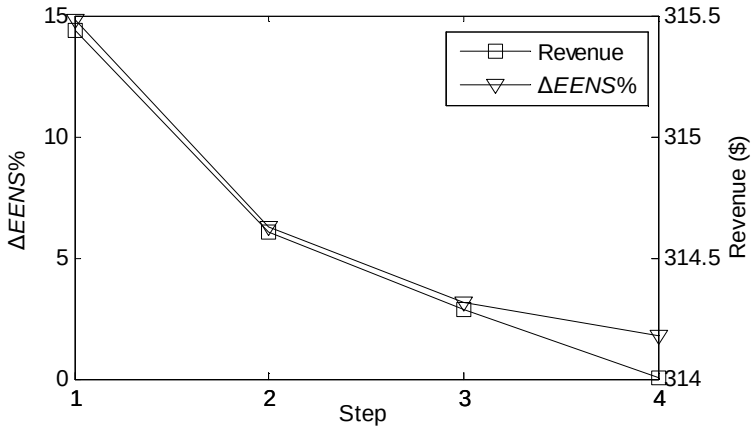

Fig. 5.18 Variation of ΔEENS and revenue versus step

The itemization of cost and EENS of the entire period is shown in Table 5.4. From Table 5.4 one sees that the proposed method can solve the problem efficiently. It can improve the results till the desirable accuracy is met. The accuracy of the method is guaranteed by the small value of Δ*EENS*.

Table 5.4 Itemization of cost and EENS

	Results of step one	Results of step four
$EENS^0$ (kW)	0.000	0.000
$EENS^1$ (kW)	0.547	0.508
$EENS^{>1}$ (kW)	N/A	0.116
Operating cost ($)	337.809	336.1922
Reserve cost ($)	6.754	7.235
EENS cost ($)	5.471	6.237
Total cost ($)	350.034	349.664
Revenue ($)	315.482	314.177

The optimal SR is shown in Fig. 5.19. From this figure one sees that when the effect of second and higher orders of outage events is considered, the reserve during optimization periods is rescheduled and more SR is required. Although the 42-unit microgrid has the same total capacity value as the 6-unit microgrid, the reserve scheduled for the 42-unit microgrid is much smaller than that in the 6-unit microgrid. From the reliability point of view, it is better to replace a large unit by a number of units with small capacity.

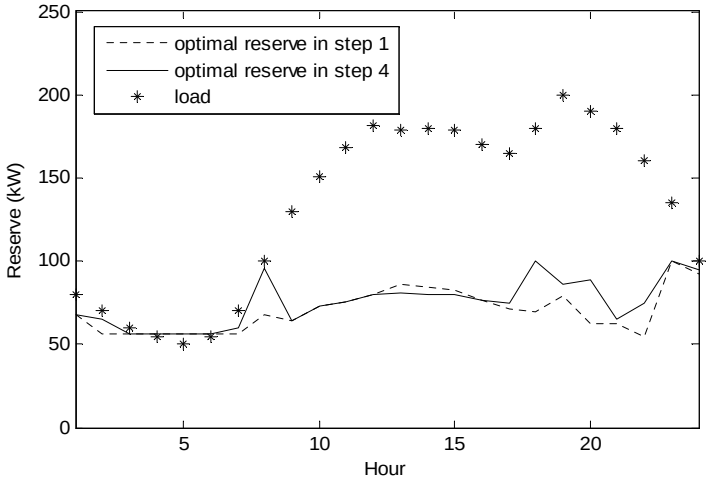

Fig. 5.19 Optimal SR in step one and four

The LOLP of each optimization period is shown in Fig. 5.20. The energy stored in ESS of each optimization period is shown in Fig. 5.21. Form Fig. 5.21 it can be found that the variation of energy stored in ESS is similar to that in the 6-unit system. In order to get profit, ESS mainly charges up when the market price is low and discharges its energy when the market price is high.

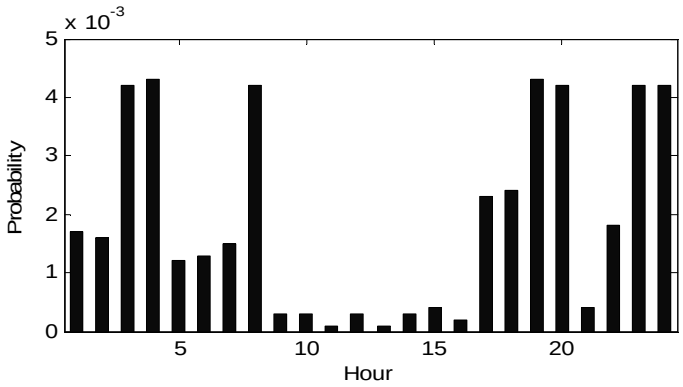

Fig. 5.20 LOLP of every hour

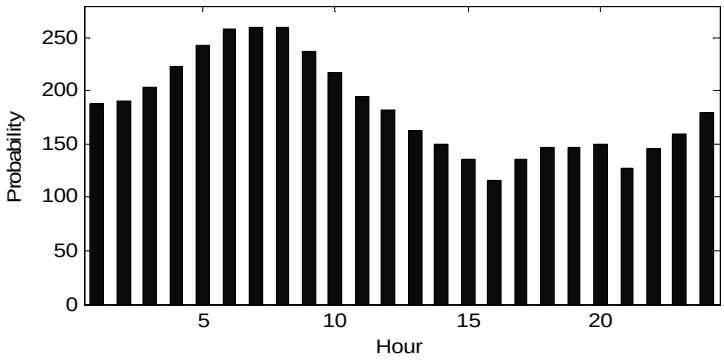

Fig. 5.21 Energy stored in ESS

If the 42-unit microgrid system is solved by optimizing the SC and EIC caused by uncertainties, first and second order outages of outage events and without using the modified multi-step method, the optimization will finally run out of memory even only the first two periods are considered.

5.3 Discussions of Results

In the proposed multi-step method, some simplifications, assumptions and approximations are frequently needed, the effect of which is often unknown [108]. In this section, a series of sensitivity analyses are implemented. These sensitive analyses are based on 24 hours unless otherwise specified.

5.3.1 Effect of Aggregation of Uncertainties

During the optimization, uncertainties caused by load, WTG, and PV outputs are combined and rounded. The number of intervals of the rounded uncertainty distribution *N* has a strong effect on the accuracy of the final optimization results. It also directly corresponds to the computation complexity.

The 6-unit microgrid is used as an example. It is assumed that the microgrid operates in grid connected mode. For simplicity only the first hour is considered. If the optimization is run over the 24-hour period, the system will run out of memory when a large number of intervals of the approximated uncertainty distribution *N* is used. The variations of the profit and run time versus *N* are shown in Fig. 5.22.

The right most point of each line in Fig. 5.22 is calculated when uncertainties are not rounded and represents the real true value. For clarity, the objective function, namely, the profit is normalized by its real true value. The difference between each square point and the value 1 represents the error due to rounding.

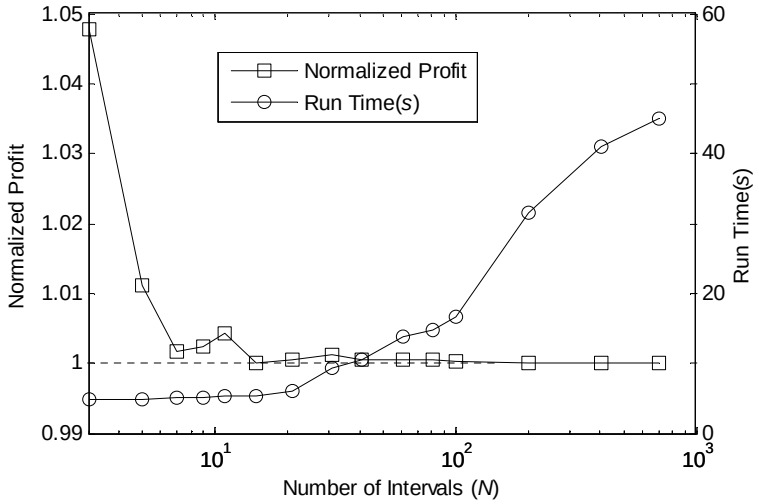

Fig. 5.22 Variations of normalized profit and run time versus *N*

From Fig. 5.22 one sees that the value of profit oscillates but eventually settles down towards the true value as N increases. The computation time also increases when N increases. There is a tradeoff between accuracy and computation complexity.

N directly corresponds to the degree of rounding of the total uncertainties which are caused by non-dispatchable DG units and load. A series of sensitivity analyses have been performed to investigate the impacts of different uncertainties on the objective function. For simplicity only the first hour is considered. The profit is normalized by its real true value.

◆ **Effect of WTG penetration level**

In the study case, the capacity of WTG is 40 kW. The total capacity of all units is 420 kW, and the WTG penetration level is about 10%. To illustrate the effect of WTG penetration level, the capacity of WTG is modified by multiplying it by a simple multiplication factor. Fig. 5.23 shows the variations of normalized profit versus N under different WTG capacities.

With the increasing WTG penetration level, the degree of uncertainties in the microgrid increases. From Fig. 5.23 one sees that with the increasing WTG penetration level, the convergence speed of the oscillation decreases. For example, if the error due to rounding is made smaller than 0.1%, from the inset one sees that when the multiplication factor is 0.5, N should be larger than 11; and when the multiplication factor is 1 and 2, N should be larger than 31 and 51 respectively. The penetration of PV has a similar effect.

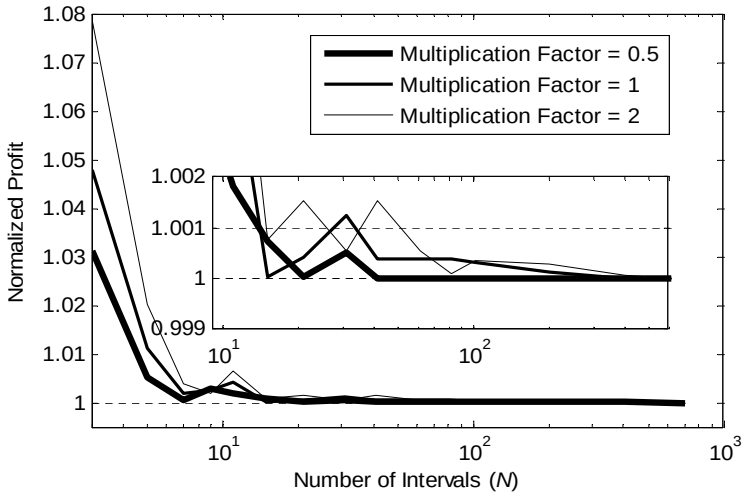

Fig. 5.23 Variations of normalized profit versus N under different WTG capacities

◆ **Effect of forecast wind speed**

To illustrate the effect of wind speed, the value of the forecast wind speed is also modified by multiplying a simple multiplication factor. Fig. 5.24 shows the variations of the normalized profit versus *N* under different wind speeds.

From Fig. 5.24 one sees that when the multiplication factor takes the value of 0.5 or 2, the convergence speed of the oscillation increases compared with that when the multiplication factor is 1.

The speed-to-power conversion function of WTG used in the study case is shown in Fig. 5.25. v_i, v_r and v_o are 5, 15, 45 miles/hour respectively. When the sample points of the wind speed fall in ranges 1, 3, and 4, the WTG output power is fixed. The variation of wind speed has no effect on the WTG output power. When the sample points of the wind speed fall in range 2, the WTG output varies according to the wind speed value. At hour 1, the forecast wind speed is about 7 miles/h. When the multiplication factor takes the value of 0.5 or 2, less sample points of the wind speed fall in range 2 compared with those when the multiplication factor is 1. The uncertainty introduced by WTG decreases. This corresponds to the increase of the convergence speed of the oscillation shown in Fig. 5.24.

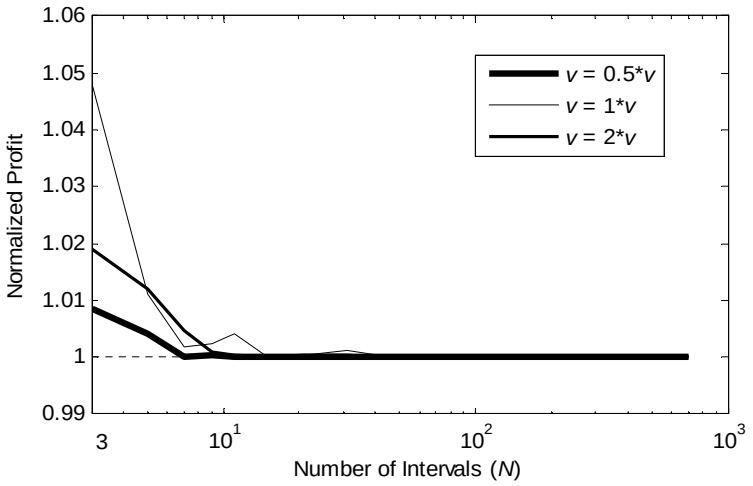

Fig. 5.24 Variations of normalized profit versus *N* under different multiplication factors of wind speeds

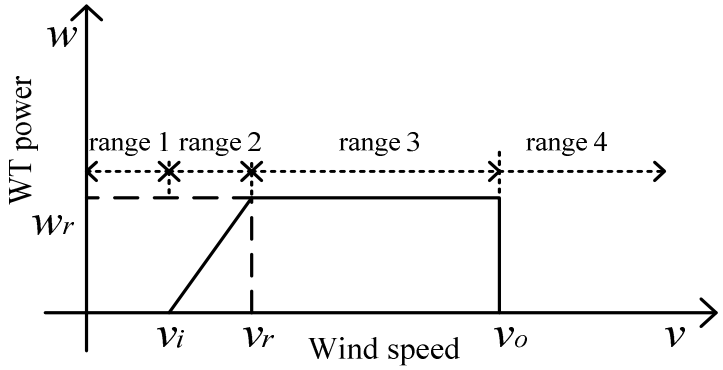

Fig. 5.25 Speed to power conversion function of WTG

◆ **Effect of standard deviation of load**

Fig. 5.26 shows the variations of normalized profit versus *N* under different standard deviations, σ of load. With the increasing σ, the degree of uncertainties in the microgrid increases. From Fig. 5.26 one sees that with the increasing σ, the convergence speed of the oscillation decreases.

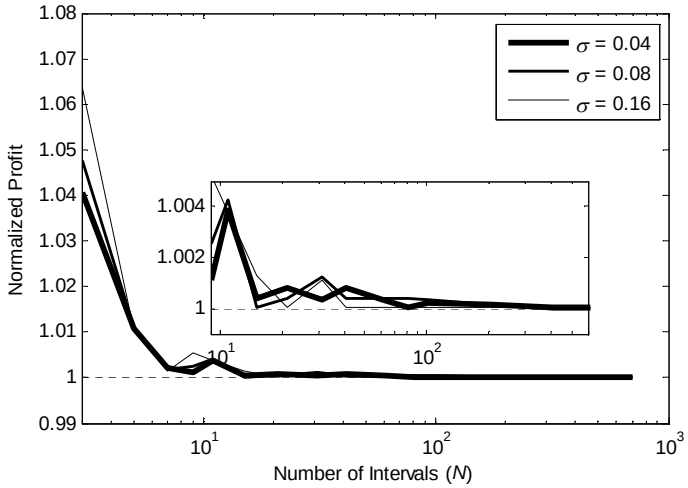

Fig. 5.26 Variations of normalized profit versus *N* under different standard deviations of load

◆ **Effect of load levels**

Fig. 5.27 shows the variations of the normalized profit versus *N* under different load levels. The wind speed is more volatile than the load. Increasing the load level is equivalent to decreasing the degree of total uncertainties in the microgrid. So with the increase in the load level, the convergence speed of the oscillation increases. Compared with the WTG capacity, wind speed, standard deviation of load, the load level has the strongest effect on the uncertainty level. From Fig. 5.27 one sees that the change of convergence speed of the oscillation is very large under different load levels.

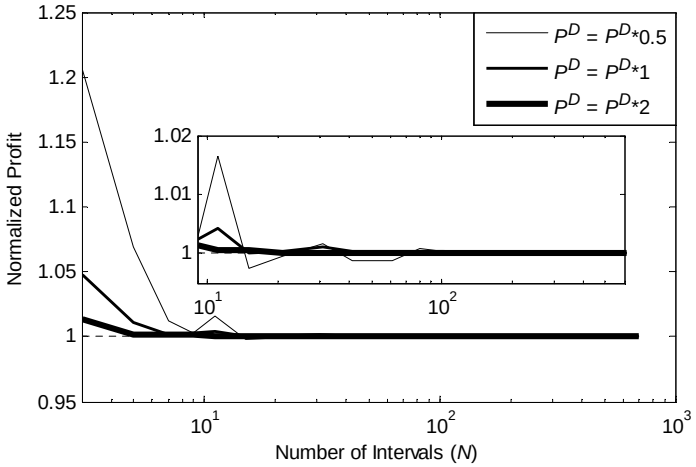

Fig. 5.27 Variations of normalized profit versus *N* under different load levels

5.3.2 Effect of Rounding Increments of Final Combined Distribution

The final combined distribution considers the effect of uncertainties and unreliabilities which are caused by second and higher orders of outage events. For computation simplicity, the final combined distribution is rounded by a fixed rounding increment during optimization.

Fig. 5.28 shows a study of the variations of the profit and number of intervals of the final combined distribution *N* as a function of rounding increments for the 6-unit microgrid. The leftmost circle/square on each line is calculated when the final combined distribution is not rounded. One sees that the profit is robust and unaffected by the variation of rounding increments. When the rounding increment increases, the number of intervals decreases. The computation complexity will decrease heavily.

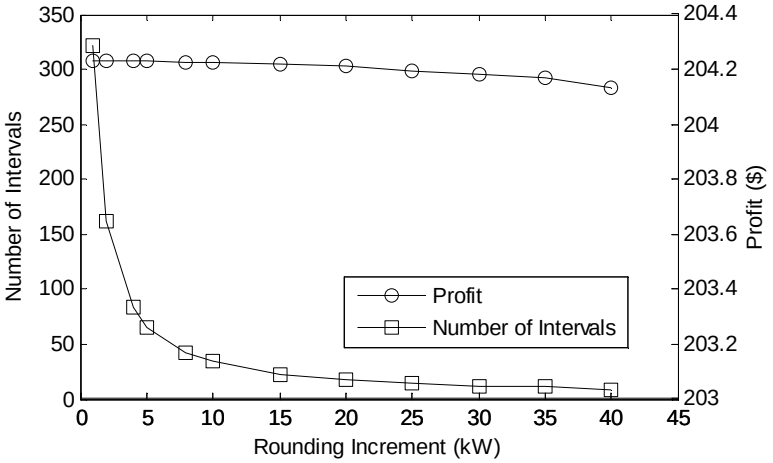

Fig. 5.28 Variation of profit and number of intervals N as a function of rounding increment of final combined distribution

5.3.3 Effect of Approximation of Probabilities

During optimization, the probabilities mainly affect the EENS value. The accuracy of $EENS^{>1}$ is affected not only by the approximation of probabilities, but also by the modified multi-step method. So $EENS^0$ and $EENS^1$ are selected to represent the effect of approximation of probabilities. The effect of approximation of probabilities can be described by $\Delta EENS^{01}$

$$\Delta EENS^{01} = \frac{\left| EENS^0_{in} + EENS^1_{in} - EENS^0_{after} - EENS^1_{after} \right|}{EENS^0_{after} + EENS^1_{after}} \tag{5.1}$$

where

$\Delta EENS^{01}$: normalized relative $EENS^{01}$ error;

$EENS^{01}$: sum of $EENS^0$ and $EENS^1$;

$EENS^0_{in}$: $EENS^0$ calculated during optimization;

$EENS^1_{in}$: $EENS^1$ calculated during optimization;

$EENS^0_{after}$: $EENS^0$ calculated after optimization via COPT; and

$EENS^1_{after}$: $EENS^1$ calculated after optimization via COPT.

In the first step $EENS^0_{\text{in}}$ and $EENS^1_{\text{in}}$ are calculated by (4.35). In other steps, they are calculated by the first and second terms of (4.36). $EENS^0_{\text{after}}$ and $EENS^1_{\text{after}}$ are calculated using optimization results based on COPT.

Obviously, the approximation of probabilities is affected by unit unreliability U_i and the number of units, N_G. To illustrate the effect of the unit unreliability, U_i is increased from 0.0001 to 0.01. The variations of $\Delta EENS^{01}$ versus U_i in step one and step two are shown in Figs. 5.29 and 5.30.

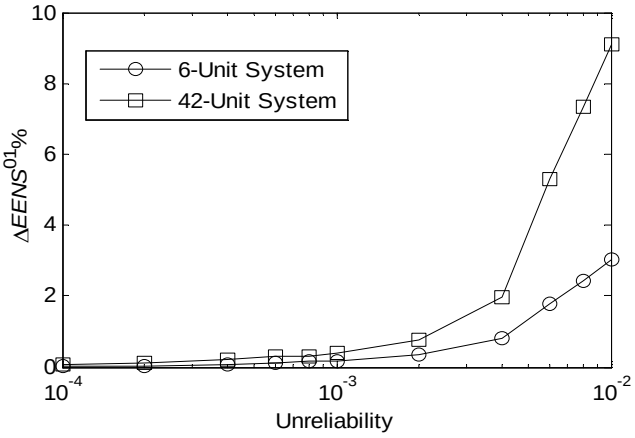

Fig. 5.29 $\Delta EENS^{01}$ versus unit unreliability in step one

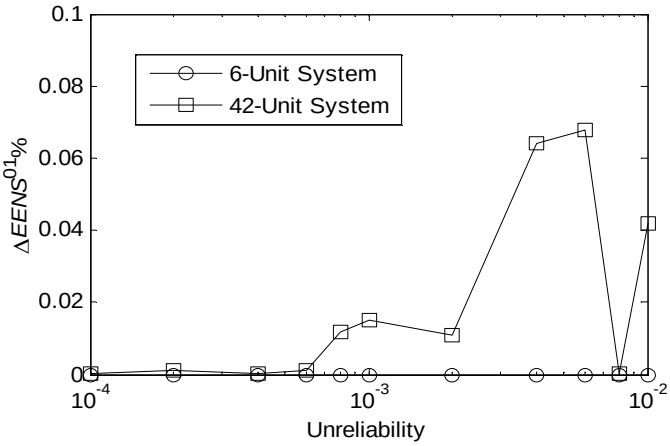

Fig. 5.30 $\Delta EENS^{01}$ versus unit unreliability in step two

From Fig. 5.29 one sees that the approximation error of probabilities increases with the increase of the unit unreliability and system size. In the first step, the approximation error is considerable and it is non-negligible for some circumstances.

From Fig. 5.30 one sees that based on the results of step one, $\Delta EENS^{01}$ calculated in step two is always smaller than 0.1%. The approximation error is greatly reduced, and is accurate enough for optimization when compared with that in step one. During the following steps, the approximation error is always at a low level of smaller than 0.1% because the probabilities are calculated based on the results of last step.

5.3.4 Effect of the Modified Multi-Step Method

The accuracy of the proposed method is guaranteed by $\Delta EENS$ which is defined in (4.40). For the 42-unit system, the variations of $\Delta EENS$ versus the processing step under different unit unreliabilities are shown in Fig. 5.31. It shows that with the increase of the unit unreliability, more steps are needed. When the unreliability is smaller than 0.002, only two steps are needed.

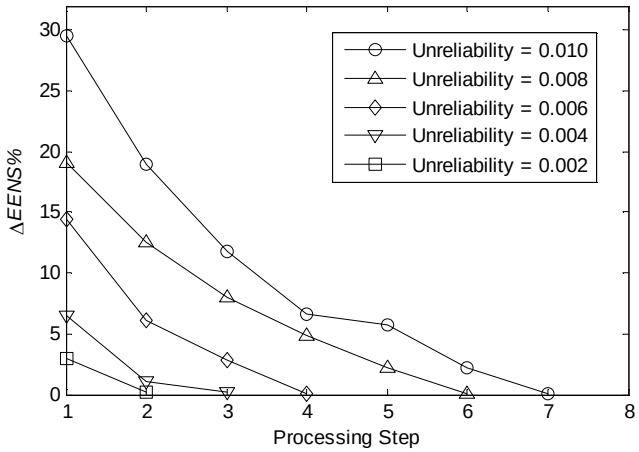

Fig. 5.31 Variations of $\Delta EENS$ versus processing step.

During optimization, $EENS^{>1}$ is computed by the modified multi-step method. The accuracy of $EENS^{>1}$ can be described by $\Delta EENS^{>1}$ which is shown in (5.2).

$$\Delta EENS^{>1} = \frac{|EENS_{in}^{>1} - EENS_{after}^{>1}|}{EENS_{after}^{>1}} \tag{5.2}$$

where

$\Delta EENS^{>1}$: normalized relative $EENS^{>1}$ error;

$EENS_{in}^{>1}$: $EENS^{>1}$ calculated during optimization, and it is corresponds to the third term of (4.36); and

$EENS_{after}^{>1}$: $EENS^{>1}$ calculated after optimization via COPT.

From (5.2) it can be found that $\Delta EENS^{>1}$ represents the $EENS^{>1}$ which is not captured by the proposed multi-step method. $\Delta EENS^{>1}$ denotes the ability of the modified multi-step method to capture the unit unreliability which is caused by the second and higher orders of outage events.

For the 42-unit system, the variations of $EENS^{>1}/EENS$ and $\Delta EENS^{>1}$ versus unit unreliability at the final step are shown in Fig. 5.32. In Fig. 5.32, when the unreliability is small, $EENS^{>1}/EENS$ is small. According to the value of $\Delta EENS^{>1}$, a magnitude of several percents of $EENS^{>1}$ is not captured, but the solution process has already satisfied the convergence criterion of (4.40). This is because $EENS^{>1}$ is much smaller than $EENS^{01}$ in the total *EENS* formed by $EENS^{01}$ and $EENS^{>1}$. With the increase of unreliability, the ratio $EENS^{>1}/EENS$ increases. In order to maintain the accuracy of the results, a larger magnitude of $EENS^{>1}$ must be captured during the optimization process so that the magnitude of $EENS^{>1}$ which is not captured decreases. This corresponds to the decreasing trend of $\Delta EENS^{>1}$ in Fig. 5.32.

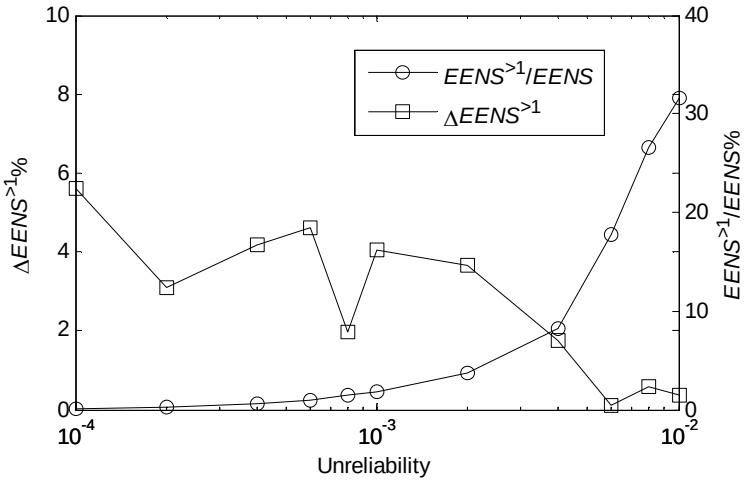

Fig. 5.32 Variations of $EENS^{>1}/EENS$ and $\Delta EENS^{>1}$ versus unreliability.

5.3.5 Run Time

The run time is affected by many factors. They include the system size, unit unreliability, load level, VOLL value, the interval of the combined uncertainty distribution, the rounding increment of the final combined distribution, convergence criterion, the duality gap of the MILP algorithm, etc. The proposed method can run faster if a larger rounding increment, convergence criterion and dual gap are used.

5.4 Summary

In this chapter, the probabilistic load, WTG, and PV models are introduced. The probabilistic WTG and PV distributions are truncated and discretized. Then the uncertainties caused by the load, WTG and PV are aggregated and rounded.

A modified multi-step method is proposed to estimate the SR in microgrids. The optimal is determined by simultaneous optimizing SC and EIC. EENS in this chapter is not only caused by various uncertainties, but also caused by unit outage events. Compared with the

multi-step method which is used in large traditional power systems, EENS in the modified multi-step is divided into two parts. EENS caused by uncertainties only, and first order of outage events and uncertainties are calculated directly during optimization using UC variables. EENS caused by uncertainties, second and higher orders of outage events are modeled as a piecewise linear function of SSR and captured step by step. Then the computation efficiency is greatly improved and accurate results can be achieved within a desirable execution time.

A hypothetical microgrid is used as the study case. This microgrid consists of a WTG, a PV, a FC, a MT, an ESS and is grid connected to the upstream grid. Both grid connected operation mode and isolated mode are considered. The optimization results are explicitly shown.

A series of sensitivity analyses are implemented to demonstrate the efficiency and robustness of the modified multi-step method proposed. The effect of aggregated uncertainties, rounding increment of the final combined distribution, approximation of probabilities and modified multi-step are all considered. The sensitivity analyses show that the proposed method is accurate, efficient and robust.

Chapter 6
Conclusions and Recommendations

6.1 Conclusions

SR is an important resource which intends to protect a power system against unforeseen events such as unit outages and/or load changes. Scheduling sufficient SR can reduce the probability and severity of loss of load. However, providing SR has a cost because it requires committing additional units and operating other units at less than their optimal output. Therefore the SR requirement needs to be assigned appropriately.

Various deterministic and probabilistic techniques can be used to determine the optimal SR requirement. Probabilistic techniques include the mainly successive iterative UC, reliability constrained UC, and cost/benefit analysis. Among these techniques, the cost/benefit analysis is the best choice. The drawback of this technique is that the calculation of reliability indices such as EENS and LOLP is rather complex during optimization.

In this thesis, a multi-step method is proposed to optimize the SR requirement in large traditional power systems. A modified multi-step method is proposed to optimize the SR requirement in microgrids. Some major research works and the contributions are further presented here.

- Modeling EENS and LOLP as a piecewise linear function of SSR only

When optimizing the SR requirement by the cost/benefit analysis, the major difficulty is the computation complexity caused by EENS and LOLP. The formulation of EENS and

LOLP are highly nonlinear and their combinatorial nature exists. In this research the EENS formulation is greatly simplified. EENS and LOLP in each optimization period can be modeled as a piecewise linear function of SSR based on a given unit schedule.

The EENS formulation is analyzed and it can be concluded that unless SSR is seen as the only variable, the EENS formulation cannot be drastically simplified. The EENS curve varies as a function of SSR only is shown based on the IEEE-RTS system data. It can be found that the EENS curve has a strong piecewise property. The reason why the piecewise property exists is analyzed. The process to determine the parameters of the piecewise function is analyzed. These parameters are by-products of COPT which is established based on a given unit schedule. The cluster property of EENS curves is discussed. It is concluded that the EENS value does not change too much for a fixed SSR when the unit schedule varies in the feasible region. The reason why the cluster property exists is also presented. Finally one can conclude that EENS can be formulated as a piecewise linear function of SSR based on a known unit schedule. This approximation can greatly reduce the computation burden.

- Optimizing SR using multi-step method in large traditional power systems

The optimal SR can be determined by optimizing SC and EIC in which EENS is formulated as a piecewise linear function. However, formulating EENS as a piecewise linear function of SSR may introduce some errors. So a multi-step method is proposed.

In step one, a base UC module without reserve constraint is implemented to produce the initial unit schedule. Then COPT for each optimization period is established. In step two, parameters of the EENS piecewise linear function are determined based on COPT. Then the optimal SR can be determined. After optimization a new unit schedule can be obtained and the corresponding COPT can be established. A convergence criterion is introduced to ensure that the error caused by the EENS approximation is guaranteed. If the convergence criterion is satisfied, the optimization will stop. Otherwise the EENS

formuation will be updated based on the newly found unit schedule and the optimizaiton runs again. The optimization runs step by step till the convergence criterion is satisfied. The proposed method is demonstrated by the IEEE-RTS system. Extensive sensitivity analyses such as the effects of VOLL, outage replacement rate (ORR) and system size are also given.

- Optimizing SR using modified multi-step method in microgrids

Before optimizing the SR in microgrids, the probabilistic load, WTG, and PV distribution models are given. These distributions are truncated and discretized. For computation simplicity, all the uncertainties are combined and aggregated.

The proposed multi-step method may have poor convergence speed or cannot converge when it is implemented in microgrids. A modified multi-step method is proposed. The difference between the multi-step method and modified multi-step method lies in the procedure of calculating EENS. In the multi-step method, the total EENS is formulated as a piecewise linear function of SSR. In the modified multi-step method, EENS is divided into two parts and calculated using two different methods. EENS caused by uncertainties only, and uncertainties and first order of outage events is calculated directly using UC variables. EENS caused by uncertainties, and second and higher orders of outage events is modeled by a piecewise linear function of SSR and captured step by step. The modified multi-step method is conducted on the 6-unit microgrid of both the grid connected and isolated modes. The studies are also extended to a 42-unit microgrid system. Various simulation results are given. A series of sensitivity analyses are implemented to demonstrate the efficiency and robustness of the proposed method.

6.2 Recommendations

For future works the research work can be expanded to further improve the schemes proposed in this thesis.

- The reason why EENS can be formulated as a piecewise linear function of SSR only is mainly based on the cluster property of EENS curves. The theoretical backing of the cluster property can be further strengthened.

- The robustness of the proposed multi-step method can be improved. For example, when VOLL is very large, the results obtained by the multi-step method deviates from the actual optimal results. There are many tradeoffs in the SR estimation problem. The main tradeoff is a compromise between SC and EIC. However, some secondary tradeoffs exist. For example, units with large capacity and relatively low cost results in a decrease of the total SC when their output increases. At the same time the EENS increases and the EIC increases due to their large capacity. Most of the time the effect of low cost outweighs the effect of large capacity. So this tradeoff is not considered in the multi-step method. However when VOLL is very large, this tradeoff is important and it will affect the performance of the multi-step method and hence may be worthy of further studies.

- For the modified multi-step method, the computation time can be sped up further. During optimization, it is obvious that some contingencies such as some first order of outage events cannot cause loss of load. For example, it is obvious that a single outage of units 1-5 of the IEEE-ETS system with a 12-MW capacity will not cause loss of load. Empirical constraints can be added into the optimization and the number of possible outage events considered in optimization decreases. The computation efficiency can be further improved in future studies.

- ❖ Transmission/distribution networks affect the SR estimation heavily. Interruptible load is also an important source of SR. The effect of network and interruptible load need to be further analyzed in the future.

References

[1] H. Singh and A. Papalexopoulos, **"**Competitive procurement of ancillary services by an independent system operator**,"** *IEEE Trans. Power Syst.*, vol. 14, no. 2, pp. 498-504, May 1999.

[2] F. S. Wen and A. K. David, "Optimally co-ordinated bidding strategies in energy and ancillary service markets," *IEE Proc.-Gener. Transm. Distrib.*, vol. 149, no. 3, pp. 331-338, May 2002.

[3] Chin-Chung Wu, Wei-Jen Lee, Chin-Lung Cheng and Hong-Wei Lan, "Role and value of pumped storage units in an ancillary services market for isolated power systems-simulation in the Taiwan power system," *IEEE Trans. Ind. Electron.*, vol. 44, no. 6, pp. 1924-1929, Nov. 2008.

[4] Tongxin Zheng and E. Litvinov, "Contingency-based zonal reserve modeling and pricing in a co-optimized energy and reserve market," *IEEE Trans. Power Syst.*, vol. 23, no. 2, pp. 277-286, May 2008.

[5] Y. Rebours and D. S. Kirschen, "What is spinning reserve?" 2005. [Online]. Available:http://eee.dev.ntweb.mcc.ac.uk/research/groups/eeps/publications/reportstheses/aoe/rebours%20et%20al_tech%20rep_2005A.pdf.

[6] Y. Rebours and D. S. Kirschen, "A survey of definitions and specifications of reserve services," 2005. [Online]. Available:http://www.eee.manchester.ac.uk/research/groups/eeps/ publications/reportstheses/aoe/rebours et al_tech rep_2005B.pdf.

[7] M. A. Ortega-Vazquez, "Optimizing the spinning reserve requirements," Ph. D. Dissertation, univ. Manchester, May 2006.

[8] A. Ahmadi-Khatir and R. Cherkaoui, "A probabilistic joint energy and spinning reserve market model," *IEEE Power Eng. Soc. General Meeting*, pp. 1-6, Jan. 2010.

[9] F. D. Galiana, F. Bouffard, J. M. Arroyo, and J. F. Restrepo, "Scheduling and pricing of coupled energy and primary, secondary, and tertiary reserves," *Proc. IEEE*, vol. 93, no. 11, pp. 1970–1983, Nov. 2005.

[10] R. Billinton and R. Karki, "Capacity_reserve_assessment_using_system_well-being analysis," *IEEE Trans. on Power Syst.*, vol. 14, no. 2, pp. 433-438, May 1999.

[11] Wu L., Shahidehpour M., and Li T., **"**Cost of reliability analysis based on stochastic unit commitment," *IEEE Trans. Power Syst.*, vol. 23, no. 3, pp. 1364-1374, Aug. 2008.

[12] R. Billinton and R. N. Allan, *Reliability evaluation of power systems*, Plenum Press, second edition, 1996.

[13] H. B. Gooi, D. P. Mendes, K. R. W. Bell, and D. S. Kirschen, "Optimal scheduling of spinning reserve," *IEEE Trans. Power Syst.*, vol. 14, no. 4, pp. 1485-1490, Nov. 1999.

[14] J. Bai, H. B. Gooi, L. M. Xia, G. Strbac and B. Venkatesh, "A probabilistic reserve market incorporating interruptible load", *IEEE Trans. on Power Syst.*, vol. 21, no. 3, pp. 1079-1087, Aug. 2006.

[15] D. Chattopadhyay and R. Baldick, "Unit commitment with probabilistic reserve," *IEEE Power Eng. Soc. Winter Meeting*, New York, vol. 1, pp. 280-285, Jan. 2002.

[16] F. Bouffard and F. D. Galiana, "An electricity market with a probabilistic spinning reserve criterion," *IEEE Trans. Power Syst.*, vol. 19, no. 1, pp. 300-307, Feb. 2004.

[17] D. N. Simopoulos, S. D. Kavatza, and C. D. Vournas, "Reliability constrained unit commitment using simulated annealing," *IEEE Trans. Power Syst.*, vol. 21, no. 4, pp. 1699-1706, Nov. 2006.

[18] F. Aminifar, M. Fotuhi-Firuzabad, and M. Shahidehpour, "Unit commitment with probabilistic spinning reserve and interruptible load considerations," *IEEE Trans. on Power Syst.*, vol. 24, no. 1, pp. 388-397, Jan. 2009.

[19] M. Jaefari-Nokandi, and H. Monsef, "Scheduling of Spinning Reserve Considering Customer Choice on Reliability," *IEEE Trans. Power Syst.*, vol. 24, no. 4, pp. 1780-1789, Nov. 2009.

[20] K. Afshar, M. Ehsan, M. Fotuhi-Firuzabad and N. Amjady, "Cost-benefit analysis and MILP for optimal reserve capacity determination in power system," *Applied Mathematics and Computation*, vol. 196, no. 2, pp. 752-61, 1 Mar. 2008.

[21] J. X. Wang, X. F. Wang, and Y. Wu, "Operating reserve model in the power market," *IEEE Trans. Power Syst.*, vol. 20, no. 1, pp. 223-229, Feb. 2005.

[22] K. Afshar, M. Ehsan, M. Fotuhi-Firuzabad and N. Amjady, "Cost-benefit analysis and MILP for optimal reserve capacity determination in power system," *Applied Mathematics and Computation*, vol. 196, no. 2, pp. 752-61, 1 Mar. 2008.

[23] Tsung-Ying Lee, "Optimal spinning reserve for a wind-thermal power system using EIPSO," *IEEE Trans. Power Syst.*, vol. 22, no. 4, pp. 1612-1621, Nov. 2007.

[24] A. Zakariazadeh, L. Alinezhad, and S. Jadid, "Optimum simultaneous clearing of energy and spinning reserve markets with high penetration of wind power," *Power and Energy Engineering Conference* (*APPEEC*), *2010 Asia-Pacific*, pp. 1-4, 28-31Mar. 2010.

[25] M. A. Ortega-Vazquez, D. S. Kirschen, and D. Pudjianto, "Optimising the scheduling of spinning reserve considering the cost of interruptions," *Proc. Inst. Elect. Eng., Gen., Transm., Distrib.*, vol. 153, no. 5, pp. 570–575, Dec. 2006.

[26] M. A. Ortega-Vazquez, and D. S. Kirschen, "Optimizing the spinning reserve requirements using a cost/benefit analysis," *IEEE Trans. Power Syst.*, vol. 22, no. 1, pp. 24-33, Feb. 2007.

[27] M. A. Ortega-Vazquez, and D. S. Kirschen, "Estimating the spinning reserve requirements in systems with significant wind power generation penetration, " *IEEE Trans. Power Syst.*, vol. 24, no. 1, pp. 114-124, Feb. 2009.

[28] A. Ahmadi-Khatir, M. Fotuhi-Firuzabad and L. Goel, "Customer choice of reliability in spinning reserve procurement and cost allocation using well-being analysis," *Elect. Power Syst. Res.*, vol. 79, no. 10, pp. 1431–1440, Oct. 2009.

[29] M. Parvania, M. Fotuhi-Firuzabad, F. Aminifar and A. Abiri-Jahromi, "Reliability-constrained unit commitment using stochastic mixed-integer

programming," *IEEE 11th International Conference on Probabilistic Methods Applied to Power Systems (PMAPS)*, pp. 200- 205, 14-17, Jun. 2010.

[30] J. M. Morales, A. J. Conejo, and J. Perez-Ruiz, "Economic valuation of reserves in power systems with high penetration of wind power," *IEEE Trans. Power Syst.*, vol. 24, no. 2, pp. 900-910, May 2009.

[31] S. Kamalinia, and M. Shahidehpour, "Generation expansion planning in wind-thermal power systems," *IET Gener. Transm. Distrib.*, vol. 4, no. 8, pp. 940-951, Aug. 2010.

[32] F. Bouffard, F. D. Galiana, and A. J. Conejo, "Market-clearing with stochastic security-part I: formulation," *IEEE Trans. Power Syst.*, vol. 20, no. 4, pp. 1818-1826, Nov. 2005.

[33] F. Bouffard, F. D. Galiana, and A. J. Conejo, "Market-clearing with stochastic security-part II: case studies," *IEEE Trans. Power Syst.*, vol. 20, no. 4, pp. 1827-1835, Nov. 2005.

[34] M. Parvania, and M. Fotuhi-Firuzabad, "Demand response scheduling by stochastic SCUC," *IEEE Trans. Smart Grid*, vol. 1, no. 1, pp. 89-98, Jun. 2010.

[35] Jichen Zhang, J. D. Fuller, and S. Elhedhli, "A stochastic programming model for a day-ahead electricity market with real-time reserve shortage pricing," *IEEE Trans. Power Syst.*, vol. 25, no. 2, pp. 703-713, May 2010.

[36] P. A. Ruiz, C. R. Philbrick, E. Zak, K. W. Cheung, and P. W. Sauer, "Uncertainty management in the unit commitment problem," *IEEE Trans. Power Syst.*, vol. 24, no. 2, pp. 642-651, May 2009.

[37] Chun-Lung Chen, "Optimal wind-thermal generating unit commitment," *IEEE Trans. Energy Convers.*, vol. 23, no. 1, pp. 273-280, Mar. 2008.

[38] Tsung-Ying Lee, "Optimal spinning reserve for a wind-thermal power system using EIPSO," *IEEE Trans. Power Syst.*, vol. 22, no. 4, pp. 1612-1621, Nov. 2007.

[39] L. Söder, "Reserve margin planning in a wind-hydro-thermal power system," *IEEE Trans. Power Syst.*, vol. 8, no. 2, pp. 564–571, May 1993.

[40] R. Doherty, and M. O'Malley, "A new approach to quantify reserve demand in systems with significant installed wind capacity," *IEEE Trans. Power Syst.*, vol. 20, no. 2, pp. 587-595, May 2005.

[41] G. Strbac, A. Shakoor, M. Black, D. Pudjianto, and T. Boppc, "Impact of wind generation on the operation and development of the UK electricity systems," *Elect. Power Syst. Res.*, vol. 77, no. 9, pp. 1214–1227, Jul. 2007.

[42] K. Liu and J. Zhong, "Generation dispatch considering wind energy and system reliability," *IEEE Power Eng. Soc. General Meeting*, vol. 1, pp. 1-7, 25-29 Jul. 2010.

[43] F. Bouffard and F.D. Galiana, "Stochastic security for operations planning with significant wind power generation," *IEEE Trans. Power Syst.*, vol. 23, no. 2, pp. 306-316, May. 2008.

[44] M. A. Matos and R. Bessa, "Operating reserve adequacy evaluation using uncertainties of wind power forecast," *IEEE Bucharest Power Tech*, pp. 1-8, Jun.-Jul., 2009.

[45] M. A. Matos, and R. J. Bessa, "Setting the operating reserve using probabilistic wind power forecasts," *IEEE Trans. Power Syst.*, IEEE early access.

[46] K. Afshar, M. Ehsan, M. Fotuhi-Firuzabad and N. Amjady, "Cost-benefit analysis and MILP for optimal reserve capacity determination in power system," *Applied Mathematics and Computation*, vol. 196, no. 2, pp. 752-61, 1 Mar. 2008.

[47] R. H. Lasseter, "MicroGrids**,"** *IEEE Power Eng. Soc. Winter Meeting*, vol. 1, pp. 305-308, 27-31 Jan. 2002.

[48] R. H. Lasseter, and P. Paigi, "Microgrid: a conceptual solution**,"** *The 35th Annual IEEE Power Electronics Specialists* Conf., vol. 6, pp. 4285-4290, 20-25 Jun. 2004.

[49] R. H. Lasseter, "Certs microgrid," *IEEE International Conference on System of Systems Engineering*, pp. 1-5**,** 16-18 Apr. 2007.

[50] N. Hatziargyriou, H. Asano, R. Iravani, and C. Marnay, "Microgrids**,"** *IEEE Power and Energy Magazine*, vol. 5, no. 4, pp. 78-94, Jul.-Aug. 2007.

[51] J. Driesen, and F. Katiraei, **"**Design for distributed energy resources**,"** *IEEE Power and Energy Magazine*, vol. 6, no. 3, pp.30-40, May-Jun. 2008.

[52] (2009) Architecture of microgrid. [Online]. Available:http://bit.ly/f98iSX.

[53] S. Chowdhury, S. P. Chowdhury and P. Crossley, *microgrids and active distribution networks*, Institution of Engineering and Technology, 2009.

[54] F. Katiraei, R. Iravani, N. Hatziargyriou, and A. Dimeas, **"**Microgrids management**,"** *IEEE Power and Energy Magazine*, vol. 6, no. 3, pp.54-65, May-Jun. 2008.

[55] A. Tsikalakis, I. Tassiou, and N. Hatziargyriou, "Impact of Energy Storage in the Secure and Economic Operation of Small Islands," *Proceedings of the MedPower 04 conference*, 15-17 Nov. 2004, Larnaca, Cyprus.

[56] K. K. Kariuki and R. N. Allan, "Evaluation of reliability worth and value of lost load," *IEE Proc.-Gener. Transm. Distrib.*, vol. 143, no. 2, pp. 171-180, Mar. 1996.

[57] B. Venkatesh, Peng Yu, H. B. Gooi, and D. Choling, **"**Fuzzy MILP unit commitment incorporating wind generators**,"** *IEEE Trans. on Power Syst.*, vol. 23, no. 4, pp. 1738-1746, Nov. 2008.

[58] A. M. Leite Da Silva, and G. P. Alvarez, "Operating reserve capacity requirements and pricing in deregulated markets using probabilistic techniques," *IET Gener. Transm. Distrib.*, vol. 1, no. 3, pp. 439-446, May 2007.

[59] A. M. L. L. da Silva, W.S. Sales, L.A. da Fonseca Manso, and R. Billinton, "Long-term probabilistic evaluation of operating reserve requirements with renewable sources," *IEEE Trans. Power Syst.*, vol. 25, no. 1, pp. 106-116, Feb. 2008.

[60] C. Wang and S. M. Shahidehpour, "Effects of ramp-rate limits on unit commitment and economic dispatch," *IEEE Trans. Power Syst.*, vol. 8, no. 3, pp. 1341-1350, Aug. 1993.

[61] C. Grigg, P. Wong, P. Albrecht, R. Allan, M. Bhavaraju, R. Billinton, Q. Chen, C. Fong, S. Haddad, S. Kuruganty, W. Li, R. Mukerji, D. Patton, N. Rau, D. Reppen, A. Schneider, M. Shahidehpour, and C. Singh, "The IEEE reliability test system - 1996," *IEEE Trans. Power Syst.*, vol. 14, no. 3, pp. 1010-1018, Aug. 1999.

[62] C. A. Floudas, *Nonlinear and Mixed-Integer Optimization: Fundamentals and Applications*. New York: Oxford Univ. Press, 1995.

[63] A. Brooke, D. Kendrick, A. Meeraus, and R. Raman: '*GAMS: A User's Guide*', (GAMS Development Corp., Washington D.C., 1998).

[64] Jeremy Bloom, "Optimization applications in the energy and power industries," [online]. Available: http://public.dhe.ibm.com/common/ssi/ecm/en/wsw14064usen/WSW14064USEN.PDF.

[65] Tao Li and M. Shahidehpour, **"**Price-based unit commitment: a case of Lagrangian relaxation versus mixed integer programming**,"** *IEEE Trans. on Power Syst.*, vol. 20, no. 4, pp. 2015-2025, Nov. 2005.

[66] M. Carrion and J. M. Arroyo, **"**A computationally efficient mixed-integer linear formulation for the thermal unit commitment problem**,"** *IEEE Trans. on Power Syst.*, vol. 21, no. 3, pp. 1371-1378, Aug. 2006.

[67] D. Streiffert, R. Philbrick, and A. Ott, **"**A mixed integer programming solution for market clearing and reliability analysis**,"** *IEEE Power Eng. Soc. General Meeting*, vol. 3, pp. 2724-2731, 12-16 Jun. 2005.

[68] Y. Fu, M. Shahidehpour, and Z. Li, "Security-constrained unit commitment with AC constraints," *IEEE Trans. on Power Syst.*, vol. 20, no. 3, pp. 1538-1550, Aug. 2005.

[69] Y. Fu, M. Shahidehpour, and Z. Li, "Fast SCUC for large-scale power systems," *IEEE Trans. on Power Syst.*, vol. 22, no. 4, pp. 2144-2151, Nov. 2007.

[70] F. Vallee, J. Lobry, and O. Deblecker, **"**Impact of the wind geographical correlation level for reliability studies,**"** *IEEE Trans. Power Syst.*, vol. 22, no. 4, pp. 2232-2239, Nov. 2007.

[71] M. R. Patel, *Wind and Solar Power Systems*. Boca Raton, FL: CRC Press, 1999.

[72] J. Hetzer, D. C. Yu, and K. Bhattarai, **"**An economic dispatch model incorporating wind power**,"** *IEEE Trans. on Energy Convers.*, vol. 23, no. 2, pp. 603-611, Jun. 2008.

[73] A. R. Daniel and A. A. Chen, "Stochastic simulation and forecasting of hourly average wind speed sequences in Jamaica," *Solar Energy*, vol. 46, no. 1, pp. 1-11, Jan. 1991.

[74] B. S. Borowy and Z. M. Salameh, **"**Optimum photovoltaic array size for a hybrid wind/PV system**,"** *IEEE Trans. on Energy Convers.*, vol. 9, no. 3, pp. 482-488, Sep. 1994.

[75] M. C. Alexiadis, P. S. Dokopoulos, and H. S. Sahsamanoglou, **"**Wind speed and power forecasting based on spatial correlation models**,"** *IEEE Trans. on Energy Convers.*, vol. 14, no. 3, pp.836-842, Sep. 1999.

[76] G. Damousis, M. C. Alexiadis, J. B. Theocharis, and P. S. Dokopoulos, "A fuzzy model for wind speed prediction and power generation in wind parks using spatial correlation," *IEEE Trans. Energy Convers.*, vol. 19, no. 2, pp. 352-361, Jun. 2004.

[77] S. Roy, **"**Market constrained optimal planning for wind energy conversion systems over multiple installation sites," *IEEE Trans. on Energy Convers.*, vol. 17, no. 1, pp. 124-129, Mar. 2002.

[78] B. S. Borowy, and Z. M. Salameh, "Methodology for optimally sizing the combination of a battery bank and PV array in a wind/PV hybrid system**,"** *IEEE Trans. on Energy Convers.*, vol. 11, no. 2, pp. 367-375, Jun. 1996.

[79] R. Billinton, and A. A. Chowdhury, "Incorporation of wind energy conversion systems in conventional generating capacity adequacy assessment," *IEE Proc. Gen., Transm., and Distrib*., vol. 139, no. 1, pp. 47-56, Jan. 1992.

[80] G. B. Shrestha, and L. Goel, "A study on optimal sizing of stand-alone photovoltaic stations,**"** *IEEE Trans. on Energy Convers.*, vol. 13, no. 4, pp.373-378, Dec. 1998.

[81] J. Tovar, F. J. Olmo, and L. Alados-Arboledas, "One-minute global irradiance probability density distributions conditioned to the optical air mass," *Solar Energy*, vol. 62, no. 6, pp. 387-393, Jun. 1998.

[82] F. Y. Ettoumi, A. Mefti, A. Adane, and M. Y. Bouroubi, "Statistical analysis of solar measurements in Algeria using beta distributions," *Renewable Energy*, vol. 26, no. 1, pp.47-67, May 2002.

[83] F. Giraud, and Z. M. Salameh, **"**Steady-state performance of a grid-connected rooftop hybrid wind-photovoltaic power system with battery storage," *IEEE Trans. on Energy Convers.*, vol. 16, no. 1, pp.1-7, Mar. 2001.

[84] Z. M. Salameh, B. S. Borowy, and A. R. A. Amin, **"**Photovoltaic module-site matching based on the capacity factors**,**" *IEEE Trans. on Energy Convers.*, vol. 10, no. 2, pp. 326-332, Jun. 1995.

[85] D. K. Khatod, V. Pant, and J. Sharma, "Analytical approach for Well-Being assessment of small autonomous power systems with solar and wind energy sources," *IEEE Trans. on Energy Convers.*, vol. 25, no. 2, pp. 535-545, Jun. 2010.

[86] M. K. C. Marwali, S. M. Shahidehpour, and M. Daneshdoost, "Probabilistic production costing for photovoltaics-utility systems with battery storage,**"** *IEEE Trans. on Energy Convers*, vol. 12, no. 2, pp. 175-180, Jun. 1997.

[87] M. K. C. Marwali, M. Haili, S. M. Shahidehpour, and K. H. Abdul-Rahman, **"**Short term generation scheduling in photovoltaic-utility grid with battery storage**,"** *IEEE Trans. on Power Syst.*, vol. 13, no. 3, pp. 1057-1062, Aug. 1998.

[88] R. Chedid, H. Akiki, and S. Rahman, "A decision support technique for the design of hybrid solar-wind power systems," *IEEE Trans. on Energy Convers.*, vol. 13, no. 1, pp. 76-83, Mar. 1995.

[89] A. G. Tsikalakis, and N. D. Hatziargyriou, "Centralized control for optimizing microgrids operation**,"** *IEEE Trans. on Energy Convers.*, vol. 23, no. 1, pp. 241-248, Mar. 2008.

[90] R. J. Yinger, "Behavior of Capstone and Honeywell microturbine generators during load changes," Jul. 2001. [Online]. Available: http://certs.lbl.gov/pdf/49095.pdf.

[91] J. D. Kueck, R. H. Staunton, S. D. Labinov, and B. J. Kirby, "Microgrid energy management System," Jan. 2003. [Online]. Available: http://www.ornl.gov/sci/btc/apps/ Restructuring/TM2002-242.pdf.

[92] Ryan Firestone and Chris Marnay, "Energy manager design for microgrids," Mar. 2005. [Online]. Available: http://certs.lbl.gov/pdf/54447.pdf.

[93] Robert H. Lasseter, and Paolo Piagi, "Control and design of microgrid components," Jan. 2006. [Online]. Available:http*://www.pserc.wisc.edu /.../lasseter_microgridcontrol_final_ project_report.pdf.*

[94] J. E. Larmine and A. Dicks, *Fuel Cell Systems Explained*. Chichester, U.K.: Wiley, 2000.

[95] S. Chiang, K. Chang, and C. Yen, "Residential photovoltaic energy storage system," *IEEE Trans. Energy Convers.*, vol. 45, no. 3, pp. 385-394, Jun. 1998.

[96] Jinhong Jeon, Seulki Kim, Changhee Cho, Jonbo Ahn, and Jangmok Kim, "Power control of a grid-connected hybrid generation system with photovoltaic/wind turbine/battery sources," *7th International Conference on Power Electronics*, pp. 506-510, 22-26 Oct. 2007.

[97] A. Oudalov, D. Chartouni, and C. Ohler, "Optimizing a battery energy storage system for primary frequency control," *IEEE Trans. on Power Syst.*, vol. 22, no. 3, pp. 1259-1266, Aug. 2007.

[98] H. T. Le and T. Q. Nguyen, "Sizing energy storage systems for wind power firming: An analytical approach and a cost-benefit analysis," in *Power & Energy Soc. General Meeting*, 20-24, Jul. 2008.

[99] H. Ibrahim, A. Ilinca, and J. Perron, "Energy storage systems-characteristics and comparisons," *Renewable and Sustainable Energy Reviews*, vol. 12, no. 5, pp. 1221-1250, Jun. 2008.

[100] X. Wang, D. Mahinda Vilathgamuwa, and S. Choi, "Determination of battery storage capacity in energy buffer for wind farm," *IEEE Trans. Energy Convers.*, vol. 23, no. 3, pp. 868 –878, Sept. 2008.

[101] C. Venu, Y. Riffonneau, S. Bacha, and Y. Baghzouz, "Battery storage system sizing in distribution feeders with distributed photovoltaic systems," *IEEE Bucharest, PowerTech*, Jun. 2009.

[102] C. Abbey and G. Joos, "A stochastic optimization approach to rating of energy storage systems in wind-diesel isolated grids," *IEEE Trans. on Power Syst.*, vol. 24, no. 1, pp. 418-426, Feb. 2009.

[103] P. Mercier, R. Cherkaoui, and A. Oudalov, "Optimizing a battery energy storage system for frequency control application in an isolated power system," *IEEE Trans. on Power Syst.*, vol. 24, no. 3, pp. 1469-1477, Aug. 2009.

[104] A. Etxeberria, I. Vechiu, H. Camblong, and J. M. Vinassa, "Hybrid energy storage systems for renewable energy sources integration in microgrids: a review," *International Power Engineering Conference* (*IPEC*) *Proceedings*, pp. 532-537, Oct. 2010.

[105] F. A. Chacra, P. Bastard, G. Fleury, and R. Clavreul, "Impact of energy storage costs on economical performance in a distribution substation," *IEEE Trans. on Power Syst.*, vol. 20, no. 2, pp. 684-691, May. 2005.

[106] Lu Bo, and M. Shahidehpour, "Short-term scheduling of battery in a grid-connected PV/battery system," *IEEE Trans. on Power Syst.*, vol. 20, no. 2, pp. 1053-1061, May. 2005.

[107] M. N. A. Hawlader, T. Y. Bong, and W. Mahmood, "Some frequently used meteorological data for Singapore," *Int. Journal of Solar Energy*, vol. 8, no. 1, pp.1-11, 1990.

[108] R. Allan, and R. Billinton, "Probabilistic assessment of power systems," *Proc. IEEE*, vol. 88, no. 2, pp.140-162, Feb. 2000.

Appendices

A.1 Data of 26-unit IEEE-RTS system

The 26-unit system is derived from the IEEE-RTS single-area system [61]. If the hydro generating units are omitted, this system consists of 26 units. The quadratic approximation of the cost functions and ramp up rates were taken from [60]. The coefficients of the quadratic cost functions are shown in Table A.1. The generator operational parameters are shown in Table A.2. The load for a 24-hour period is shown in Table A.3.

Table A.1 Coefficients of quadratic production costs of generating units

Unit	a_i ($/MW^{2}h)	b_i ($/MWh)	c_i ($/h)	Unit	a_i ($/MW^{2}h)	b_i ($/MWh)	c_i ($/h)
1	0.02533	25.5472	24.3891	14	0.00623	18.0000	217.8952
2	0.02649	25.6753	24.4110	15	0.00612	18.1000	218.3350
3	0.02801	25.8027	24.6382	16	0.00598	18.2000	218.7752
4	0.02842	25.9318	24.7605	17	0.00463	10.6940	142.7348
5	0.02855	26.0611	24.8882	18	0.00473	10.7154	143.0288
6	0.01199	37.5510	117.7551	19	0.00481	10.7367	143.3179
7	0.01261	37.6637	118.1083	20	0.00487	10.7583	143.5972
8	0.01359	37.7770	118.4576	21	0.00259	23.0000	259.1310
9	0.01433	37.8896	118.8206	22	0.00260	23.1000	259.6490
10	0.00876	13.3272	81.1364	23	0.00263	23.2000	260.1760
11	0.00895	13.3538	81.2980	24	0.00153	10.8616	177.0575
12	0.00910	13.3805	81.4641	25	0.00194	7.4921	310.0021
13	0.00932	13.4073	81.6259	26	0.00195	7.5031	311.9102

Table A.2 Generator operational parameters

Unit	P_i^{min} (MW)	P_i^{max} (MW)	SC_i ($/WM)	IC_i (h)	P_i^0 (MW)	T_i^{on} (h)	T_i^{off} (h)	UR_i (MW/h)	DR_i (MW/h)	MTTF (h)
1	2.4	12	68	-1	0	1	1	48	60	2940
2	2.4	12	68	-1	0	1	1	48	60	2940
3	2.4	12	68	-1	0	1	1	48	60	2940
4	2.4	12	68	-1	0	1	1	48	60	2940
5	2.4	12	68	-1	0	1	1	48	60	2940
6	4	20	5	-1	0	1	1	30.5	70	450
7	4	20	5	-1	0	1	1	30.5	70	450
8	4	20	5	-1	0	1	1	30.5	70	450
9	4	20	5	-1	0	1	1	30.5	70	450
10	15.2	76	596	3	15.2	3	2	38.5	80	1960
11	15.2	76	596	3	15.2	3	2	38.5	80	1960
12	15.2	76	596	3	15.2	3	2	38.5	80	1960
13	15.2	76	596	3	15.2	3	2	38.5	80	1960
14	25	100	566	-3	0	4	2	51	74	1200
15	25	100	566	-3	0	4	2	51	74	1200
16	25	100	566	-3	0	4	2	51	74	1200
17	54.25	155	953	5	125	5	3	55	78	960
18	54.25	155	953	5	121.4	5	3	55	78	960
19	54.25	155	953	5	121.4	5	3	55	78	960
20	54.25	155	953	5	121.4	5	3	55	78	960
21	68.95	197	775	-4	0	5	4	55	99	950
22	68.95	197	775	-4	0	5	4	55	99	950
23	68.95	197	775	-4	0	5	4	55	99	950
24	140	350	4468	10	350	8	5	70	120	1150
25	100	400	0	10	400	8	5	50.5	100	1100
26	100	400	0	10	400	8	5	50.5	100	1100

Table A.3 Load for 26-unit system

Hour	Load (MW)	Hour	Load (MW)	Hour	Load (MW)	Hour	Load (MW)
1	1700	7	2000	13	2590	19	2500
2	1730	8	2430	14	2550	20	2550
3	1690	9	2540	15	2620	21	2600
4	1700	10	2600	16	2650	22	2480
5	1750	11	2670	17	2550	23	2200
6	1850	12	2590	18	2530	24	1840

A.2 Data of 6-unit Microgrid System

A hypothetical microgrid is used in this thesis. The load profile and energy price are derived from [18]. They are shown in Figs. A.1 and A.2. Four DG units are installed in this microgrid. They include a WTG, a PV, a FC and a MT. The microgrid with an ESS can be connected to the upstream grid. It can be seen as a 6-unit system. Table A.4 summarizes their parameters. Here a linear bidding production cost function is used. The offer coefficients of DG units are derived from [18]. For the ESS, P_{max}^{E} is 20 kW; η^{E} is 0.9; and C_S, C_E, C_{min}, C_{max} are 180, 180, 100, 260 kWh respectively.

The average hourly wind speed and irradiance shapes of WTG and PV are taken from [23]. They are shown in Figs. A.3 and A.4. For WTG, v_i, v_r and v_o are 5, 15 and 45 miles/hour respectively. J = 10, k = 2 and $c = v_{mean}/0.9$ miles/hour are assumed for all hours. For PV, η^{PV} = 12%, and S^{PV} = 270 m^2 while K = 10, ω = 0.3, k_1 = 2, k_2 = 10, $c_2 = g_{mean}/0.95$ and $c_1 = 0.4c_2$ for all hours. For the aggregated uncertainty distribution, M = 7 is used. For the final combined distribution, the fixed rounding increment is 5 kW. An indicative combinatorial distribution of the WTG, PV and load uncertainties at hour 12 is shown in Fig. A.5. The corresponding aggregated uncertainty distribution is shown in Fig. A.6.

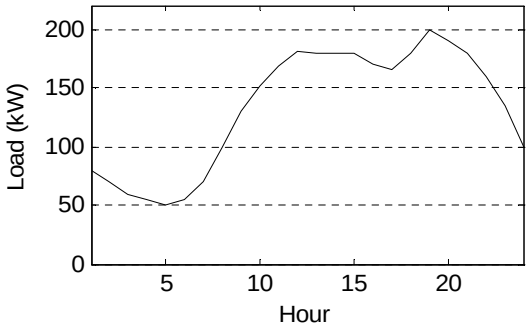

Fig. A.1 Load profile of the study case

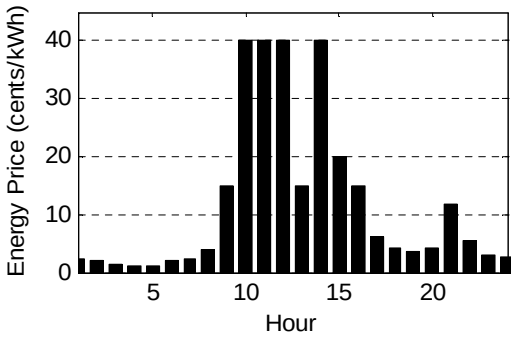

Fig. A.2 Energy price of every hour

Table A.4 Parameters of DG units, ESS and upstream Grid

Unit Type	WTG	PV	FC	MT	ESS	Upstream Grid
$P_i^{\min}$ (kW)	0	0	10	30	-20	-100
$P_i^{\max}$ (kW)	40	30	100	150	20	100
SC_i (cents/kW)	0	0	53	45	0	0
IC_i (h)	1	0	0	1	1	1
P_i^0 (kW)	8.14	0	0	30	20	21.86
T_i^{on} (h)	1	1	1	1	1	0
T_i^{off} (h)	1	1	1	1	1	0
UR_i (kW/h)	600	600	900	900	600	600
DR_i (kW/h)	600	600	900	900	600	600
Failure rate γ_i	0.006	0.006	0.006	0.006	0.006	0.006
$b_{i,t}$ (cents/kWh)	10.63	54.84	2.84	4.37	0	$MP(t)$
$c_{i,t}$ (cents/h)	0	0	850	425	10	0

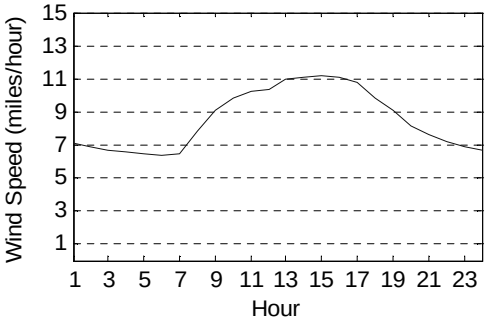

Fig. A.3 Hourly wind speed of WTG

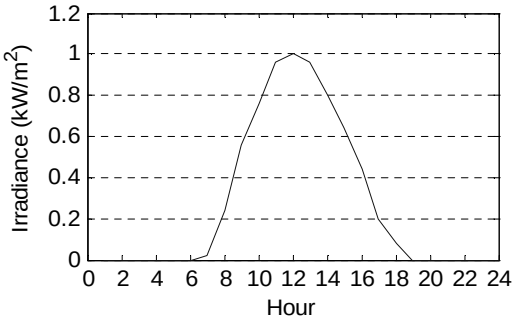

Fig. A.4 Hourly irradiance of PV

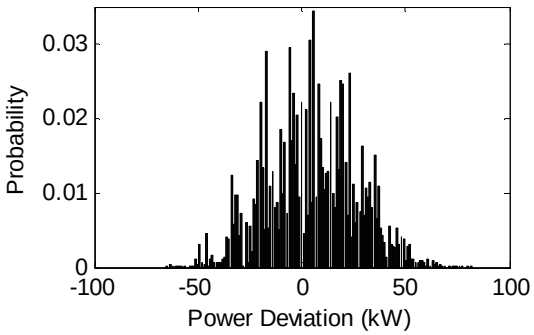

Fig. A.5 A combinational distribution of uncertainties

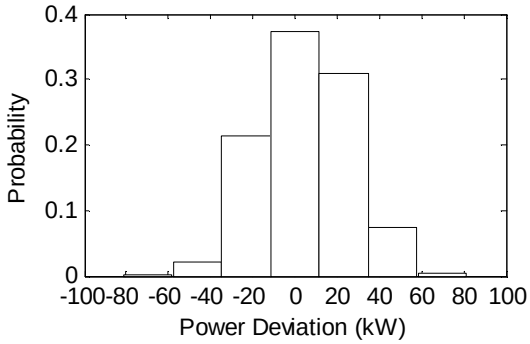

Fig. A.6 The aggregated distribution of uncertainties

A.3 Mixed Integer Linear Programming Model

◆ Linear expressions of quadratic unit production cost function

The quadratic polynomial approximation of the unit production costs ($a_i \cdot P_{i,t}^2 + b_i \cdot P_{i,t} + c_i$) can be approximated by piecewise linear functions. A three-segment piecewise linear function is usually used. The linearization of the quadratic cost function is shown in Fig. A.7.

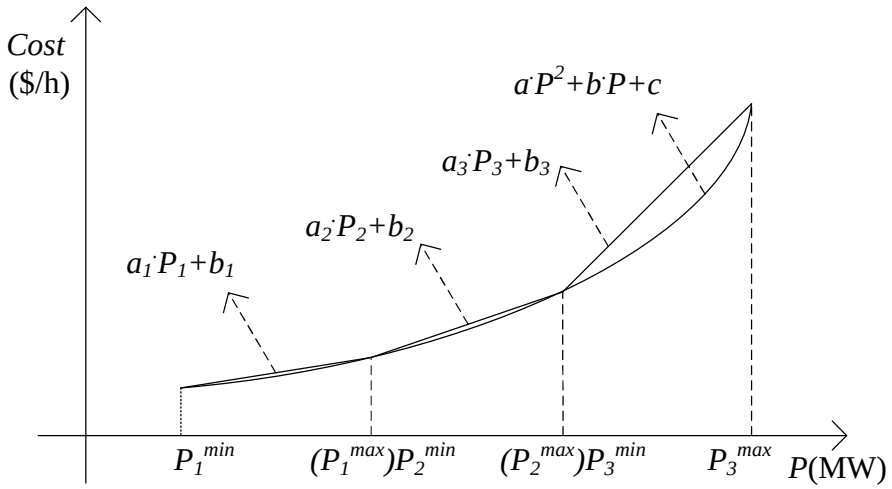

Fig. A.7 Linearization of the quadratic production cost function

The three-segment piecewise linear function can be formulated as

$$C_{i,t} = \sum_{m=1}^{3} (a_{m,i} \cdot P_{m,i,t} + b_{m,i} \cdot U_{m,i,t}) \tag{A.1}$$

in which

$$a_{m,i} = \frac{[a_i (P_{m,i}^{\max})^2 + b_i P_{m,i}^{\max} + c_i] - [a_i (P_{m,i}^{\min})^2 + b_i P_{m,i}^{\min} + c_i]}{P_{m,i}^{\max} - P_{m,i}^{\min}} \qquad \forall m{=}1,2,3; \forall i \in I \tag{A.2}$$

$$b_{m,i} = [a_i (P_{m,i}^{\min})^2 + b_i P_{m,i}^{\min} + c_i] - a_{m,i} \cdot P_{m,i}^{\min} \qquad \forall m{=}1,2,3; \forall i \in I \tag{A.3}$$

$$\begin{cases} P_{1,i}^{\min} = P_i^{\min} \\ P_{1,i}^{\max} = P_i^{\min} + (P_i^{\max} - P_i^{\min})/3 \end{cases} \tag{A.4}$$

$$\begin{cases} P_{2,i}^{\min} = P_i^{\min} + (P_i^{\max} - P_i^{\min})/3 \\ P_{2,i}^{\max} = P_i^{\min} + 2\times(P_i^{\max} - P_i^{\min})/3 \end{cases} \quad \text{(A.5)}$$

$$\begin{cases} P_{3,i}^{\min} = P_i^{\min} + 2\times(P_i^{\max} - P_i^{\min})/3 \\ P_{3,i}^{\max} = P_i^{\max} \end{cases} \quad \text{(A.6)}$$

where

$P_{m,i,t}$ output power when unit *i* operates in segment *m* during period *t*;

$U_{m,i,t}$ status (0/1) when unit *i* operates in segment *m* during period *t*;

$P_{m,i}^{\max}$ maximum output power when unit *i* operates in segment *m*;

$P_{m,i}^{\min}$ minimum output power when unit *i* operates in segment *m*; and

$P_i^{\min}$: minimum output power of unit *i*.

◆ **Generation limit**

The power generation limits are formulated as follows

$$P_{i,t} = \sum_{m=1}^{3} P_{m,i,t} \quad \text{(A.7)}$$

$$P_{m,i}^{\min} \cdot U_{m,i,t} \le P_{m,i,t} \le P_{m,i}^{\max} \cdot U_{m,i,t} \qquad \forall m=1,2,3; \forall i \in I; \forall t \in T \quad \text{(A.8)}$$

$$\sum_{m=1}^{3} U_{m,i,t} \le 1 \quad \text{(A.9)}$$

$$P_i^{\min} \cdot U_{i,t} \le P_{i,t} \le P_i^{\max} \cdot U_{i,t} \qquad \forall i \in I; \forall t \in T \quad \text{(A.10)}$$

◆ **Startup cost**

The startup cost is considered in the model. Once a unit is synchronized it generates a fixed cost $SC_i \cdot K_{i,t}$. The auxiliary binary variable $K_{i,t}$ satisfies

$$\begin{cases} K_{i,1} = U_{1,t} & \text{when } IC_i < 0 \\ K_{i,t} \ge U_{i,t} - U_{i,t-1} & \text{when } t = 2, 3, \ ..., \ N_T \end{cases} \quad \text{(A.11)}$$

where

IC_i initial state of unit *i*. A positive value means this unit is on and a negative value means this unit is off.

◆ **Power balance constraint**

At all hours, the total power output must match the load P_t^L.

$$\sum_{i=1}^{N_G} P_{i,t} = P_t^L \tag{A.12}$$

◆ **SR constraint**

The SR provided by a unit is constrained by its power output and ramp rate

$$R_{i,t} \le \min\{U_{i,t} \cdot P_i^{\max} - P_{i,t},\ U_{i,t} \cdot \tau \cdot UR_i\} \tag{A.13}$$

It can be linearized as

$$\begin{cases} R_{i,t} \le U_{i,t} \cdot P_i^{\max} - P_{i,t} \\ R_{i,t} \le U_{i,t} \cdot \tau \cdot UR_i \end{cases} \tag{A.14}$$

And the system spinning reserve SSR_t satisfies

$$SSR_t = \sum_{i=1}^{N_G} R_{i,t} \tag{A.15}$$

◆ **Minimum up time and down time constraints**

Minimum up time constraint

$$(U_{i,t+1} - U_{i,t})T_i^{on} - \sum_{s=t+2}^{\min\{t+T_i^{on},\, N_T\}} U_{s,t} \le \max\{1, T_i^{on} - N_T + t + 1\} \quad \forall t = 1,\ \ldots,\ N_T - 2 \tag{A.16}$$

where T_i^{on} is the minimum up time of unit *i*.

Minimum down time constraint

$$(U_{i,t} - U_{i,t+1})T_i^{off} + \sum_{s=t+2}^{\min\{t+T_i^{off},\, N_T\}} U_{s,t} \le T_i^{off} \quad \forall t = 1, \ldots, N_T - 2 \tag{A.17}$$

where T_i^{off} is the minimum down time of unit *i*.

◆ **Ramp up and ramp down constraints**

The auxiliary binary variables $U_{i,t}^{up}$ and $U_{i,t}^{dn}$ are introduced to represent whether unit *i* starts up or shuts down during period *t*. $U_{i,t}^{up}$ and $U_{i,t}^{dn}$ are defined as

$$U_{i,t}^{up} = U_{i,t}(1 - U_{i,t-1}) \tag{A.18}$$

$$U_{i,t}^{dn} = U_{i,t-1}(1 - U_{i,t}) \tag{A.19}$$

As a product of two binary variables, both of them can be linearized. The linearization of the product of some binary variables is shown in A.4.

In this thesis, it is assumed that the thermal units can be started up only at their minimum generation limit $P_i^{\min}$ when the minimum generation limit $P_i^{\min}$ is larger than the product of the ramp up rate UR_i and duration time d_T. Similarly, the thermal units can be shut down only at their minimum generation limit $P_i^{\min}$ when $P_i^{\min}$ is larger than the product of the ramp down rate DR_i and duration time d_T.

The ramp up and ramp down constraints are

$$P_{i,t} - P_{i,t-1} \le UR_i d_T \cdot (1\text{-}U_{i,t}^{up}) + \max\{P_i^{\min}, UR_i d_T\} \cdot U_{i,t}^{up} \quad \forall t = 2, \ldots, T \tag{A.20}$$

$$P_{i,t-1} - P_{i,t} \le DR_i d_T \cdot (1\text{-}U_{i,t}^{dn}) + \max\{P_i^{\min}, DR_i d_T\} \cdot U_{i,t}^{dn} \quad \forall t = 2, \ldots, T \tag{A.21}$$

where

UR_i: ramp up rate of unit *i*;

DR_i: ramp down rate of unit *i*.

◆ **Initial condition constraints**

Initial ramp up constraint

$$\begin{cases} P_{i,1} - P_i^0 \le UR_i d_T U_{i,1} & \text{when } IC_i > 0 \\ P_{i,1} - P_i^0 \le \max\{P_i^{\min}, UR_i d_T\} \cdot U_{i,1} & \text{when } IC_i \le -T_i^{off} \end{cases} \tag{A.22}$$

where

P_i^0 initial power of unit *i*.

Initial ramp down constraint

$$P_i^0 - P_{i,1} \le DR_i d_T \cdot U_{i,1} + \max\{P_i^{\min}, DR_i d_T\}(1 - U_{i,1}) \quad \exists\, IC_i > T_i^{on} \tag{A.23}$$

Initial minimum up time constraint

$$\sum_{t=1}^{T_i^{on} - IC_i} U_{i,t} \ge T_i^{on} - IC_i \quad \forall i \in I \quad \text{when } IC_i > 0 \text{ and } IC_i < T_i^{on} \tag{A.24}$$

Initial minimum down time constraint

$$\sum_{t=1}^{T_i^{off} + IC_i} U_{i,t} \le 0 \quad \forall i \in I \quad \text{when } IC_i < 0 \text{ and } IC_i > -T_i^{off} \tag{A.25}$$

A.4 Linear Expressions of the Product of Some Binary Variables

Denote *z* as a product of some binary variables as follows:

$$z = \prod_{i=1}^{n} x_i \tag{A.26}$$

The equivalent linear expressions of *z* are [62]

$$\begin{cases} z \le \dfrac{\sum_{i=1}^{n} x_i}{n} \\ z \ge \dfrac{\sum_{i=1}^{n} x_i - n + 1}{n} \end{cases} \tag{A.27}$$

or

$$\begin{cases} z \geq 0 \\ z \leq x_i \quad \forall\ i\ =\ 1,\ \ldots,\ n \\ z \geq \sum_{i=1}^{n} x_i - n + 1 \end{cases} \tag{A.28}$$

A.5 Linear Expressions of the Product of a Binary Variable and a Bounded Continuous Variable

Denote z is a product of a binary variable and a bounded continuous variable as follows

$$z = x \cdot y,\ y \in [y^{\min}, y^{\max}] \tag{A.29}$$

The equivalent linear expressions of z are [62]

$$\begin{cases} xy^{\min} \leq z \leq xy^{\max} \\ y - y^{\max}(1-x) \leq z \leq y - y^{\min}(1-x) \end{cases} \tag{A.30}$$

VITA

Wang Ming Qiang was born in 1982 in P. R. China. He received his B.E. and M.Eng. in Electrical Engineering from Shandong University, Jinan, China in 2004 and 2007 respectively. He is pursuing his PhD degree at Nanyang Technological University. His research areas are power system economic operation and microgrids. Since December, 2011, he has been a Research associate in Energy Research Institute @ Nanyang Technological University (NTU).

This research work has led to the following publications.

Journal Papers:

M. Q. Wang and H. B. Gooi, "Spinning reserve estimation in microgrids," *IEEE Trans. Power Syst.*, vol.26, no.3, pp. 1164-1174, Aug. 2011.

M. Q. Wang, H. B. Gooi and S. X. Chen, "Optimizing probabilistic spinning reserve using an analytical EENS formulation," *IET Gener. Transm. Distrib.*, vol. 5, no. 7, pp. 772-780, Jul., 2011.

S. X. Chen, H. B. Gooi and M. Q. Wang, "Sizing of energy storage for microgrids," *IEEE Trans. Smart Gird*, vol. 3, no. 1, pp. 142-151, Mar. 2012.

Conference Papers:

M. Q. Wang and H. B. Gooi, "Spinning reserve estimation in microgrids," *Transmission & Distribution Conference & Exposition: Asia and Pacific*, pp. 1-4, 26-30 Oct. 2009, Seoul, South Korea.

M. Q. Wang and H. B. Gooi, "Optimizing probabilistic reserve in large power systems," *Transmission & Distribution Conference & Exposition: Asia and Pacific*, pp. 1-4, 26-30 Oct. 2009, Seoul, South Korea.

M. Q. Wang and H. B Gooi, "Effect of uncertainty on spinning reserve estimation in microgrids," *International Power and Energy Conference*, IPEC 2010, Singapore.